Investigation of BRD9 inhibition as alternative treatment option for testicular germ cell tumors

Dissertation

zur

Erlangung des Doktorgrades (Dr. rer. nat.)

der

Mathematisch-Naturwissenschaftlichen Fakultät

der

Rheinischen Friedrich-Wilhelms-Universität Bonn

vorgelegt von

Aylin Hansen

aus

Koblenz

Bonn, 2025



Teile dieser Arbeit wurden bereits in folgender Publikation veröffentlicht:

¹ Aylin Hansen, Christine Sanders, Florian Fronhoffs, Kai Funke, Glen Kristiansen, Hubert Schorle. BRD9 inhibition as potential treatment option for testicular germ cell tumors. *Andrology*. 2025; 1-14. https://doi.org/10.1111/andr.70038

LIST OF ABBREVIATIONS

| Abbreviation | Meaning |
|--------------|--|
| -R | cisplatin-resistant |
| °C | degree celsius |
| μg | microgram |
| μΙ | microliter |
| μM | micromolar |
| μm | micrometer |
| Ac | acetyl group |
| AFP | α-Fetoprotein |
| AKT | serine/threonine-protein kinase |
| ALDH | aldehyde dehydrogenase |
| AML | acute myeloid leukemia |
| APS | ammonium persulfate |
| ASH1L | histone-lysine N-methyltransferase ASH1L |
| ATM | ataxia telangiectasia mutated |
| ATP | adenosine triphosphate |
| ATP7A | copper-transporting ATPase 1 |
| ATP7B | copper-transporting ATPase 2 |
| AUC | area under the curve |
| BAF | BRG1/BRM-associated factor |
| Bax | apoptosis regulator BAX |
| BCA | bicinchoninic acid assay |
| Bcl-xL | B-cell lymphoma-extra large |
| ВСР | bromodomain-containing protein |
| BEP | bleomycin, etoposide and platinum chemotherapy |
| BER | base excision repair |
| BET | bromodomain and extra terminal |
| ВМР | bone morphogenetic protein |
| BRAD1 | BRCA1-associated RING domain 1 |
| BRCA1 | breast cancer type 1 susceptibility protein |
| BRCA2 | breast cancer type 2 susceptibility protein |

| Abbreviation | Meaning |
|-----------------|---|
| BRD | bromodomain |
| BRD2 | bromodomain-containing protein 2 |
| BRD3 | bromodomain-containing protein 3 |
| BRD4 | bromodomain-containing protein 4 |
| BRD7 | bromodomain-containing protein 7 |
| BRD9 | bromodomain-containing protein 9 |
| BRDT | bromodomain testis-specific protein |
| BRIP1 | BRCA1 interacting helicase 1 |
| BSA | bovine serum albumin |
| Casp6 | caspase-6 |
| Сс | choriocarcinoma |
| CDK | cyclin-dependent kinase |
| cDNA | complementary deoxyribonucleic acid |
| CDX2 | homeobox protein CDX-2 |
| CH ₃ | methyl group |
| CHEK2 | checkpoint kinase 2 protein |
| CLDN1 | claudin-1 |
| CLEC1 | C-type lectin domain family 1 |
| cm | centimeter |
| cm ² | square centimeter |
| CNS | central nervous system |
| CO ₂ | carbon dioxide |
| COAD | colon adenocarcinoma |
| CRISPR | clustered regularly interspaced short palindromic repeats |
| CTR1 | copper transporter 1 |
| DAPI | 6-diamidino-2-phenylindole dihydrochloride |
| DAZL | deleted in azoospermia-like |
| DLX6 | homeobox protein DLX-6 |
| DMEM | dulbecco's modified eagle's medium |
| DMF | N,N-dimethylformamide |
| DMSO | dimethyl sulfoxide |
| DNA | deoxyribonucleic acid |

| Abbreviation | Meaning |
|--------------|---|
| DND1 | dead end protein homolog 1 |
| DNMT | DNA methyltransferase |
| DNMT33B | DNA (cytosine-5)-methyltransferase 33 B |
| DNMT3L | DNA (cytosine-5)-methyltransferase 3 L |
| dNTP | deoxynucleotide triphosphates |
| DPPA3 | developmental pluripotency-associated protein 3 |
| DUSP6 | dual specificity phosphatase 6 |
| EC | embryonal carcinoma |
| ECL | enhanced chemiluminescence |
| EDTA | ethylenediaminetetraacetic acid |
| ERCC1 | excision repair cross-complementing 1 |
| et al. | et alii, aliae, alia; latin: and others |
| EtOH | ethanol |
| ExE | extraembryonic endoderm |
| EXO1 | exonuclease 1 |
| FACS | fluorescence activated cell sorting |
| FAS | fatty acid synthase |
| FASL | fatty acid synthase ligand |
| FBS | fetal bovine serum |
| FDA | food and drug administration |
| FDR | false discovery rate |
| FES | tyrosine-protein kinase Fes/Fps |
| FGF3 | fibroblast growth factor 3 |
| FGF4 | fibroblast growth factor 4 |
| FLIP | filamin-A-interacting protein |
| fwd | forward |
| FZD5 | frizzled-5 |
| FZD6 | frizzled-6 |
| FZD10 | frizzled-10 |
| g | gram |
| GADD45 | growth arrest and DNA-damage-inducible protein 45 |
| GAPDH | glyceraldehyde-3-phosphate dehydrogenase |

| Abbreviation | Meaning |
|------------------|--|
| GATA4 | transcription factor GATA-4 |
| GATA5 | transcription factor GATA-5 |
| GBC | gallbladder cancer |
| GCNIS | germ cell neoplasia in situ |
| GCT | germ cell tumor |
| GEO | gene expression omnibus |
| GFP | green fluorescent protein |
| GO | gene ontology |
| GSH | glutathione |
| h | hour |
| H ₂ O | water |
| HAND1 | heart- and neural crest derivatives-expressed protein 1 |
| HAT | histone acetyltransferase |
| HCI | hydrochloric acid |
| HDAC | histone deacetylase |
| hESC | human embryonic stem cell |
| HESX1 | homeobox expressed in ES cells 1 |
| HEYL | hairy/enhancer-of-split related with YRPW motif-like protein |
| HHR | homologous recombination machinery |
| HMGB1 | high-mobility group box protein 1 |
| hPGCLC | human primordial germ cell like cell |
| HR | homologous recombination |
| HRAS | GTPase HRas |
| HRP | horseradish per |
| HRR | homologus recombination repair |
| HSF4 | heat shock factor protein 4oxidase |
| IF | immunofluorescence |
| IGCCCG | international germ cell cancer collaborative group |
| IHC | immunohistochemistry |
| ISWI | imitation SWItch |
| Kac | ε-N-acetylation of lysine residues |
| kDa | kilo dalton |

| Abbreviation | Meaning |
|-------------------|---|
| KIT | mast/stem cell growth factor receptor Kit |
| KLF2 | krueppel-like factor 2 |
| KLF4 | krueppel-like factor 4 |
| KLF5 | krueppel-like factor 5 |
| KLF15 | krueppel-like factor 15 |
| LACC | locally advanced cervical cancer |
| LDH | lactate dehydrogenase |
| LEF1 | lymphoid enhancer-binding factor 1 |
| М | molar |
| MDM2 | E3 ubiquitin-protein ligase Mdm2 |
| MeOH | methanol |
| mg | milligram |
| MgCl ₂ | magnesium chloride |
| min | minute |
| ml | milliliter |
| MLH1 | DNA mismatch repair protein Mlh1 |
| mm | millimeter |
| mM | millimolar |
| MMR | mispaired base repair |
| mRNA | messenger ribonucleic acid |
| MRP | multidrug resistance proteins |
| MRT | malignant rhabdoid tumor |
| MSH2 | DNA mismatch repair protein Msh2 |
| MT | metallothionein |
| mTOR | mammalian target of rapamycin |
| NAE1 | NEDD8-activating enzyme E1 regulatory subunit |
| NANOG | homeobox protein NANOG |
| NCAM | neural cell adhesion molecule 1 |
| NBS1 | nibrin |
| ncBAF | non-canonical BAF |
| NEAA | non-essential amino acid |
| NER | nucleotide excision pathway |

| Abbreviation | Meaning |
|-----------------|---|
| NH ₃ | amine |
| NHL | non-hodgkin lymphoma |
| nm | nanometer |
| nM | nanomolar |
| N-MYC | N-MYC proto-oncogene protein |
| NODAL | nodal homolog |
| NOTCH2 | neurogenic locus notch homolog protein 2 |
| ns | not significant |
| OCT | organic cation transporter |
| PAGE | polyacrylamid gel electrophoresis |
| PALB2 | partner and localizer of BRCA2 |
| PARP | poly (ADP-ribose) polymerase |
| PBAF | polybromo-associated BAF |
| PBRM1 | protein polybromo-1 |
| PBS | phosphate buffered saline |
| PBST | phosphate buffered saline tween |
| PCR | polymerase chain reaction |
| PD-1 | programmed cell death 1 |
| PDGF | platelet-derived growth factor |
| PDGFb | platelet-derived growth factor subunit B |
| PDGFRb | platelet-derived growth factor receptor b |
| PD-L1 | programmed cell death ligand 1 |
| PE | platinum and etoposide chemotherapy |
| PFA | paraformaldehyde |
| PGC | primordial germ cell |
| PI3K | phosphoinositid-3-kinase |
| PMS | N-methyl dibenzo pyrazine methyl sulfate |
| PMS2 | mismatch repair endonuclease PMS2 |
| POU5F1 | POU domain, class 5, transcription factor 1 |
| PRDM1 | PR domain zinc finger protein 1 |
| PRDM14 | PR domain zinc finger protein 14 |
| PROTAC | proteolysis targeting chimera |

| Abbreviation | Meaning |
|--------------|--|
| p-RPLND | primary retroperitoneal lymph node dissection |
| PTM | posttranslational modification |
| PUMA | P53 upregulated modulator of apoptosis |
| PVDF | polyvinylidene fluoride |
| qRT-PCR | quantitative real-time polymerase chain reaction |
| RAD51 | DNA repair protein RAD51 |
| RAD54 | DNA repair protein RAD54 |
| rev | reverse |
| RIN | RNA integrity |
| RIPA | radioimmunoprecipitation assay buffer |
| RNA | ribonulceic acid |
| ROS | reactive oxygen species |
| rpm | rounds per minute |
| RPMI | roswell park memorial institute medium |
| SALL4 | SAL-like protein 4 |
| SAMSN1 | SAM domain-containing protein SAMSN-1 |
| SD | standard deviation |
| SDS | sodium dodecyl sulfate |
| sec | second |
| SEMA3C | semaphorin-3C |
| SFRP1 | secreted frizzled-related protein 1 |
| SFRP4 | secreted frizzled-related protein 4 |
| shRNA | small hairpin RNA |
| siRNA | small interfering RNA |
| SMARCA2 | probable global transcription activator SNF2L2 |
| SMARCA4 | transcription activator BRG1 |
| SOX2 | transcription factor SOX-2 |
| SOX15 | transcription factor SOX-15 |
| SOX17 | transcription factor SOX-17 |
| SOX21 | transcription factor SOX-21 |
| SPG | spermatogonia |
| SqCLC | squamous cell lung cancer |

| Abbreviation | Meaning |
|--------------|--|
| SSC | spermatogonial stem cell |
| SWI/SNF | SWItch/sucrose non-fermentable |
| TAE | tris-acetate-EDTA-buffer |
| TEMED | tetramethyl ethylenediamine |
| TFAP2C | transcription factor AP-2 gamma |
| TGCT | testicular germ cell tumor |
| TKI | tyrosine kinase |
| TMA | tissue microarray |
| U | unit |
| UTF1 | undifferentiated embryonic cell transcription factor 1 |
| UV | ultraviolet |
| V | volt |
| v/v | volume per volume |
| VEGFR | vascular endothelial growth factor receptor |
| VIP | etoposide, ifosfamide and platinum chemotherapy |
| w/v | weight per volume |
| WB | western blot |
| WHO | world health organistation |
| WNT2B | protein Wnt-2b |
| xg | relative centrifugal force |
| XPA | DNA repair protein complementing XP-A cells |
| XPF | xeroderma pigmentosum complementation group F |
| XTT | 2,3-Bis-(2-methoxy-4-nitro-5-sulfenyl)-(2H)-tetrazolium-5- |
| | carboxanilid |
| YST | yolk sac tumor |
| ZMYND8 | MYND-type zinc finger-containing chromatin reader ZMYND8 |
| ZSCAN10 | zinc finger and SCAN domain-containing protein 10 |
| β-hCG | beta subunit of human chorionic gonadotropin |

TABLE OF CONTENTS

| LIST OF AB | BREVIATIONS | IV |
|-------------|-------------------------------|-----|
| TABLE OF (| CONTENTS | XII |
| LIST OF FIC | GURES | XIV |
| LIST OF TA | BLES | XV |
| 1 INTROI | DUCTION | 1 |
| 1.1 Ge | rm cell development | 1 |
| 1.2 Ge | rm cell tumors | 2 |
| 1.2.1 | Type I germ cell tumors | 4 |
| 1.2.2 | Type II germ cell tumors | 4 |
| 1.2.3 | Type III germ cell tumors | 6 |
| 1.3 Tre | eatment of TGCTs | 6 |
| 1.3.1 | Non-Seminomas | 6 |
| 1.3.2 | Seminomas | 7 |
| 1.3.3 | Cisplatin | 7 |
| 1.4 Cis | splatin resistance | 10 |
| 1.4.1 | Pre-target | 10 |
| 1.4.2 | On-target | 10 |
| 1.4.3 | Post-target | 12 |
| 1.4.4 | Off-target | 12 |
| 1.5 Alte | ernative treatment options | 13 |
| 1.5.1 | Targeted therapy | 13 |
| 1.5.2 | Immunotherapy | 13 |
| 1.5.3 | Other therapeutic agents | 14 |
| 1.5.4 | Epigenetic drugs | 14 |
| 1.6 Bro | omodomain-containing proteins | 15 |
| 1.6.1 | BRD9 | 16 |
| 1.6.2 | I-BRD9 | 17 |
| 1.6.3 | TGCT cell lines | 19 |
| 1.7 Ain | n of the project | 19 |
| | RIALS | |
| | II lines | 20 |

| | 2.2 | Cell culture media and reagents | 21 |
|---|--------------|--|----|
| | 2.3 | Consumables | 22 |
| | 2.4 | Chemicals and reagents | 23 |
| | 2.5 | Buffers and solutions | 24 |
| | 2.6 | Kits | 25 |
| | 2.7 | Enzymes | 26 |
| | 2.8 | Equipment | 26 |
| | 2.9 | Antibodies | 28 |
| | 2.10 | Oligonucleotides | 28 |
| | 2.11 | Software | 29 |
| 3 | ME | THODS | 31 |
| | 3.1 | Affymetrix expression microarray analysis of GCT tissues | 31 |
| | 3.2 | Tissue microarray | 31 |
| | 3.3 | Immunohistochemistry staining | 31 |
| | 3.4 | Cell culture maintenance | 31 |
| | 3.5 | Illumina HT-12v4 expression microarray analysis of TGCT cell lines | 32 |
| | 3.6 | Protein extraction, SDS PAGE and Western Blot analysis | 32 |
| | 3.7 | Cell viability assay | 33 |
| | 3.8 | DAPI/ AnnexinV (Apoptosis) FACS analysis | 34 |
| | 3.9 | Hoechst (Cell Cycle) FACS Analysis | 34 |
| | 3.10 | RNA isolation | 34 |
| | 3.11 | 3'mRNA sequencing analysis | 35 |
| | 3.12 | RNAseq data analysis | 35 |
| | 3.13 | Quantitative RT-PCR | 36 |
| | 3.14 | Immunofluorescence staining | 36 |
| | 3.15 | Statistical analysis | 37 |
| 4 | RES | SULTS | 38 |
| | 4.1 | BRD9 is expressed in TGCT tissue as well as cell lines | 38 |
| | 4.2 depen | Inhibition of BRD9 decreases viability in TGCT cell lines in a dose- and timedent manner | |
| | 4.3 | I-BRD9 led to induction of apoptosis and G1-phase cell cycle arrest in TG | CT |

| | 4.4 differ | BRD9 inhibition in embryonal carcinoma and seminoma induces rentiation to an epithelial cell fate and loss of pluripotency | 47 |
|-----|---------------|--|-----|
| | 4.5 level | Confirmation of induction of apoptosis and cell cycle arrest on trans | • |
| 5 | DIS | SCUSSION | 59 |
| 6 | BIE | BLIOGRAPHY | 65 |
| 7 | AP | PENDIX | 85 |
| 8 | AC | CKNOWLEDGEMENT | 90 |
| LI | ST (| OF FIGURES | |
| Fiç | gure | 1: Overview of effects of I-BRD9 in TGCTs | XVI |
| Fiç | gure | 2: Human germ line development | 1 |
| Fiç | gure | 3: New cases in testis cancer in 2022 worldwide | 3 |
| Fiç | gure 4 | 4: Development of GCTs | 4 |
| Fiç | gure | 5: Human PGC-like cells resemble seminoma (TCam-2) cells | 5 |
| Fiç | gure | 6: Chemical structure of cisplatin | 8 |
| Fiç | gure | 7: Mode of action of cisplatin in cancer treatment | g |
| Fi | gure | 8: Mechanisms of cisplatin resistance | 11 |
| Fi | gure | 9: Mechanisms of cisplatin resistance | 12 |
| Fiç | gure | 10: Structure of the bromodomain of human BRD4 | 15 |
| Fiç | gure | 11: Epigenetic modifications in TGCTs | 17 |
| Fiç | gure | 12: K _{ac} mimetic I-BRD9 binds to the bromodomain of BRD9 | 18 |
| Fiç | gure | 13: Expression of BRD9 in TGCT tissues | 39 |
| Fiç | gure | 14: Expression of BRD9 in TGCT cell lines | 40 |
| Fiç | gure | 15: Viability of TGCT cell lines treated with I-BRD9 | 42 |
| Fiç | gure | 16: Viability of TGCT cell lines treated with I-BRD9 | 43 |
| Fiç | gure | 17: BRD9 inhibition induced apoptosis in TGCT cell lines | 45 |
| Fiç | gure | 18: I-BRD9 induced G1-phase cell cycle arrest in TGCT cell lines | 46 |
| Fiç | gure | 19: Differentially expressed genes in 2102 EP cells | 48 |
| Fiç | gure : | 20: Differentially expressed genes in TCam-2 cells | 48 |
| Fiç | gure : | 21: Differentially expressed genes in MPAF cells | 49 |

| Figure 22: Epithelium development is enriched in 2102 EP and 1 Cam-2 cells while |
|--|
| metabolic processes are upregulated in MPAF cells 5 |
| Figure 23: Genes associated with epithelium development were upregulated in 2102 |
| EP and TCam-2 cells5 |
| Figure 24: Downregulation of genes associated with stem cell population |
| maintenance in 2102 EP and TCam-2 cells |
| Figure 25: Stem cell population maintenance associated genes were downregulated |
| in 2102 EP and TCam-2 cells 5 |
| Figure 26: NANOG and PRDM14 were downregulated in 2102 EP cells on protein |
| level5 |
| Figure 27: NANOG and PRDM14 were downregulated in TCam-2 cells on protein |
| level5 |
| Figure 28: Transcriptome analysis confirmed induction of apoptosis 5 |
| Figure 29: Transcriptome analysis confirmed induction of cell cycle arrest 5 |
| Figure S 1: Example images for the staining intensities of SALL4 in seminomas, |
| embryonal carcinomas and GCNIS 8 |
| Figure S 2: Original Western Blot images of BRD9 protein level and corresponding |
| load control β -actin in different TGCT cell lines as well as control cell lines |
| Figure S 3: Utilization of logarithmic regression curve for calculation of IC ₅₀ values |
| based on XTT assay data (Figure 15) 8 |
| Figure S 4: Utilization of logarithmic regression curve for calculation of IC ₅₀ values |
| based on XTT assay data (Figure 15) |
| Figure S 5: STRING-based interaction analysis of all upregulated genes associated |
| with epithelium development in 2102 EP cells after 24h of treatment with I-BRD9 8 |
| Figure S 6: STRING-based interaction analysis of all upregulated genes associated |
| with epithelium development in TCam-2 cells after 24h of treatment with I-BRD9 8 |
| LIST OF TABLES |
| Table 1: Expression of BRD9 in testicular tumor and normal testis tissue 3 |
| Table 2: IC ₅₀ values of TGCT cell lines and control cell lines 4 |

SUMMARY

Type II germ cell tumors are the most prevalent tumor in young men between the ages of 15 and 35 years. They arise from a block in primordial germ cell differentiation leading to a precursor lesion called germ cell neoplasia in situ (GCNIS). They are subgrouped into seminomas and non-seminomas. Non-seminomas comprise embryonal carcinomas which are able to differentiate into cells of all three germ layers as well as extraembryonic tissue classified as teratoma, yolk sac tumor and choriocarcinoma.

The standard treatment of testicular germ cell tumors (TGCT) is orchiectomy followed by cisplatin-based chemotherapy leading to high 5-year survival rates of 95 % but unfortunately 15-20 % of patients are still resistant to the treatment. Therefore, we found it very important to investigate alternative treatment options like epigenetic drugs. BET protein inhibitors interfering with the epigenetic landscape have already been shown to be effective in different cancer types like prostate cancer, glioblastoma and breast cancer. The bromodomain-containing protein-9 (BRD9) is part of a chromatin remodeling complex and an epigenetic reader which binds to acetylated lysine residues to activate gene expression by recruitment of other transcription factors. BRD9 shows significantly increased protein levels in cervical cancer and in malignant rhabdoid tumor (MRT) cells. For example, in acute myeloid leukemia (AML) cells the inhibition of BRD9 led to reduction of cell growth. Therefore, we found it very interesting to investigate the effect of the BRD9 inhibitor I-BRD9 in TGCTs.

First, we analyzed the expression of the target BRD9 in TGCT tissues and cell lines. Meta-analysis of microarray data in tissues as well as cell lines showed expression of BRD9. On protein level Western Blot also revealed comparable protein levels in TGCT cell lines while a tissue microarray (TMA) showed heterogenous expression of BRD9 in TGCT tissues. On the other hand, the lowest expression was found in the control cell line MPAF and in normal testis tissue indicating a promising starting point for testing the BRD9 inhibitor in TGCTs. XTT viability assays after I-BRD9 application led to reduced cell growth in all TGCT cells while the control cells were only slightly affected. FACS analysis revealed induction of apoptosis as well as G1-phase cell cycle arrest already after 24 hours of treatment with I-BRD9 in the TGCT cell lines while the control cells remained unaffected. RNAseq analysis displayed downregulation of a prominent network of pluripotency markers including NANOG, NODAL and KLF4 while

genes involved in epithelium development were upregulated. These data suggest loss of the pluripotency state and differentiation towards an epithelial cell fate (Figure 1).

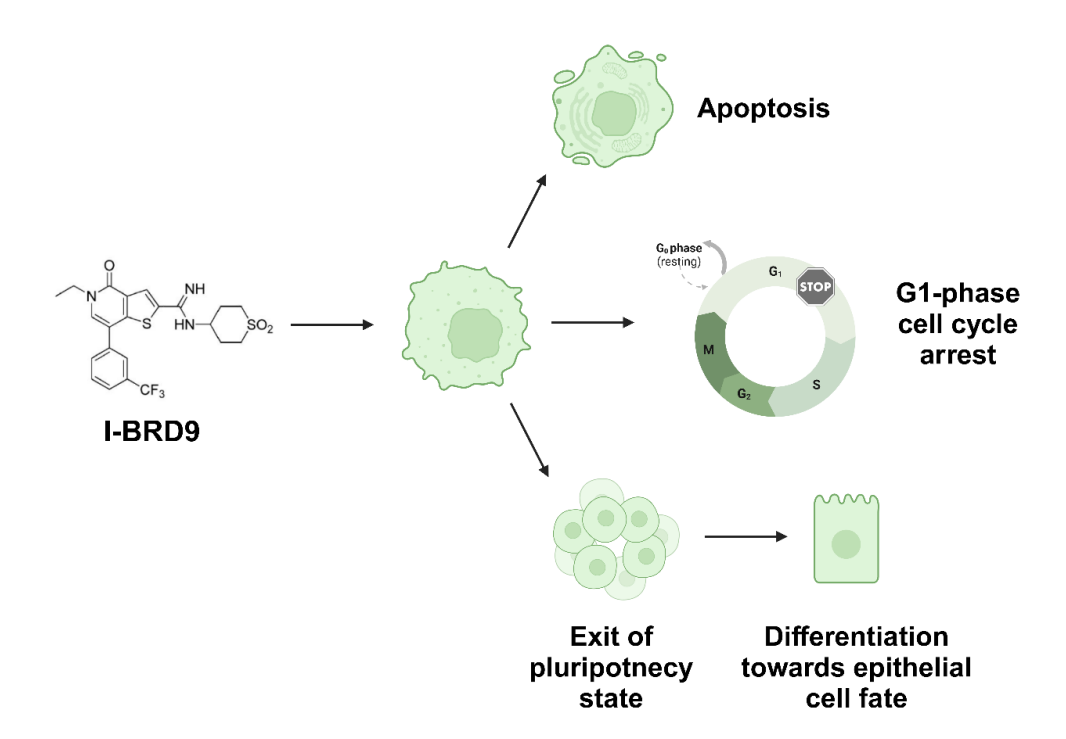


Figure 1: Overview of effects of I-BRD9 in TGCTs. BRD9 inhibition led to induction of apoptosis as well as G1-phase cell cycle arrest. Transcriptome analysis revealed downregulation of pluripotency markers and induction of epithelium development. Created in https://BioRender.com.

Taken together, the BRD9 inhibitor I-BRD9 led to severe effects in TGCT cell lines like reduction of viability, induction of apoptosis and G1-phase cell cycle arrest while the control cells were only slightly affected. BRD9 inhibition induces loss of the pluripotency state and differentiation towards an epithelial cell fate. Most importantly, the data suggest I-BRD9 as a potential treatment alternative for TGCTs.

1 INTRODUCTION

1.1 Germ cell development

The start of every mammalian embryo is the fertilization of the oocyte by the sperm resulting in a totipotent zygote. The zygote arises all cell lineages including the germ line (Figure 2) ². Origin of the germ cell lineage are primordial germ cells (PGC) which give rise to spermatogonia or oocytes ^{3,4}.

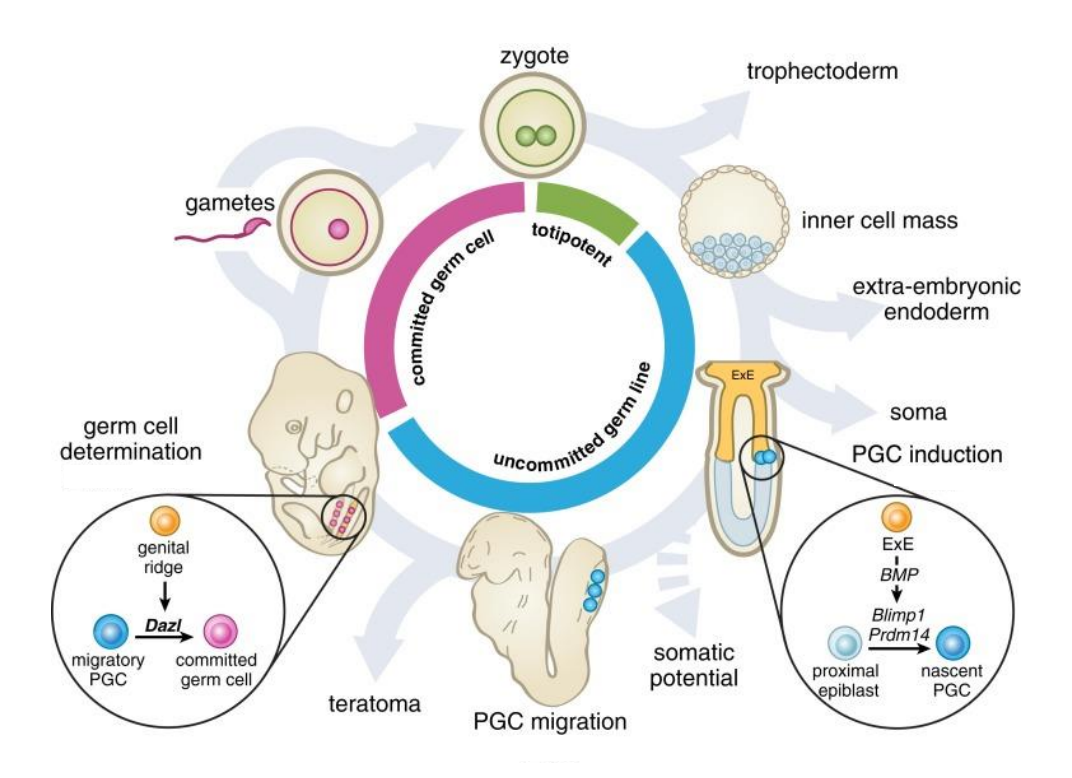


Figure 2: Human germ line development. The fertilized oocyte develops into the zygote which further develops into the blastocyst. The pre-implantation epiblast cells arise all lineages including the germ line. PGCs are found near the yolk sac before they migrate to the genital ridge. Meiosis and gametogenesis give rise to gametes (oocytes and sperm) which are able to restart the circle by fertilization. PGC – primordial germ cell, ExE – Extraembryonic endoderm. Modified from ⁵.

Specification occurs during early embryonic development and is orchestrated by a specific network of genes which is induced by signals from the extra-embryonic tissues ^{2,6}. BMP and WNT signaling result in induction of expression of BLIMP1 which specifies PGCs ^{6,7}. Afterwards, PRDM14 as well as TFAP2C are upregulated ⁸. They represent a regulatory transcription factor network of PGCs ^{2,6}. During migration of the PGCs

along the developing hindgut to the genital ridges global DNA methylation as well as deletion of imprinting occurs ⁷. At the genital ridge PGCs undergo licensing in preparation for gametogenesis which is induced by DAZL ⁹. Furthermore, PGCs differentiate into gonocytes and enter cell cycle arrest in G0-phase and therefore are prevented from mitosis until after birth. Afterwards, gonocytes differentiate into spermatogonia (SPG) which stay dormant for 5-7 years. Mitosis starts and the number of SPGs is increased to enable differentiation into spermatozoa in the process of spermiogenesis ¹⁰.

Upon PGC specification, pluripotency markers including OCT4, LIN28, SOX2, KLF2, KLF5, N-MYC and NANOG are expressed in PGCs. In contrast to induced pluripotency PGC fate is already initiated in the epiblast cells which comprise key factors of pluripotency ⁴. PGCs maintain the expression of SOX2, KLF2, KLF5, N-MYC and NANOG during specification while migratory PGCs express POU5F1, PRDM1, SALL4 and NANOG ^{4,11}. After arrival in the gonadal niche PGCs downregulate pluripotency markers ¹². Of note, the expression of many pluripotency factors in PGCs as well as absence of correct germ cell differentiation signals might lead to the development of germ cell tumors ¹³.

1.2 Germ cell tumors

According to the World Health Organization (WHO) the second leading cause of death worldwide is cancer accounting nearly 10 million deaths in 2018. The prevalent cancers in males are lung, prostate, colorectal, stomach and liver cancer while breast, colorectal, lung, cervical and thyroid cancer are most predominant in females ¹⁴. Testis cancer only accounted 72040 (1.7 %) of new cases in 2022 but germ cell tumors (GCT) are the most prominent cancer in younger males between the ages of 15 and 35 (Figure 3) ^{15,16}.

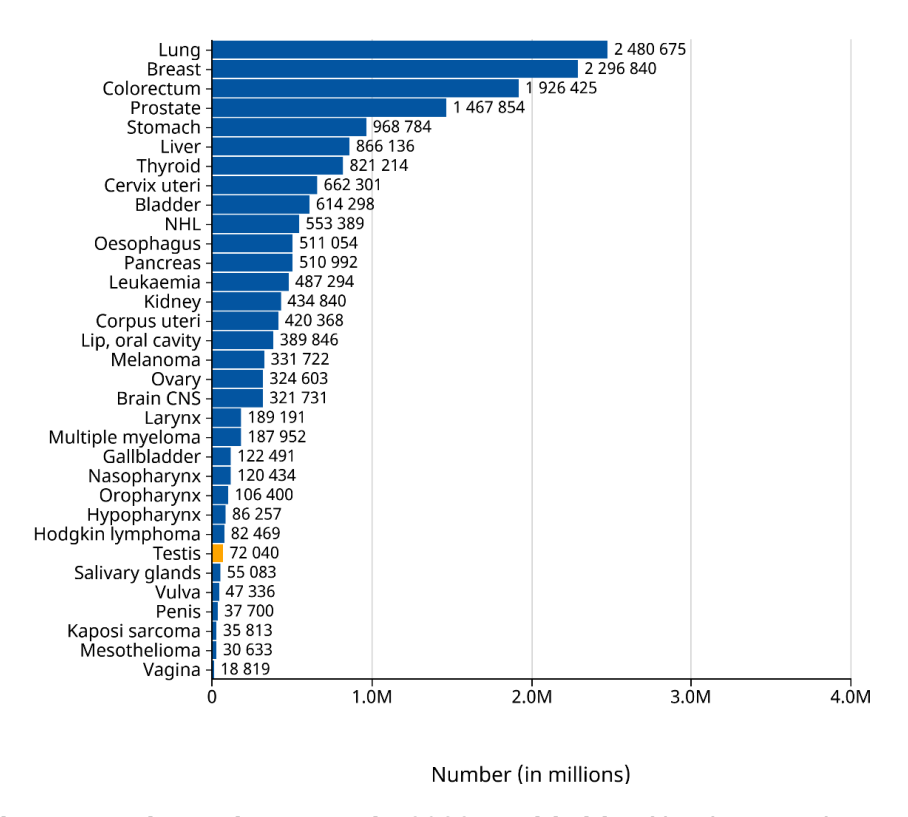


Figure 3: New cases in testis cancer in 2022 worldwide. Absolute numbers of incidences in both sexes in 2022. Testis cancer accounted for 72040 new cases. NHL – Non-Hodgkin lymphoma; CNS – central nervous system. Modified from ¹⁵.

GCTs are a group of rare neoplasms which occur in the gonads (ovary and testis), in extragonadal sites along the body midline and in the midline of the brain ^{12,16}. Incidences are rising steadily highlighting the clinical importance. A high prevalence is visible in the Caucasian populations and in total there is a five times higher incidence rate in industrialized countries compared to less developed regions ^{16,17}. The familial risk factor is higher than in most other cancers and the predominant abnormality is a short arm of the chromosome 12 ^{16,18}. Other risk factors are for example cryptorchidism, infertility, contralateral testicular cancer or Klinefelter's syndrome ¹⁹. Based on the cell of origin, sex and age of the patient and developmental potential 7 types (Type 0-VI) of GCT were classified ¹².

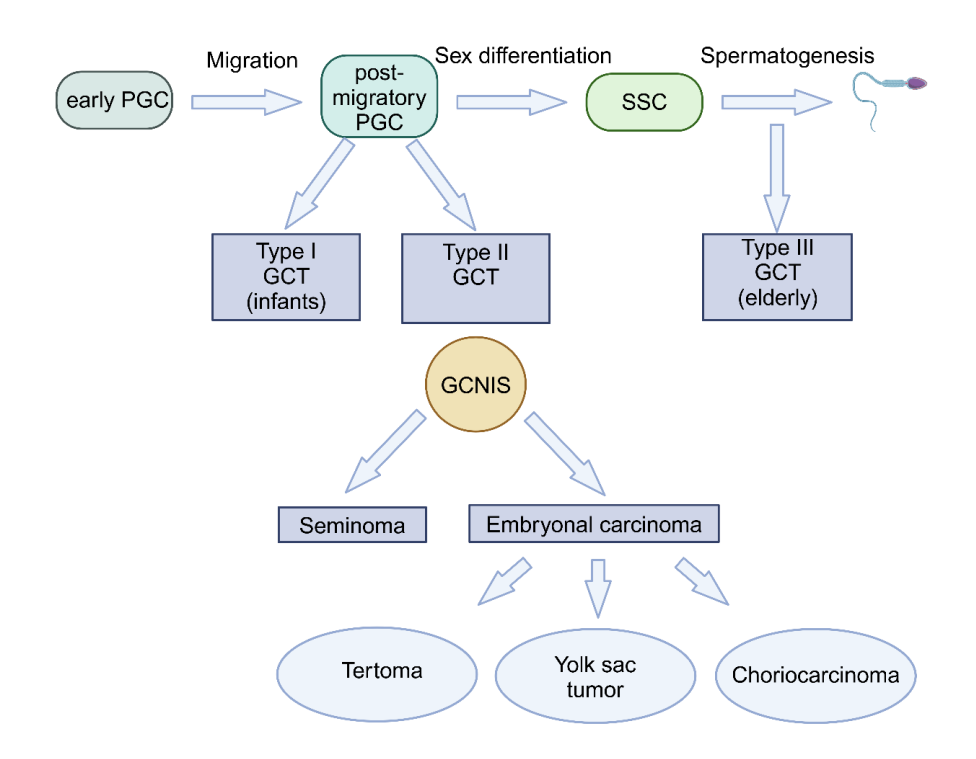


Figure 4: Development of GCTs. Type I GCTs derive directly from post-migratory PGCs. In contrast, type II GCTs arise from a precursor lesion called germ cell neoplasia in situ (GCNIS). They subgroup in seminoma and non-seminoma (embryonal carcinomas) which comprise teratoma, yolk sac tumor and choriocarcinoma. Type III GCTs arise in spermatogenesis. PGC – primordial germ cell; SSC – spermatogonial stem cell; GCT – germ cell tumor; GCNIS – germ cell neoplasia in situ. Modified from ⁷. Created in https://BioRender.com.

1.2.1 Type I germ cell tumors

Type I GCTs are yolk sac tumors and teratomas of neonates and children up to 6 years ¹⁷. They occur along the midline of the body corresponding to the PGC migration route. The origin of these tumors are PGCs or gonocytes (Figure 4) ¹². Downregulation of PGC-specific genes like TFAP2C, PRDM1 and PRDM14 is initiated but they fail to also downregulate pluripotency markers ⁷. Type I teratomas usually have no chromosomal abnormalities while type I yolk sac tumors show aneuploidy with chromosomal changes ²⁰.

1.2.2 Type II germ cell tumors

Type II GCTs occur mainly in the testis where they are referred to as testicular germ cell tumors (TGCT). Only in a few cases (5 %) tumors localize extragonadal along the body midline. TGCTs account for 60 % of all malignant tumors in young men (20-40 years). The gain of chromosome 12p was found in 80 % of all TGCTs indicating

importance for development of TGCTs ²⁰. They arise from a precursor lesion called germ cell neoplasia in situ (GCNIS) ⁷. Arrested PGCs with (epi-) genetic aberrations fail to downregulate pluripotency and germ cell markers and give rise to this lesions ^{7,21}. GCNIS stay dormant until puberty accumulating chromosomal abnormalities which activate malignant growth developing into seminoma or embryonal carcinoma (Figure 4) ²¹. Seminomas display restricted abilities of differentiation and therefore are considered to be the default pathway of GCNIS development. They share gene expression patterns of PGC maintaining pluripotency markers including OCT4, NANOG and LIN28 ⁷. Irie et al. found that seminoma derived TCam-2 cells aligned with human PGC- like cells (hPGCLC) and gonadal hPGCs in PCA indicate the progress of the early germline from pre-induced cells over hPGCLCs and TCam-2 cells to gonadal hPGCs (Figure 5). All three share expression of early germ cell markers (BLIMP1, TFAP2C, DND1 and KIT) ²².

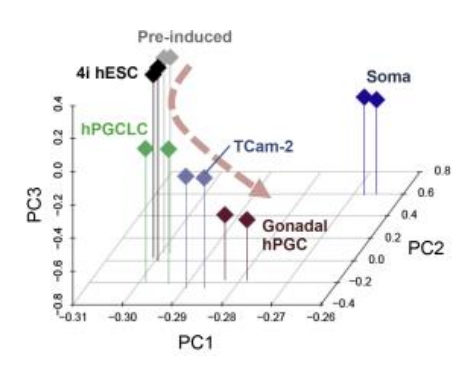


Figure 5: Human PGC-like cells resemble seminoma (TCam-2) cells. Principle component analysis (PCA) of RNA-seq data. Arrowline indicates possible progression of the germline. hESC – human embryonic stem cell; hPGCLC – human primordial germ cell-like cell; hPGC – human primordial germ cell. Modified from ²².

Of note, seminoma cells (TCam-2) also express SOX17 which is the key specifier for PGC fate. SOX17 regulates BLIMP1, PRDM14 and TFAP2C which are necessary for depletion of somatic genes and therefore inducing latent pluripotency ²².

Embryonal carcinomas are totipotent and able to differentiate into all three germ layers (meso-, ecto- and endoderm) as well as extraembryonic tissue and therefore differentiating into teratoma, yolk sac tumor or choriocarcinoma (Figure 4) ⁷. Non-seminomas share the expression of OCT4, NANOG and DPPA3 with seminomas but in addition also express NODAL, DNMT33B, DNMT3L and CD30 ²³. Of note, in

embryonal carcinomas SOX2 is upregulated ¹². Therefore, SOX2 and SOX17 are used as diagnostic biomarkers for distinguishing TGCT subtypes ²⁴.

1.2.3 Type III germ cell tumors

Type III GCTs are spermatocytic tumors of older males between 40 and 55 years. The origin of these tumors are probably germ cells capable of spermatogonia maturation (Figure 4) ⁷. Mutations in FGF3 and HRAS are predisposing for type III GCTs ¹². Chromosomal abnormalities are rare, the repetitive change are losses or gains of whole chromosomes ¹².

1.3 Treatment of TGCTs

TGCTs are diagnosed as an unilateral palpable mass by the patient or incidentally via scrotal ultrasonography. Patients may also report scrotal pain, flank or back pain and in very few cases gynaecomastia ^{25,26}. To support the diagnosis serum tumor marker levels including α-Fetoprotein (AFP), beta subunit of human chorionic gonadotropin (β-hCG) and lactate dehydrogenase (LDH) are determined. These markers correlate with germ cell cancer histology ²⁵. Radical orchiectomy allows for histopathologic reports on tumor size, histology and lymphovascular invasion ²⁶. Staging is performed based on the International Germ Cell Cancer Collaborative Group (IGCCCG). Seminomas and non-seminomas can be distinguished in clinical stages I-III.

1.3.1 Non-Seminomas

Stage I non-seminomas are diagnosed in 70 % of patients at this stage and are grouped into low-risk or high risk according to absence or presence of vascular invasion and display high survival rates of 98-100 % ^{26,27}. For low-risk patients active surveillance is the recommended procedure and as an alternative one cycle of bleomycin, etoposide and platinum (BEP) chemotherapy is used. High risk patients are usually treated with one adjuvant BEP cycle but surveillance can also be an alternative ²⁵. Non-seminoma stage II tumors involve also the retroperitoneal lymph nodes and are distinguished according to involved lymph node size in IIA (nodes <2 cm), IIB (nodes 2-5 cm) and IIC (nodes >5 cm) ²⁶. For stage IIA with negative tumor markers close follow up of the lymph node is recommended with primary retroperitoneal lymph

node dissection (p-RPLND) when volume of the lymph node increases. Alternatively, tumors are treated with 3 cycles of BEP chemotherapy or 4 cycles of platinum and etoposide (PE) chemotherapy. In case of stage IIA with positive tumor marker as well as stage IIC chemotherapy is recommended ²⁶. For stage IIB and III tumors treatment is based on good, intermediate or poor prognosis. Stage III tumors are defined as tumors that involve lymph nodes or any other organs ^{25,26}. In case of good prognosis tumors are treated by 3 cycles of BEP, 4 cycles of PE or RPLND. For intermediate prognosis 4 cycles of BEP or 4 cycles of etoposide, ifosfamide and platinum (VIP) chemotherapy are recommended. In patients with poor prognosis 4 cycles of either BEP or VIP including dose intensification are used ²⁵.

1.3.2 Seminomas

About 80 % of patients are diagnosed at stage I and the 5-year relapse rates after orchiectomy account 15-20 % ²⁶. After orchiectomy there are different treatment options based on low and high risk. Stage I tumors with low risk undergo active surveillance while high risk tumors are treated by 1-2 cycles of platinum-based chemotherapy at a dose in the area under the curve (AUC) of 7 or also surveillance ²⁵. For Stage IIA tumors radiotherapy or chemotherapy with either 3 BEP cycles or 4 PE cycles are recommended ²⁶. Stage IIB-III tumors are treated by 3-4 cycles of BEP chemotherapy ²⁵.

1.3.3 Cisplatin

Cisplatin is the first generation of platinum-based drugs and was first synthesized in 1844 while the chemical structure was discovered in 1893. In 1965 Dr. Rosenberg unrevealed the ability of cell division inhibition and cisplatin was FDA approved for cancer treatment in 1978 ^{28–32}. In patients with testis cancer the survival rate was significantly increased by the establishment of cisplatin-based chemotherapy. Before treatment with cisplatin the 5-year survival rate was 72 % while the use of cisplatin increased the survival rate to 95 % ³³. Cisplatin is a metallic coordination molecule with square planar geometry. It is composed of a platinum ion enclosed by two amine (NH₃) ligands and two chloride (CI) ligands (Figure 6). At room temperature cisplatin is a white or yellow crystalline powder and is soluble in *N,N*-dimethylformamide (DMF) ²⁹.

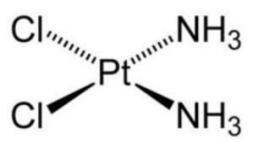


Figure 6: Chemical structure of cisplatin. Pt – platinum; CI – chloride; NH_3 – amine. Modified from 29 .

Cisplatin enters the tumor cells through the copper transporter 1 (CTR1). Afterwards, activation is initiated by significantly lower intracellular chloride ion concentration which leads to the replacement of the chloride ligands by water molecules. Following chemical reactions in the cytoplasm enable cisplatin to bind to DNA and therefore changing the DNA structure leading to DNA damage ³⁰. Oxidative stress is common in cisplatin induced cytotoxic effects. It is defined by formation of reactive oxygen species (ROS) as well as reduced mitochondrial glutathione (GSH) resulting in DNA damage ^{28,29}. Ataxia telangiectasia mutated (ATM) leads to phosphorylation and therefore the activation of p53 followed by GADD45, p21 and MDM2 mediated cell cycle arrest ²⁸. In addition, p53 results in apoptosis by several mechanisms including activation of Bax, PUMA and Casp6 as well as degradation of FLIP or inhibition of the antiapoptotic role of Bcl-xL (Figure 7) ²⁹.

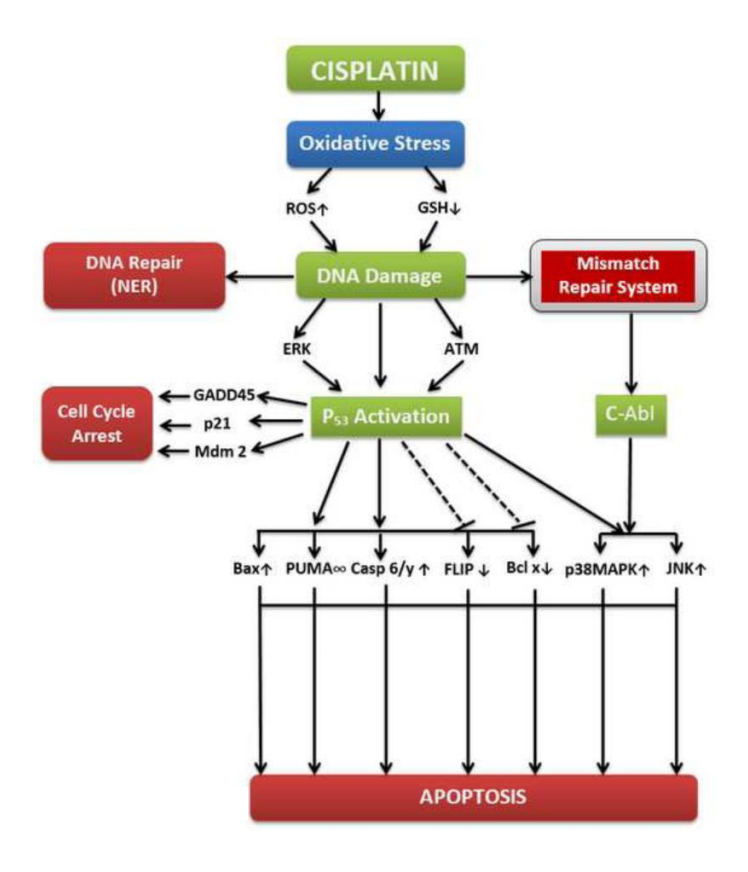


Figure 7: Mode of action of cisplatin in cancer treatment. Modified from ²⁹.

Sensitivity of TGCTs to cisplatin is based on impaired DNA repair induced by DNA damage as well as increased apoptotic response ³⁴. Cisplatin-induced DNA damage is usually repaired by the nucleotide excision pathway (NER) ³⁵. In TGCTs proteins involved in NER including ERCC1, XPA and XPF show low expression levels and therefore sensitizing TGCT cells for cisplatin therapy ³⁴. Furthermore, cisplatin induces increased expression of the FAS receptor which is a target of p53 and results in the activation of the intrinsic apoptosis pathway executed by the interaction of FAS and its ligand FASL ³⁶. Of note, DNA methylation correlates with cisplatin-sensitivity. While seminomas are hypomethylated, embryonal carcinomas show an intermediate methylation profile and the more differentiated tumors including yolk sac tumors, choriocarcinomas and teratomas display hypermethylation. In line, seminomas as well as embryonal carcinomas show high sensitivity towards cisplatin while on the other hand, highly differentiated teratomas are insensitive to cisplatin ³⁷.

1.4 Cisplatin resistance

While survival rates improve there are still 15-20 % of patients resistant to the treatment and 50 % of patients develop intrinsic resistance or establish multidrug resistance after treatment with cisplatin ^{38,39}. Cisplatin resistance is multifactorial and is divided in pre, on-, post- and off target resistance (Figure 8, Figure 9) ⁴⁰. Pre-target mechanisms play a role prior to binding of cisplatin to the DNA while on-target mechanisms are directly involved in cisplatin-induced DNA damage. Pathways activated by cisplatin-induced DNA damage are grouped in post-target mechanisms. Off-target mechanisms comprise pathways not directly related to cisplatin-induced DNA lesions ⁴¹.

1.4.1 Pre-target

Pre-target mechanisms are based on reduction of cisplatin influx, increase of cisplatin efflux as well as cisplatin inactivation (Figure 8) ³⁹. Cisplatin uptake into the cell is mediated by passive diffusion or facilitated transport by the copper transporter CTR1 or organic cation transporters (OCT) while copper efflux transporters ATP7A and ATP7B as well as multidrug resistance proteins (MRP) enable the export of cisplatin ^{40,42}. Application of copper (substrate of CTR1) resulted in less cytotoxic effects of cisplatin, whereas copper chelators lead to accumulation of cisplatin and escalate cytotoxicity ^{43,44}. In TGCTs cisplatin resistance is not related to drug transporters ³⁸. Detoxification is performed by cytoplasmic scavengers like metallothioneins (MT) or glutathione (GSH) binding to cisplatin and therefore reducing the amount of active cisplatin ^{45,46}. Low levels of scavengers were found in TGCTs suggesting no significant contribution of pre-target mechanisms to cisplatin resistance in TGCTs ^{38,47}.

1.4.2 On-target

Cisplatin induces DNA damage which usually results in apoptotic signals ⁴⁰. However, cisplatin-resistant cells are able to repair adducts by activation of DNA repair mechanisms or cells can tolerate unrepaired DNA lesions ^{39,40}. Nucleotide excision repair (NER) is the most common system to overcome cisplatin-induced DNA damage (Figure 8) ⁴⁸. The bonds formed between cisplatin and DNA are removed by excision repair cross-complementing 1 (ERCC1) and Xeroderma pigmentosum complementation group F (XPF) proteins ³⁹. ERCC1 expression is negatively

correlated with sensitivity to cisplatin in different cancer types including bladder and ovarian cancer ^{49,50}. In TGCTs high-mobility group box protein 1 (HMGB1) which binds to cisplatin DNA crosslinks and interferes with NER is highly expressed leading to cisplatin resistance ³⁸. Tolerance of cisplatin-induced DNA damage is related to impaired mismatch base repair (MMR) ³⁹. Cisplatin-induced DNA lesions are detected but not repaired by MMR-related proteins including MSH2 and MLH1 ^{40,51,52}. In TGCT patients impaired MMR is correlated with treatment failure and relapse. Decreased expression of MHL2 in refractory TGCTs indicate defective MMR as a mechanism of cisplatin resistance in TGCTs ³⁸. The homologous recombination machinery (HHR) usually repairs cisplatin-induced DNA double-strand breaks ³⁹. Two components of the HHR are BRCA1 and BRCA2 which are both mutated in ovarian and breast cancer ⁵³. HHR deficiency is correlated with increased sensitivity to cisplatin ^{54–56}. Poly (ADP-ribose) polymerase (PARP) plays a role in repair of single-strand breaks induced by cisplatin via base excision repair (BER) ³⁸. In TGCTs overexpression of PARP was detected suggesting to be involved in a possible on-target mechanism in TGCTs ^{57,58}.

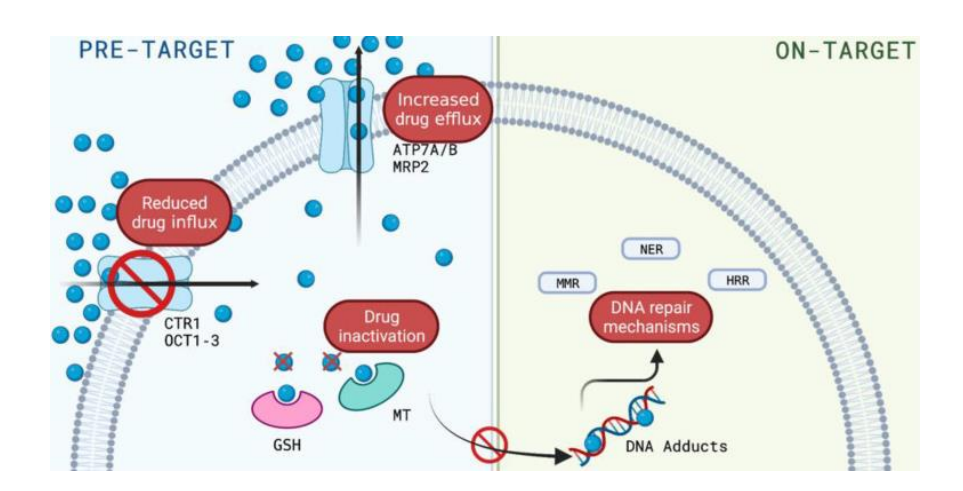


Figure 8: Mechanisms of cisplatin resistance. Mechanisms are subgrouped into pre-, on-, post- and off-target. Pre-target mechanisms comprise reduced drug influx, increased drug efflux as well as drug inactivation. On-target mechanisms are based on DNA repair mechanisms. MMR – mismatch base repair; NER – nucleotide excision repair; HRR – homologous recombination repair. Modified from ³⁹.

1.4.3 Post-target

The inactivation of the TP53 gene encoding for the p53 protein is the predominant post-target mechanism (Figure 9) ⁵⁹. Depletion of p53 results in reduction of apoptosis and induction of resistance in 50 % of cancers ⁶⁰. Of note, TGCTs are among few cancers showing rarely inactivation of TP53 ⁶¹. In fact, hyperactivation of p53 leads to increased sensitivity to cisplatin in TGCTs ^{62–64}. High abundance of MDM2 interacting with p53 is related to cisplatin resistance in TGCTs ³⁶. Upregulation of platelet-derived growth factor receptor b (PDGFRb) and its ligand PDGF-b in TGCT results in activation of PDGFR/ PI3K/ AKT pathway and subsequent phosphorylation of p21 and activation of MDM2. Thus, cells are prevented from apoptosis and induce G1-phase cell cycle arrest ^{65,66}. Another mechanism is the inactivation of caspases like caspase 3, 8 and 9 which are important in apoptosis. Caspase inactivation is related to cisplatin resistance in different types of cancer ^{39,67}.

1.4.4 Off-target

A general pathway in response to stress is autophagy or heat-shock response which are classified as off-target mechanism (Figure 9) ^{40,68,69}. In ovarian and non small cell lung cancer upregulation of proteins of the autophagy pathway is positively correlated with cisplatin resistance while inhibition of autophagy resensitized cells to cisplatin ^{70,71}.

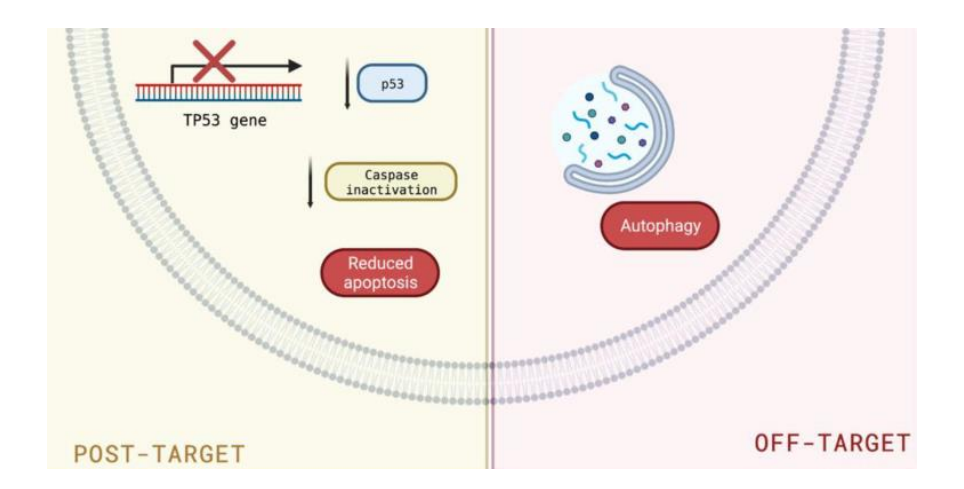


Figure 9: Mechanisms of cisplatin resistance. Mechanisms are subgrouped into pre-, on-, post- and off-target. Post-target mechanisms result in reduced apoptosis. Autophagy is categorized as off-target mechanisms. Modified from ³⁹.

All these pre-, on-, post- and off-target mechanisms contribute to cisplatin resistance emphasizing the necessity of investigating alternative treatments.

1.5 Alternative treatment options

Different preclinical and clinical trials studied various alternative treatment options for refractory GCTs including targeted therapy, immunotherapy epigenetic drugs and other therapeutic agents ⁷².

1.5.1 Targeted therapy

One possibility of targeted therapy are tyrosine kinase inhibitors (TKI) inhibiting receptor tyrosine kinases for example vascular endothelial growth factor receptor (VEGFR) and platelet-derived growth factor (PDGF) which are overexpressed in GCTs ^{66,72}. Sunitinib, a multikinase inhibitor, re-sensitized cisplatin-resistant GCT cell lines to cisplatin and in a phase II clinical trial sunitinib led to a response rate of 13 % ^{73,74}.

Another target is the mammalian target of rapamycin (mTOR) which upon overactivation is associated with enhanced cell growth, proliferation and survival. The mTOR inhibitor everolimus was tested in phase II clinical trials but showed only limited efficacy ^{75–77}.

Targeted therapy also includes the inhibition of PARP. High PARP expression is correlated with lower overall survival in GCTs ⁵⁷. Olaparib inhibiting PARP was tested in phase II clinical trials with marginal efficacy ⁷⁸.

Possible targets are cyclin-dependent kinases (CDK). Inhibitors of cell cycle-associated CDKs (CDK1/2/4/6) like palbicicilib and ribocicilib were investigated in phase II clinical studies ^{79,80}. Transcriptional CDK (CDK7/8/9/12/13) inhibitors were studied in vitro and showed cytotoxic effects in TGCT cell lines ⁸¹.

1.5.2 Immunotherapy

The Programmed cell death 1 (PD-1)/ Programmed cell death ligand 1 (PD-L1) interaction is the main target of immune checkpoint inhibitors. PD-L1 is highly expressed in GCTs compared to normal testis tissue ^{82,83}. Unfortunately, phase II

clinical trials of pembrolizumab (PD-1 inhibitor) showed no objective response ^{84,85}. Only one refractory GCT patient responded rapidly to pembrolizumab ⁸⁶. The PD-L1 inhibitor avelumab also showed no efficacy in patients with multiple relapsed non-seminomas ⁸⁷.

1.5.3 Other therapeutic agents

Aldehyde dehydrogenase (ALDH) showed high expression in GCTs compared to normal testis tissue. Inhibition of ALDH by disulfiramin in combination with cisplatin led to synergistic effects in cisplatin-resistant embryonal carcinoma cell lines as well as inhibition of growth in resistant xenografts ⁸⁸. A phase II clinical trial is still ongoing ⁷².

Targeting the WNT/ β -catenin signaling pathway which is deregulated in GCT by the inhibitor PRI-724 led to apoptosis in cisplatin-resistant GCTs ⁸⁹. Unfortunately, no clinical trials are initiated ⁷².

Inhibition of the interaction of MDM2 and p53 by the small-molecule MDM2 inhibitor Nutlin-3 led to induction of apoptosis and in combination with cisplatin synergistic effects were observed ^{36,90}. Again, clinical studies are missing ⁷².

1.5.4 Epigenetic drugs

Since DNA hypermethylation as well as histone deacetylation are known to be involved in cisplatin resistance targeting DNA methyltransferases (DNMT) and histone deacetylases (HDAC) was investigated ⁹¹. A hypomethylating agent guadecitabine led to induction of complete regression of cisplatin-resistant embryonal carcinoma xenografts ⁹². A phase I clinical study of combination of guadecitabine and cisplatin also showed complete response in two patients ⁹³.

HDAC inhibitors indicated preclinical efficacy in vitro and in vivo ⁷². Romidepsin led to decreased viability in TGCT cell lines as well as reduced tumor growth in xenografted mice treated with romdepsin ⁹⁴.

BET protein inhibitors like the bromodomain inhibitor JQ1 inhibiting BRD4 induced apoptosis as well as cell cycle arrest in TGCT cell lines and reduced tumor growth in xenografted mice ⁹⁵.

Taken together, in contrast to promising preclinical studies targeted therapy including TKI, mTOR and PARP inhibitors as well as immune checkpoint inhibitors led to questionable results in clinical trials. Only inhibitors interfering with the epigenetic landscape showed the most promising results. Therefore, investigation of alternative treatment options like epigenetic drugs is very important.

1.6 Bromodomain-containing proteins

Bromodomains (BRD) are able to bind specifically to ϵ -N-acetylation of lysine residues (K_{ac}) which are the most frequent posttranslational modification (PTM) in proteins ^{96,97}. BRDs got the name from the Drosophila gene brahma where the bromodomain was first reported by Tamkun et al. in 1992 ^{98,99}. They are evolutionary conserved and comprise ~110 amino acids. All BRDs share a fold including a left-handed bundle of four α helices (α_Z , α_A , α_B , α_C) which are linked by two interhelical loops (ZA and BC loops) forming a hydrophobic binding pocket including the Kac binding site and therefore influencing the binding specificity (Figure 10) ^{97,100,101}.

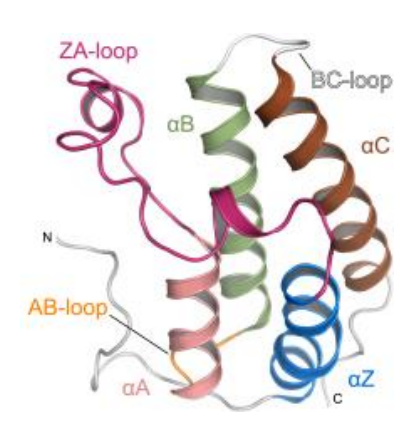


Figure 10: Structure of the bromodomain of human BRD4. Modified from 97.

Proteins containing BRDs have various functions like chromatin remodeling, recruitment of transcription factors and histone modifications ¹⁰². In humans 61 bromodomains are known in 46 different bromodomain-containing proteins (BCP). They are subgrouped in bromodomain and extra-terminal (BET) and non-BET families ¹⁰³. BET proteins comprise BRD2, BRD3, BRD4 and testis-specific BRDT while non-BET proteins comprise histone acetyltransferases (HAT), SWI/SNF complexes, AAA ATPase proteins, ISWI complexes and E3 SUMO/ubiquitin ligases ^{102,103}. Since BRDs

play important roles in chromatin-based gene transcription targeting BCPs by small molecules is a promising starting point to overcome therapy resistance and to discover alternative treatment options for TGCTs. The inhibition of BET proteins has already been shown to be effective. Therefore, we focused on BRD9. The effect of BRD9 inhibition is not studied yet in TGCTs but seems to be a possible target for an alternative treatment option.

1.6.1 BRD9

BRD9 comprises 597 amino acids and contains one bromodomain ¹⁰³. It belongs to the non-BET families and is classified as a group IIIa member. Group IIIa comprises chromatin remodeling factors like SMARCA2, SMARCA4, PBRM1, BRD7 and BRD9. They are subunits of the Switch/Sucrose Non-Fermentable (SWI/SNF) complex which remodels chromatin in an ATP-dependent manner. The SWI/SNF complex regulates DNA damage, gene transcription and cell growth as well as differentiation ¹⁰⁴. The ATPase component of the complex contains several functional domains including BRD which mediates histone binding ¹⁰². The SWI/SNF complexes are subgrouped into three classes: canonical ATPase BRG1/BRM-associated factor (BAF), polybromo-associated BAF (PBAF) and non-canonical BAF (ncBAF) complexes ¹⁰⁵. BRD7 is part of the PBAF complex while the smallest ncBAF complex comprises BRD9. The bromodomain and its K_{ac} binding ability mediate the assembly of the complex by propelling ATPase-driven movement along the chromatin ¹⁰². Therefore, BRD9 is an epigenetic reader activating gene expression by recruitment of transcriptions factors (Figure 11) ⁴¹.

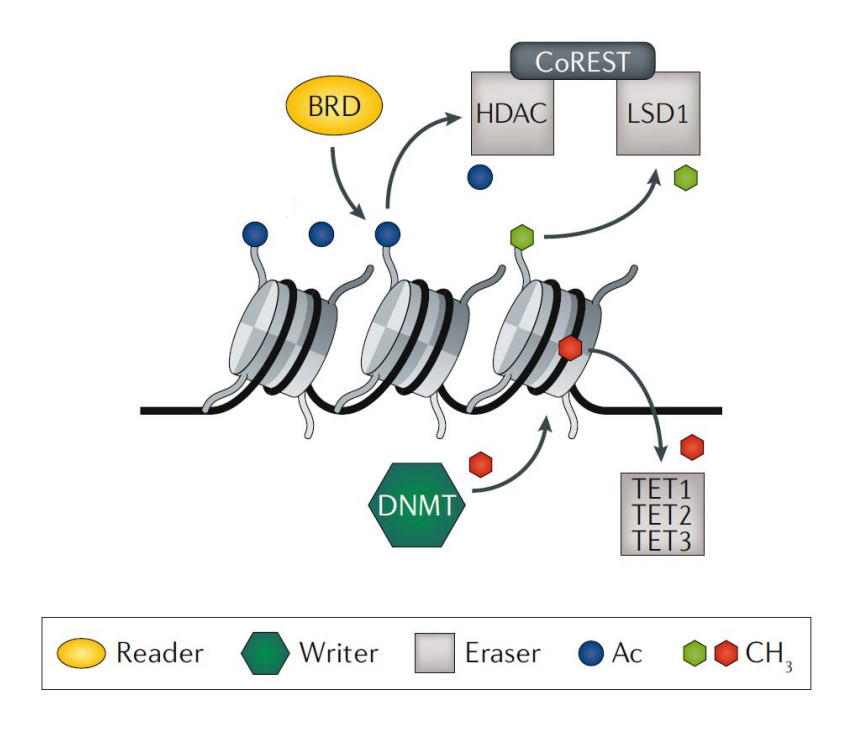


Figure 11: Epigenetic modifications in TGCTs. BRDs are epigenetic readers activating or repressing gene expression by recruitment of transcription factors. BRD – bromodomain proteins; HDAC – histone deacetylase; DNMT – DNA methyltransferase; Ac – acetyl group; CH₃ – methyl group. Modified from ⁴¹.

Furthermore, BRD9 is known to play an oncogenic role, promotes tumor progression and is deregulated in 23 malignancies ¹⁰⁶. For example, BRD9 is upregulated in acute myeloid leukemia (AML) cells and targeting BRD9 led to decreased proliferation of mouse and human AML cells ¹⁰⁷. In squamous cell lung cancer (SqCLC) inhibition of BRD9 by overexpression of miR-140-3p reduced tumorigenesis by downregulation of c-myc ¹⁰⁸. LP99 was the first BRD7/BRD9 inhibitor that revealed anti-inflammatory ability in human monocytic leukemia cells ¹⁰⁹. Two BRD9-specific inhibitors BI-7273 and BI-9564 were designed and showed both antiproliferative effects in AML cells while BI-9564 also showed decreased tumor burden in xenografted mice ¹¹⁰. I-BRD9 is the most selective and potent BRD9 inhibitor ¹⁰². Of note, BRD9 inhibition was not studied in TGCTs yet.

1.6.2 I-BRD9

I-BRD9 is a chemical probe that was described by Theodoulou et al. in 2016 (Figure 12 A). It is a K_{ac} mimetic binding to the bromodomain binding pocket of BRD9 (Figure

12 B) ¹¹¹. I-BRD9 was discovered by structure-based design and showed more than 700-fold selectivity over BET proteins and 200-fold higher over BRD7 ¹⁰³.

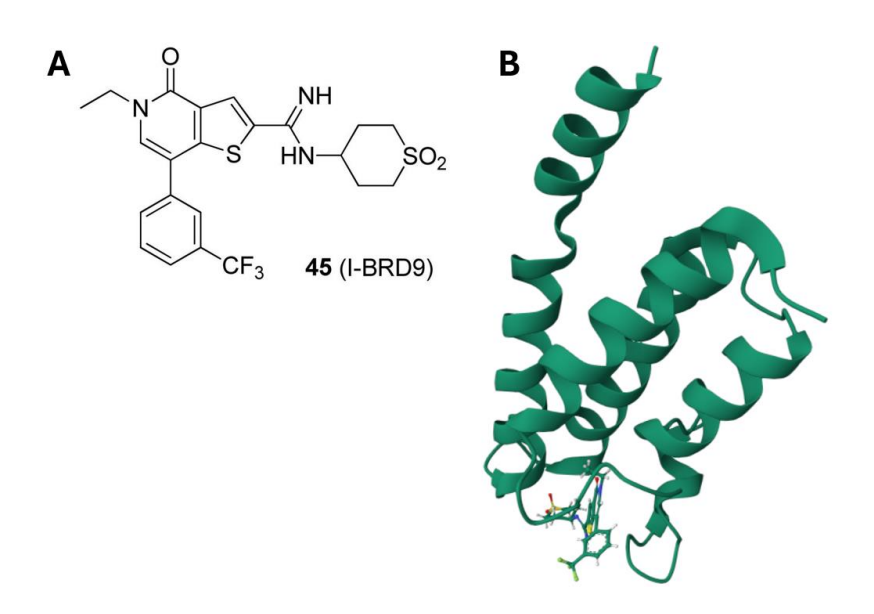


Figure 12: K_{ac} mimetic I-BRD9 binds to the bromodomain of BRD9. (A) Structure of I-BRD9 111 . (B) Crystal structure of I-BRD9 binding to BRD9. Image from the RCSB PDB (RCSB.org) of PDB ID 6V1B 112 . Modified from 111,112 .

The thienopyridine I-BRD9 led to downregulation of immunology and cancer-related genes including CLEC1, FES, SAMSN1 and DUSP6 ^{113–116}. In AML cells I-BRD9 led to reduction of cell growth as well as induction of apoptosis ¹¹⁷. I-BRD9 resulted in decreased cell proliferation in gallbladder cancer (GBC) as well as reduction of tumor growth in a GBC mouse tumor model without significant side-effects ¹¹⁸. In colon adenocarcinoma (COAD) cells application of I-BRD9 suppressed cell growth as well as reduced tumor growth in xenografted mice ¹¹⁹. Treatment of rhabdoid tumors with I-BRD9 resulted in reduction of cell proliferation, induction of apoptosis as well as G1-phase cell cycle arrest ¹²⁰. These data suggest I-BRD9 as an effective compound in different tumors. Of note, I-BRD9 was not studied in TGCTs so far. Therefore, investigation of the effect of I-BRD9 in TGCTs is an interesting approach to elucidate alternative treatment options.

1.6.3 TGCT cell lines

For in vitro studies of TGCTs there are several cell lines described. Embryonal carcinoma cell lines 2102 EP, NCCIT and NT2/D1 were derived from mixed non-seminoma patients ^{121–123}. NCCIT and NT2/D1 cells are pluripotent while 2102 EP cells display a nullipotent character ^{123–125}. Cisplatin-resistant subclones 2102 EP-R, NCCIT-R and NT2/D1-R were established by cisplatin treatment with increasing sublethal concentrations ^{126,127}. JAR cell line resembles choriocarcinoma and was derived from a trophoblastic tumor of the placenta from the male fetus ¹²⁸. The cell line TCam-2 was established from a testicular seminoma ¹²⁹. As control cells FS1 and MPAF were used. Immortalized adult human sertoli cells (FS1) were derived from testis tissue of a Frasier syndrome patient ¹³⁰. MPAF cells are human adult fibroblasts.

1.7 Aim of the project

In this project the aim was to elucidate an alternative treatment option for testicular germ cell tumors to overcome cisplatin therapy resistance. Therefore, the BRD9 inhibitor I-BRD9 which has already been shown to be effective in different cancer types but was not yet tested in TGCTs was studied. First, expression of the target BRD9 was analyzed on RNA level by meta-analysis of microarray data in TGCT tissues as well as cell lines and for protein level Western Blot as well as TMA were performed. In different TGCT cell lines cytotoxicity of the inhibitor was measured by viability assays. The effect of application of I-BRD9 on apoptosis as well as cell cycle distribution were assessed via FACS. To reveal changes on transcriptome level induced by BRD9 inhibition 3'mRNA sequencing was performed.

The findings will elucidate the effect of the BRD9 inhibitor I-BRD9 in TGCTs and the possibility to be used as alternative treatment option with reduced side effects and to overcome therapy resistance.

2 MATERIALS

2.1 Cell lines

| Cell line | Description | Standard culture | Source |
|-----------|-----------------|-------------------------|------------------------|
| | | medium | |
| 2102 EP | Embryonal | DMEM, 10% FBS, 1% | Prof. Dr. L. Looijenga |
| | carcinoma | penicillin/streptomycin | (Princess Máxima |
| | | (10,000 U/ml), 1% L- | Center for Pediatric |
| | | glutamine (200 mM) | Oncology, Utrecht, |
| | | | Netherlands) |
| 2102 EP-R | Cisplatin- | DMEM, 10% FBS, 1% | PD Dr. F. Honecker |
| | resistant | penicillin/streptomycin | (ZeTup Silberturm, St. |
| | subline derived | (10,000 U/ml), 1% L- | Gallen, Switzerland) |
| | from 2102EP | glutamine (200 mM) | |
| NCCIT | Embryonal | DMEM, 10% FBS, 1% | Prof. Dr. L. Looijenga |
| | carcinoma | penicillin/streptomycin | (Princess Máxima |
| | | (10,000 U/ml), 1% L- | Center for Pediatric |
| | | glutamine (200 mM) | Oncology, Utrecht, |
| | | | Netherlands) |
| NCCIT-R | Cisplatin- | DMEM, 10% FBS, 1% | PD Dr. F. Honecker |
| | resistant | penicillin/streptomycin | (ZeTup Silberturm, St. |
| | subline derived | (10,000 U/ml), 1% L- | Gallen, Switzerland) |
| | from NCCIT | glutamine (200 mM) | |
| NT2/D1 | Embryonal | DMEM, 10% FBS, 1% | Prof. Dr. L. Looijenga |
| | carcinoma | penicillin/streptomycin | (Princess Máxima |
| | | (10,000 U/ml), 1% L- | Center for Pediatric |
| | | glutamine (200 mM) | Oncology, Utrecht, |
| | | | Netherlands) |
| NT2/D1-R | Cisplatin- | DMEM, 10% FBS, 1% | PD Dr. F. Honecker |
| | resistant | penicillin/streptomycin | (ZeTup Silberturm, St. |
| | subline derived | (10,000 U/ml), 1% L- | Gallen, Switzerland) |
| | from NT2/D1 | glutamine (200 mM) | |
| | | | |

| Cell line | Description | Standard culture | Source |
|-----------|-----------------|-------------------------|------------------------|
| | | medium | |
| TCam-2 | Seminoma | RPMI, 10% FBS, 1% | Prof. Dr. L. Looijenga |
| | | penicillin/streptomycin | (Princess Máxima |
| | | (10,000 U/ml), 1% L- | Center for Pediatric |
| | | glutamine (200 mM) | Oncology, Utrecht, |
| | | | Netherlands) |
| JAR | Choriocarcinoma | DMEM, 10% FBS, 1% | ATCC (Manassas, |
| | | penicillin/streptomycin | VA, USA) |
| | | (10,000 U/ml), 1% L- | |
| | | glutamine (200 mM) | |
| FS1 | Sertoli cells | DMEM, 20% FBS, 1% | Dr. Valerie |
| | | penicillin/streptomycin | Schumacher |
| | | (10,000 U/ml), 1% L- | (Nephrology |
| | | glutamine (200 mM) | Research Center, |
| | | | Boston, USA) |
| MPAF | Fibroblasts | DMEM, 10% FBS, 1% | PD Dr. M. Peitz |
| | | penicillin/streptomycin | (Institute of |
| | | (10,000 U/ml), 1% L- | Reconstructive |
| | | glutamine (200 mM), 1% | Neurobiology, Bonn |
| | | non-essential amino | University, Bonn, |
| | | acids (100x) | Germany) |

2.2 Cell culture media and reagents

| Medium/ reagent | Manufacturer |
|------------------------------------|--|
| 0.05% Trypsin-EDTA | Thermo Fisher Scientific, Waltham, USA |
| Dimethyl sulfoxide (DMSO) | AppliChem, Darmstadt, Germany |
| Dulbecco's Modified Eagle's Medium | Thermo Fisher Scientific, Waltham, USA |
| (DMEM) high glucose | |
| Fetal bovine serum (FBS) | Merck, Darmstadt, Germany |
| L-Glutamine 200 mM | Thermo Fisher Scientific, Waltham, USA |
| Non-essential amino acids (NEAA) | Thermo Fisher Scientific, Waltham, USA |
| Penicillin/ streptomycin | Thermo Fisher Scientific, Waltham, USA |

| Medium/ reagent | Manufacturer |
|--|--|
| Phosphate buffered saline (PBS) | Thermo Fisher Scientific, Waltham, USA |
| Roswell Park Memorial Institute (RPMI) | Thermo Fisher Scientific, Waltham, USA |
| medium | |
| Sodium pyruvate | Merck, Darmstadt, Germany |

2.3 Consumables

| Consumable | Manufacturer |
|---|--------------------------------------|
| 384-well micro titer plate | 4titude, Wotton, UK |
| Cell Culture Dishes 55 cm ² | VWR, Darmstadt, Germany |
| Cell Culture Flasks, Filter Cap, | Greiner bio-one, Frickenhausen, |
| CELLSTAR® (T25, T75) | Germany |
| Cell Culture Multiwell Plates (6-, 12-, 24- | TPP, Trasadingen, Austria |
| , 96-well-plate) | |
| Cell scraper 25 cm | SARSTEDT, Nümbrecht, Germany |
| Cryogenic vials 2 ml, internal thread | Greiner bio-one, Frickenhausen, |
| | Germany |
| Eppendorf tubes (1.5 ml, 2 ml) | Eppendorf, Hamburg, Germany |
| Extra Thick Blot Filter Paper | BioRad Laboratories, Hercules, USA |
| FACS tubes | BD Biosciences, Heidelberg, Germany |
| Filter tips (10 µl, 100 µl, 1000 µl) | Nerbe Plus, Winsen/Luhe, Germany |
| Microplate, 96 well, PS, F-bottom, clear | Greiner bio-one, Frickenhausen, |
| | Germany |
| Microscope Cover Glasses 14 mm | Marienfeld GmbH, Lauda- |
| | Königshofen, Germany |
| Microscope slides | Marienfeld GmbH, Lauda- |
| | Königshofen, Germany |
| Parafilm M® | Pechiney Plastic Packaging, Menasha, |
| | USA |
| PCR® strip tubes | Axygen Scientific, Union City, USA |
| Petri dishes | Greiner bio-one, Frickenhausen, |
| | Germany |

| Consumable | Manufacturer |
|---|---------------------------------|
| Pipette tips (10 μl, 100 μl, 1000 μl) | Greiner bio-one, Frickenhausen, |
| | Germany |
| Polypropylene tubes CELLSTAR® (15 | Corning, Amsterdam, Netherlands |
| ml, 50 ml) | |
| Roti-PVDF membrane | Carl Roth, Karlsruhe, Germany |
| Stripettes Costar® (5 ml, 10 ml, 25 ml) | Greiner bio-one, Frickenhausen, |
| | Germany |

2.4 Chemicals and reagents

| Chemical/ Reagent | Manufacturer |
|---|--|
| 2-Mercaptoethanol | Merck, Darmstadt, Germany |
| 6-Diamidino-2-phenylindole | AppliChem, Darmstadt, Germany |
| dihydrochloride (DAPI) | |
| 10x reaction buffer + MgCl ₂ | Thermo Fisher Scientific, Waltham, USA |
| Albumin fraction V (BSA) | AppliChem, Darmstadt, Germany |
| Ammonium persulfate (APS) | Carl Roth, Karlsruhe, Germany |
| AnnexinV binding buffer | BioLegend, San Diego, USA |
| BRD9 inhibitor I-BRD9 (SML1534) | Sigma-Aldrich, St. Louis, USA |
| cOmplete™ ULTRA Tablets, Mini | Roche, Basel, Switzerland |
| Protease Inhibitor Cocktail | |
| Coomassie Brillant Blue G250 | Biomol, Hamburg, Germany |
| Ethylenediaminetetraacetic acid (EDTA) | Thermo Fisher Scientific, Waltham, USA |
| (50 mM) | |
| Ethanol | VWR, Darmstadt, Germany |
| Fluoroshield™ | Merck, Darmstadt, Germany |
| Glycine | Carl Roth, Karlsruhe, Germany |
| Hematoxylin | Merck, Darmstadt, Germany |
| Hoechst bisBenzimid H 33342 | Sigma-Aldrich, St. Louis, USA |
| Isopropanol | AppliChem, Darmstadt, Germany |
| Maxima SYBR Green/ROX qPCR | Thermo Fisher Scientific, Waltham, USA |
| Master Mix (2X) | |

| Chemical/ Reagent | Manufacturer |
|---|--|
| Methanol | VWR, Darmstadt, Germany |
| Oligo(dT) ₁₈ primer | Thermo Fisher Scientific, Waltham, USA |
| PageRuler™ Plus Prestained Protein | Thermo Fischer Scientific, Waltham, |
| Ladder, 10 bis 250 kDa | USA |
| PE-AnnexinV | BioLegend, San Diego, CA USA |
| PBS tablets | AppliChem, Darmstadt, Germany |
| Phenazine methosulfate (PMS) | Sigma-Aldrich, St. Louis, USA |
| RiboLock RNase Inhibitor (40 U/μl) | Thermo Fischer Scientific, Waltham, |
| | USA |
| Roti-Load 1, reducing, 4 x concentrated | Carl Roth, Karlsruhe, Germany |
| Rotiphorese ® Gel 30 (37,5:1) | Carl Roth, Karlsruhe, Germany |
| Rotiphorese ®10x SDS-PAGE | Carl Roth, Karlsruhe, Germany |
| Sodium dodecyl sulfate (SDS) | Merck, Darmstadt, Germany |
| Tetramethyl ethylenediamine (TEMED) | VWR, Darmstadt, Germany |
| Tris-HCl | Carl Roth, Karlsruhe, Germany |
| Triton X-100 | AppliChem, Darmstadt, Germany |
| Tween 20 | AppliChem, Darmstadt, Germany |
| UltraPure™ agarose | Invitrogen™, Thermo Fisher Scientific, |
| | Waltham, USA |
| Water, nuclease free | Thermo Fisher Scientific, Waltham, USA |
| XTT sodium salt | AppliChem, Darmstadt, Germany |

2.5 Buffers and solutions

| Buffer/ Solution | Recipe/ Supplier |
|--------------------------------|--|
| 5x RT buffer | Thermo Fisher Scientific, Waltham, USA |
| Ammonium persulfate (APS) 10% | 10 % (w/v) ammonium persulfate in H ₂ O |
| BSA-Blocking solution | 5 % (w/v) BSA in PBST |
| BSA-Antibody dilution solution | 1 % (w/v) BSA in PBS |
| PBST | 200 ml 10x PBS, 1 ml Tween20, ad 2l |
| | H ₂ O |
| RIPA buffer | Cell Signaling, Danvers, USA |

| Buffer/ Solution | Recipe/ Supplier |
|---------------------------------------|--|
| SDS Polyacrylamide gel | 12 % separation gel: 3.2 ml H ₂ O, 4 ml |
| | Rotiphorese® Gel 30 (37,5:1), 2.6 ml |
| | 1.5 M Tris-HCl (pH 8.8), 100 µl 10 % |
| | SDS, 100 µl 10 % APS, 4 µl TEMED |
| | 5 % stacking gel: 3.4 ml H ₂ O, 830 μl |
| | Rotiphorese® Gel 30 (37,5:1), 630 µl 1 |
| | M Tris-HCl (pH 6.8), 50 μl 10 % SDS, 50 |
| | μl 10 % APS, 5 μl TEMED |
| SDS running buffer | 100 ml ROTIPHORESE® 10x SDS- |
| | PAGE, ad 1I H₂O |
| Tris-acetate-EDTA-buffer (TAE) (50 x) | 2 M Tris base, 50 mM EDTA, 1 M acetic |
| | acid |
| Western Blot transfer buffer (10x) | 20 mM Tris, 192 mM Glycine, 0.1% |
| | (w/v) SDS, 20% (v/v) Methanol |
| Western Blot transfer buffer (1x) | 200 ml Methanol, 100 ml Western Blot |
| | transfer buffer (10X), ad 1 I H ₂ O |

2.6 Kits

| Kit | Manufacturer |
|---|------------------------------|
| Pierce™ BCA protein assay kit | Thermo Fisher, Waltham, USA |
| RNA 6000 Nano Kit | Agilent Technologies, Santa |
| | Clara, USA |
| RNeasy Mini Kit | Qiagen, Hilden, Germany |
| SuperSignal™ West Femto Maximum Sensitivity | Thermo Fisher, Waltham, USA |
| Substrate | |
| DyLight™ 594 Antibody Kit, R.T.U. (DI-2794) | Vector Laboratories, Newark, |
| | CA, USA |
| VectaFluor™ Horse Anti-Rabbit IgG, DyLight™ | Vector Laboratories, Newark, |
| 594 Antibody Kit, R.T.U. (DI-1794-15) | CA, USA |
| WESTAR NOVA 2.0 Western Blot Substrate | Cyanagen, Bologna, Italy |

2.7 Enzymes

| Enzyme | Manufacturer |
|--------------------------------------|--|
| DNasel | Thermo Fisher Scientific, Waltham, USA |
| Maxima H Minus Reverse Transkriptase | Thermo Fisher Scientific, Waltham, USA |
| (200 U/µI) | |
| RNase A | AppliChem, Darmstadt, Germany |

2.8 Equipment

| Equipment | Manufacturer |
|--------------------------------------|--|
| 2100 Bioanalyzer Instrument | Agilent Technologies, Santa Clara, USA |
| Advanced Digital Shaker | VWR, Darmstadt, Germany |
| Agarose gel chamber | Peqlab, Erlangen, Germany |
| Autostainer BenchMark Ultra | Roche, Basel, Switzerland |
| Balance BP211S | Sartorius, Göttingen, Germany |
| Balance PT 120 | Sartorius, Göttingen, Germany |
| BD FACSCanto II Flow Cytometer | BD Biosciences, New Jersey, USA |
| Cell culture hood BSB 6A | Gelaire, Sydney, Australia |
| Cell culture hood Safety cabinet | Kendro, Langenselbold, Germany |
| HERAsafe® | |
| Centrifuge 5417R | Eppendorf, Hamburg, Germany |
| Centrifuge Heraeus™ Megafuge™ 1.0 | Thermo Fisher Scientific, Waltham, USA |
| Centrifuge Heraeus™ Multifuge™ 3 S-R | Thermo Fisher Scientific, Waltham, USA |
| ChemiDoc MP Imaging System | BioRad Laboratories, Hercules, USA |
| Electrophoresis Power Supply Consort | Peqlab, Erlangen, Germany |
| EV243 | |
| Gel Documentation System GEL iX20 | Intas Science Imaging Instruments |
| Imager | GmbH,Göttingen, Germany |
| HiSeq 2500 V4 | Illumina, San Diego, USA |
| Incubator Heracell 240i | Thermo Fisher Scientific, Waltham, USA |
| Incubator UM200 | Memmert, Schwabach, Germany |
| iMark™ Microplate Absorbance Reader | BioRad Laboratories, Hercules, USA |
| Magnetic stirrer MR 3001 | Heidolph, Schwabach, Germany |

| Equipment | Manufacturer |
|-------------------------------------|--|
| Mini-PROTEAN® Tetra Cell Casting | BioRad Laboratories, Hercules, USA |
| Module | |
| Mini-PROTEAN® Tetra Vertical | BioRad Laboratories, Hercules, USA |
| Electrophoresis Cell | |
| Microscope Labovert FS | Leica Microsystems, Wetzlar, Germany |
| Microscope Axiovert 40C | Zeiss, Jena, Germany |
| Multichanel pipette | Eppendorf, Hamburg, Germany |
| Neubauer improved counting chamber | Brand, Wertheim, Germany |
| pH-Meter | Schott Instruments, Mainz, Germany |
| Pipette controller Accu-Jet® Pro | Brand, Wertheim, Germany |
| Pipettes (10, 20, 100, 1000 µl) | Eppendorf, Hamburg, Germany |
| Spectrophotometer Nano Drop 1000 | Thermo Fisher Scientific, Waltham, USA |
| Sonicator Bioruptor® | Diagenode, Seraing, Belgium |
| Thermal cycler 2720 | Applied Biosystems® by Thermo Fisher |
| | Scientific Inc., Carlsbad, USA |
| Thermomixer Compact | Eppendorf, Hamburg, Germany |
| Tilt/roller mixer RS-TR 05 | Phoenix Instrument, Garbsen, Germany |
| Trans-Blot® Turbo™ Transfer System | BioRad Laboratories, Hercules, USA |
| ViiA 7 Real-Time PCR System | Thermo Fisher Scientific, Waltham, USA |
| VisiScope CSU-W1 | Vistron Systems, Puchheim, |
| | Germany |
| Vortex Genie 2 | Scientific Industries Inc., New York, |
| | USA |
| Waterbath TW8 | Julabo, Seelbach, Germany |
| Western Blot Imaging System | Bio-Rad Laboratories, Hercules, USA |
| ChemiDoc MP | |
| Western Blot Transfer System Trans- | Bio-Rad Laboratories, Hercules, USA |
| Blot® Turbo™ | |

2.9 Antibodies

| Antibody | Manufacturer | Order | Species | Application | Dilution |
|----------|----------------------|----------|---------|-------------|----------|
| | | number | | | |
| SALL4 | Cell Marque, | 385M | Mouse | IHC | 1:50 |
| | Rocklin, USA | | | | |
| BRD9 | Abcam, Cambridge, | ab277488 | Rabbit | IHC | 1:500 |
| | UK | | | | |
| BRD9 | Cell Signaling, | 58906S | Rabbit | WB | 1:1000 |
| | Danvers, USA | | | | |
| β-actin | Merck, Darmstadt, | A5441 | Mouse | WB | 1:10000 |
| | Germany | | | | |
| Anti- | Agilent | P0448 | Goat | WB | 1:2000 |
| Rabbit | Technologies | | | | |
| HRP | (Dako), Santa Clara, | | | | |
| | USA | | | | |
| Anti- | Agilent | P0260 | Rabbit | WB | 1:2000 |
| Mouse | Technologies | | | | |
| HRP | (Dako), Santa Clara, | | | | |
| | USA | | | | |
| PRDM14 | Cell Signaling, | 83527 | Rabbit | IF | 1:100 |
| | Danvers, USA | | | | |
| NANOG | Abcam, Cambridge, | ab109250 | Rabbit | IF | 1:250 |
| | UK | | | | |

2.10 Oligonucleotides

| Gene | Forward primer (5'-3') | Reverse primer (5'-3') |
|--------|------------------------|-------------------------|
| HSF4 | GGACCAGTTTCCTCGTAAGCGA | CTCACCACCTTCCGAAAACCGT |
| SEMA3C | TTTGCGTGTTGGTTGGAGTAT | TCCTGTAGTCTAAAGGATGGTGG |
| DLX6 | TCGCTTTCAGCAGACACAGT | CGGCTTCTTGCCACACTTAT |
| LEF1 | GGTCCTCCTGGTCCCCACACAA | TCATGCTGAGGCTTCACGTGCA |
| GATA5 | CCTGCGGCCTCTACCACAA | GGCGCGGCGGGACGAGGAC |
| HEYL | GAGAAACAGGGCTCTTCCAA | CTTCAAGGACCCCCAGGTA |

| Gene | Forward primer (5'-3') | Reverse primer (5'-3') |
|--------|------------------------|------------------------|
| NANOG | ATGGAGGAGGAGAGAGA | GATTTGTGGGCCTGAAGAAA |
| NODAL | ATGCCAGATCCTCTTGTTGG | AGACATCATCCGCAGCCTAC |
| KLF4 | ATCTCAAGGCACACCTGCG | CCTGGTCAGTTCATCTGAGCG |
| PRDM14 | TCCACACAGGGGGTGTACTT | GAGCCTTCAGGTCACAGAGC |
| FGF4 | GGCGAGAGCTCCAGCAG | CGGCTCTACTGCAACGTG |
| GAPDH | GTCTCCTCTGACTTCAACAGCG | ACCACCCTGTTGCTGTAGCCAA |

2.11 Software

| Name | Description | Source |
|---------------------|--------------------------|----------------------------------|
| BD FACSDiva™ | Flow cytometer | BD Biosciences, New Jersey, |
| Software | application setup for | USA |
| | data acquisition | |
| Bioconductor v3.20 | Software packages for | https://www.bioconductor.org/ |
| | R-based analysis of | |
| | omics data | |
| BioRender Online | Creation of scientific | https://www.biorender.com/ |
| Tool | schematics | |
| Enrichr | Pathway analysis tool | https://maayanlab.cloud/Enrichr/ |
| | for transcriptome data | |
| GraphPad Prism 10 | Statistical analysis and | https://www.graphpad.com/ |
| | visualization of graphs | |
| | and figures | |
| ImageJ | Image processing and | https://imagej.net/ij/ |
| | analysis | |
| Image Lab Software | Acquisition and analysis | BioRad Laboratories, Hercules, |
| | software for Western | USA |
| | Blot | |
| Microsoft 365 | Word and data | Microsoft, Redmond, USA |
| (Word, Excel, Power | processing and | |
| Point) | presentation software | |
| Microplate Manager | Acquisition software for | BioRad Laboratories, Hercules, |
| Software 6 | XTT data | USA |

| Name | Description | Source |
|-------------------|---|---|
| NCBI Pubmed | Literature database | https://pubmed.ncbi.nlm.nih.gov/ |
| QuPath | Software for bioimage analysis | https://qupath.github.io/ |
| R v4.4.2 | Software environment for statistical computing and graphics | https://www.r-project.org/ |
| R studio | Coding environment for | https://posit.co/ |
| v024.09.1+394 | R | |
| STRING | Protein-protein interaction network and functional enrichment analysis tool | https://string-db.org/ |
| ViiA™ 7 Software | Acquisition of qRT-PCR data | Thermo Fisher Scientific, Waltham, USA |
| VisiView Software | Imaging software | Vistron Systems GmbH, Puchheim, Germany |
| Zotero | Reference management software | https://www.zotero.org/ |

3 METHODS

3.1 Affymetrix expression microarray analysis of GCT tissues

The Affymetrix expression microarray was previously published by Eckert et al. ¹³¹. The data were re-analyzed in context of this study regarding BRD9 expression in normal testis tissue (n=4), GCNIS (n=3), seminoma (n=4), embryonal carcinoma (n=3) and teratoma (n=3).

3.2 Tissue microarray

For tissue microarray (TMA) a cohort of 159 clinically annotated TGCT patients with curative or palliative surgical treatment (2005-2011) at the University Hospital Bonn and diagnosed by the Institute of Pathology was used. Approval of the study was given by the institutional review board of the University of Bonn (#187/16). TMA was performed by Dr. Christine Sanders and Dr. Florian Fronhoffs.

3.3 Immunohistochemistry staining

Immunohistochemical staining of BRD9 or SALL4 in the different tissues was performed using the Autostainer BenchMark Ultra. The antibodies are listed in the material (2.9). The counterstaining of the tissue sections was done with hematoxylin. The images were analyzed and quantified in QuPath and the mean H-score was determined. The analysis was performed by Dr. Christine Sanders.

3.4 Cell culture maintenance

The cell lines 2102 EP ¹²⁵, 2102 EP-R ¹²⁶, NCCIT ¹²², NCCIT-R ¹²⁶, NT2/D1 ¹²³, NT2/D1-R ¹²⁷ (embryonal carcinoma cell lines), JAR ¹³² (choriocarcinoma cell line), FS1 ¹³³ (sertoli cell line) and MPAF ¹³⁴ (human adult fibroblast cell line) were cultured in standard culture medium (2.1) in the incubator at 37 °C and 7.5 % CO₂. Splitting was performed twice a week. Cells were washed with PBS. For detachment 0.05 % Trypsin-EDTA was added and incubated for 5 minutes in the incubator. Cells were resuspended in standard culture medium. In a specific ratio cells were transferred into a cell culture flask for further maintenance. For long-term storage cell suspension was

centrifuged at 400 g for 5 minutes, media was discarded and cell pellet was resuspended in freezing medium (50 % FBS, 40 % standard culture medium and 10 % DMSO). Cells were aliquoted in cryogenic vials and stored at -80 °C. Thawing of cells was performed by incubation of the vial at 37 °C in a water bath and subsequent transfer into a cell culture flask filled with standard culture medium.

3.5 Illumina HT-12v4 expression microarray analysis of TGCT cell lines

The Illumina expression microarray was previously published by Nettersheim et al. ⁹⁴. The dataset is publicly available at GEO (ncbi.nlm.nih.gov/geo/, GSE71239). The data were re-analyzed in context of this study regarding BRD9 expression in 2102 EP (n=5), NCCIT (n=4), TCam-2 (n=5), JAR (n=2), FS1 (n=4) and MPAF (n=4) cells.

3.6 Protein extraction, SDS PAGE and Western Blot analysis

For protein extraction all steps need to be performed on ice. Cells were lysed with RIPA buffer supplemented with protease inhibitor cOmplete ULTRA Tablets. Lysate was sonicated for 30 seconds at medium intensity and centrifuged for 15 minutes at 20817 g and 4 °C. Cell debris were pelleted and protein containing supernatant was transferred into a fresh tube. Protein lysates were stored at -20 °C.

For determination of protein concentration BCA assay was performed using the PierceTM BCA Protein Assay Kit according to the manufacturer's manual. In brief, 9 bovine serum albumin (BSA) standards in different concentrations (25, 125, 250, 500, 750, 1000, 1500, 2000 μg/ml) were prepared. Triplicates of standards as well as diluted (1:10) lysates were pipetted into a microplate and 200 μl working solution (50:1 ratio of BCA reagents A and B) were added. The plate was incubated at 37 °C for 30 minutes. Absorbance was measured at a wavelength of 595 nm in a plate reader. Using the standard curve generated by the measurements of the different BSA standards protein concentrations of lysates were determined.

For sodium dodecyl sulfate – polyacrylamide gel electrophoresis (SDS-PAGE) protein lysates were diluted (1:10) and mixed with 4x ROTI-Load (reducing) and subsequently denatured for 10 minutes at 95 °C in a heating block. A SDS gel with a 5 % stacking

gel and a 12 % separation gel was used. The gel was prepared with a Mini-PROTEAN® Tetra Cell Casting Module. 30 µg of protein were loaded in the pocket. The PageRuler™ Plus Prestained Protein Ladder (10 bis 250 kDa) was used to determine the size of the proteins. The electrophoresis was performed in a Mini-PROTEAN® Tetra Vertical Electrophoresis Cell for 10 minutes at 90 V and afterwards at 120 V for approximately 1.5 hours in SDS running buffer.

Proteins were transferred to a methanol-activated PVDF membrane by the Trans-Blot® Turbo™ Transfer System using transfer buffer. Coomassie staining was performed to evaluate equal protein amounts. Membrane was blocked in 5 % BSA in PBST for 1 hour at room temperature. Primary antibodies were diluted in 5 % BSA in PBST and incubated over night at 4 °C. The antibodies are listed in the materials (2.9). Membrane was washed three times in PBST for 10 minutes on a shaking plate. Incubation with secondary antibody coupled to horseradish peroxidase (HRP) diluted in 5 % BSA in PBST was conducted for 1 hour at room temperature. Three washing steps with PBST for 10 minutes were performed. For detection of bands WESTAR NOVA 2.0 enhanced chemiluminescent (ECL) substrate or for more sensitive detection SuperSignal™ West Femto Maximum Sensitivity Substrate was used. Substrate A and B were mixed in a 1:1 ratio and applied to the membrane. Detection was performed using the ChemiDoc MP Imaging System.

3.7 Cell viability assay

For measurement of viability XTT assay was performed. Cells were seeded at a concentration of 3 x 10^4 cells/ml and $100~\mu l$ of cell suspension were transferred in wells of a 96 well plate. The next day treatment with BRD9 inhibitor or corresponding solvent control DMSO was performed in five different concentrations (2, 10, 15, 20 and 25 μM). Viability was assessed after 24, 48 and 72 hours. XTT was dissolved in medium without supplements in a concentration of 0.7 mg/ml. PMS (1.25 mM) was added and 50 μl of XTT/PMS solution was pipetted onto the cells. Incubation was performed in the incubator for 4 hours. Afterwards, absorbance was measured in a plate reader at 450 and 650 nm.

3.8 DAPI/ AnnexinV (Apoptosis) FACS analysis

For fluorescence activated cell sorting (FACS) analysis cells were seeded in a 6 well plate in a concentration of 1.5 x 10^5 cells/well. The next day treatment with 15 μ M I-BRD9 or DMSO control was performed. After 24 and 48 hours of treatment the supernatant was collected in a FACS tube and harvested cells were added. Three washing steps with PBS and subsequent centrifugation at 400 g for 5 minutes were performed. For staining cells were resuspended in 100 μ I staining solution (100 μ I AnnexinV binding buffer, 0,1 μ I DAPI and 4 μ I PE-AnnexinV) and incubated at 37 °C for 30 minutes in the dark. Afterwards, 200 μ I of PBS were added and measurement was performed at the Flow Cytometry Core Facility (University Bonn, Germany) at the BD FACSCanto II Flow Cytometer and analyzed with the BD FACSDiva softwareTM.

3.9 Hoechst (Cell Cycle) FACS Analysis

Cells were seeded in a 6-well plate (1.5 x 10⁵ cells/well) and the next day treated with 15 μM I-BRD9 or DMSO control. Measurement was performed after 24 and 48 hours of treatment. Washing with PBS and subsequent centrifugation at 400 g for 5 minutes was applied three times. Cells were fixed with ice-cold methanol for 60 minutes at 4 °C. Washing with PBS and centrifugation was performed and afterwards cells were incubated in staining solution (1.2 μg/ml Hoechst33258 and 50 μg/ml RNaseA in PBS) for 30 minutes at 37 °C. Measurement was performed at the Flow Cytometry Core Facility (University Bonn, Germany) at the BD FACSCanto II Flow Cytometer and analyzed with the BD FACSDiva softwareTM. For further analysis FlowJoTMv10.8 software was used.

3.10 RNA isolation

For isolation of RNA cell suspension was centrifuged at 10621 g for 5 minutes. Cell pellet was washed with PBS two times with subsequent centrifugation. Afterwards the RNeasy Mini Kit was used according to the manufacturer's manual. Concentration was measured with the Spectrophotometer Nano Drop 1000 and purity was checked by the 260 nm/ 280 nm ratio. High purity was considered at a ratio between 1.8 and 2.1.

3.11 3'mRNA sequencing analysis

For transcriptome analysis 2102 EP, TCam-2 and MPAF cells were seeded in a concentration of 2 x 10^5 cells/ well in a 6 well plate. Cells were treated with I-BRD9 (15 μ M) or DMSO control the next day for 24 hours. RNA was isolated as described in chapter 3.10. RNA integrity (RIN) was determined by NANO 6000 Assay kit with the Agilent Bioanalyzer 2100 system. RNA samples with RNA integrity > 7 were used for RNA sequencing analysis. The Core Facility Next Generation Sequencing (University of Bonn) performed RNA quality control, library preparation (QuantSeq 3'-mRNA Library Prep) and RNA sequencing using Illumina HiSeq 2500 V4 device at 10M reads per sample. The data are publicly available at Gene Expression Omnibus (GEO) with the accession number GSE282367 135 .

3.12 RNAseq data analysis

The Core Facility Bioinformatics (University of Bonn) performed the bioinformatic analysis. For preprocessing and quantification of the reads using default parameters nf-core RNAseq pipeline (version 3.17) was applied ¹³⁶. First quality and adapter trimming were performed with TrimGalore followed by alignment of the trimmed reads against the human genome (GRCh38) with STAR (version 2.7.11b) ¹³⁷. Pseudoalignment of the aligned data to estimate transcript abundances was performed using Salmon (version 1.9.0) ¹³⁸. To obtain gene-level expression estimates the transcript-level quantifications were aggregated. R environment (version 4.2.0) was used to execute statistical analyses ¹³⁹. Only genes with a minimum count of 5 in at least three samples were used for the inference analysis to ensure the robustness of the results. For differential gene expression analysis the Bioconductor package DESeq2 was utilized ^{140,141}. For calculation of multiple testing adjusted p-values (false discovery rate, FDR) for each contrast the Benjamini-Hochberg method was applied. Differential expression data obtained by the Core Facility Bioinformatics were further analyzed using STRING 11.5 database and Enrichr analysis tools ^{142,143}.

3.13 Quantitative RT-PCR

RNA isolation of cells was performed as described in 3.10. For DNase digest 1 µg of RNA were mixed with 1 μ I 10x Buffer + MgCl₂, 0.5 μ I DNasel filled up to 10 μ I with H₂O. Incubation was performed at 37 °C for 30 minutes. For deactivation of DNasel 1 µl EDTA was added and incubated for 10 minutes at 75 °C. For cDNA synthesis 1 µl oligo(dT)₁₈ primer as well as 1 µl dNTP mix (10 mM) were added and filled up to 14.5 μl with H₂O. Incubation was performed for 5 minutes at 65 °C. Afterwards, 4 μL 5x RT buffer, 0.5 µl RiboLock RNase inhibitor and 1 µl Maxima H Minus reverse transcriptase were added and incubated for 30 minutes at 65 °C and subsequent at 85 °C for 5 minutes. The cDNA was diluted 1:16 in H₂O and master mix containing 15 µl SYBR Green qPCR Master Mix (2x) as well as 1 µl forward primer (10 mM) and 1 µl reverse primer (10 mM) was prepared. Oligonucleotide sequences are listed in the materials (2.10). 16 µl of diluted cDNA was mixed with 16 µl of master mix and triplicates of 10 µl were pipetted into a 384 well plate. A master mix only (without cDNA) control was used for each primer pair. The housekeeping gene GAPDH was utilized as control. For quantitative real-time polymerase chain reaction (qRT-PCR) the Applied Biosystems ViiA™ 7 Real-Time PCR System was used. The expression fold change 2-△△CT was calculated 144.

3.14 Immunofluorescence staining

For immunofluorescence staining cells were seeded in a concentration of 1 x 10⁴ cells/ml in a 24 well plate onto coverslips. Treatment with I-BRD9 (15 µM) or DMSO control was performed the following day for 72 hours. Cells were washed with PBS and fixation was performed with 4 % PFA for 15 minutes. Afterwards cells were washed with PBS for 5 minutes three times. Permeabilization was performed by incubation with 0.3 % Triton-X100 in PBS for 10 minutes. Afterwards three washing steps were applied. For blocking normal horse serum was utilized for 20 minutes followed by three washing steps. Second blocking was performed with 5 % BSA in PBS for 30 minutes. The cells were washed three times. Primary antibody was incubated in 1 % BSA in PBS overnight at 4 °C. All antiboides are listed in the materials (2.9). Next day, three washing steps were performed. Secondary antibody kit (VectaFluor Horse Anti-Rabbit IgG, DyLight[™] 594 Antibody Kit, R.T.U. or VectaFluor Horse Anti-Mouse IgG, DyLight 594 Antibody Kit, R.T.U.) was used for 1 hour in the dark. Three washing steps were

performed. Cells were stained with Hoechst Bisbenzimid H 33342 (0.01 mg/ml) diluted 1:1000 in PBS for 10 minutes. The cells were washed three times. Coverslips were mounted with Fluoroshield on slides. For imaging the VisiScope CSU-W1 (Vistron, Puchheim, Germany) of the Core Facility Microscopy (University of Bonn) with the VisiView Software was used.

3.15 Statistical analysis

All independent biological replicates are presented as mean with standard deviation as error bars. Statistical significance was calculated by student's t test. P-values < 0.05 were considered significant and were indicated by asterisk (ns: not significant; *p < 0.05; **p < 0.01; ***p < 0.001). Statistical analysis was performed with GraphPad Prism 10.

4 RESULTS

TGCT patients have high 5-year survival rates of up to 95 %. The standard treatment regime is orchiectomy followed by cisplatin-based chemotherapy but unfortunately 15-20 % of the patients are resistant to the standard therapy ^{38,39}. Therefore, investigation of alternative treatment options like epigenetic drugs is very important to address and eventually overcome therapy resistance. Further, new treatment options could offer reduction of side effects.

4.1 BRD9 is expressed in TGCT tissue as well as cell lines

Expression of the target BRD9 in TGCT tissues was analyzed by meta-analysis of previously published Affymetrix expression microarray data in normal testis tissue, GCNIS, seminoma, embryonal carcinoma and teratoma ¹³¹. The analysis revealed the highest expression of BRD9 in embryonal carcinoma while GCNIS displayed the lowest expression. Of note, normal testis tissue also showed high expression of BRD9 (Figure 13A). A tissue microarray comprising GCNIS, seminoma and embryonal carcinoma of 159 patients as well as 5 normal testis tissues was performed and validated by SALL4 staining (Figure S 1). Immunohistochemical staining showed protein level and distribution of BRD9 in the different tissues. BRD9 was upregulated (moderate or high protein level) in 35.2 % of the tumor tissues compared to normal testis tissue. The protein levels of BRD9 showed significant differences between GCNIS, seminoma and embryonal carcinoma (p=0.001). The highest BRD9 protein level was found in GCNIS while tumor associated normal testis tissue displayed no or weak protein levels of BRD9 (Figure 13 B,C, Table 1).

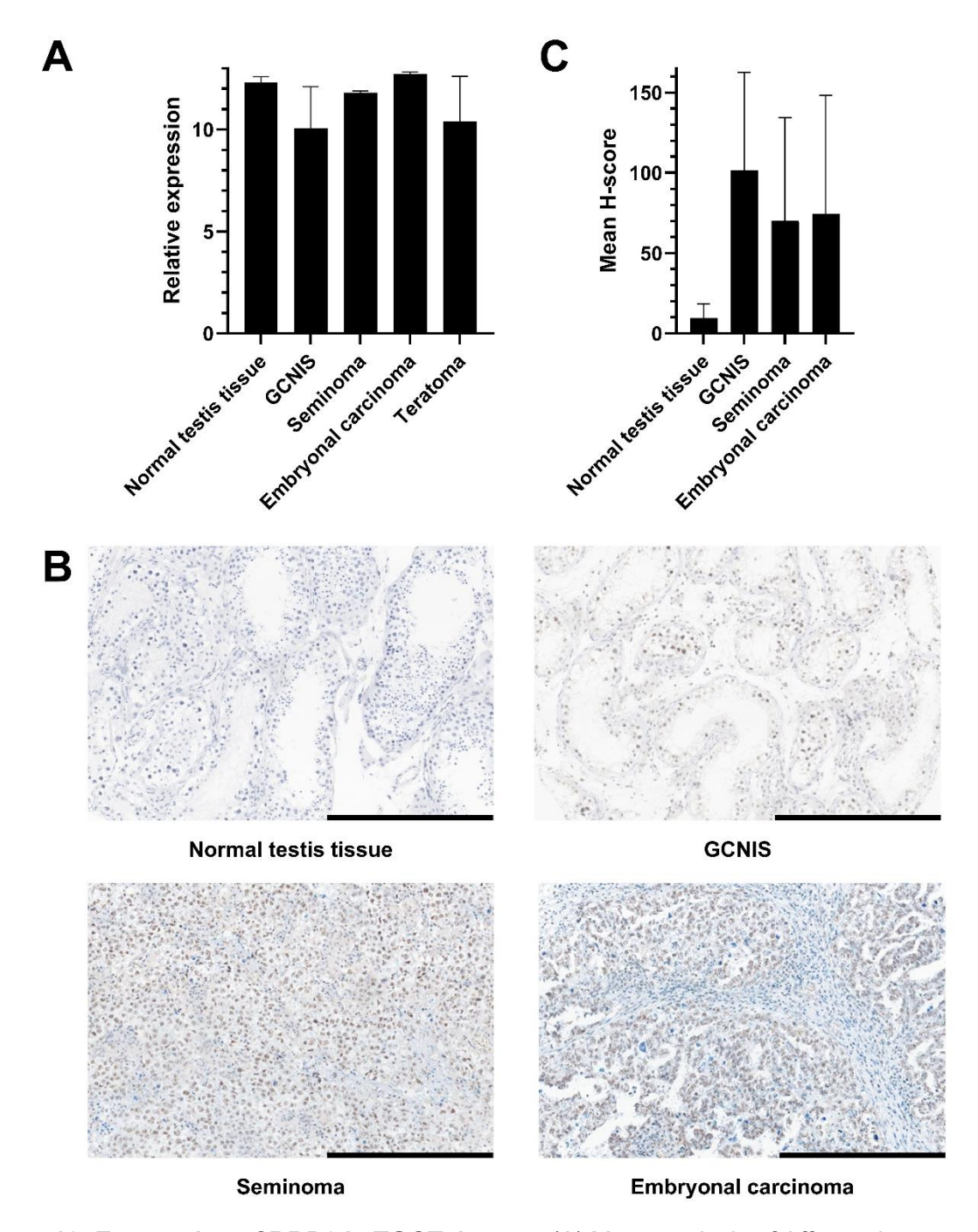


Figure 13: Expression of BRD9 in TGCT tissues. (A) Meta-analysis of Affymetrix expression microarray data in normal testis tissue, GCNIS, seminoma, embryonal carcinoma and teratoma. (B) Representative images of immunohistochemical stainings of BRD9 in normal testis tissue, GCNIS, seminoma and embryonal carcinoma (TMA). Scale bar: 500 μm. (C) Mean staining intensity (H-score) of BRD9 in normal testis tissue, GCNIS, seminoma and embryonal carcinoma. TMA as well as analysis was performed by Dr. Christine Sanders and Dr. Florian Fronhoffs. GCNIS – germ cell neoplasia in situ. Modified from ¹.

Table 1: Expression of BRD9 in testicular tumor and normal testis tissue. Testing for differences in BRD9 expression between histological subtypes (Pearson-Chi-Square, p=0.001). The analysis was performed by Dr. Christine Sanders. SD – standard derivation; GCNIS – germ cell neoplasia in situ. Modified from ¹.

| Tissue | Number | Mean | Visual analysis in categories | | | |
|-----------|----------|---------|-------------------------------|-------------|-------------|-----------|
| | of | H-score | 0 1 | | 2 | 3 |
| | patients | [SD] | negative | weak | moderate | high |
| GCNIS | 52 | 101.35 | 4 (7.7 %) | 24 (46.2 %) | 20 (38.5 %) | 4 (7.7 %) |
| | | [61.23] | | | | |
| Seminoma | 82 | 70.08 | 33 (40.2 %) | 28 (34.1 %) | 15 (18.3 %) | 6 (7.3 %) |
| | | [64.19] | | | | |
| Embryonal | 25 | 74.27 | 9 (36 %) | 5 (20 %) | 10 (40 %) | 1 (4 %) |
| carcinoma | | [74.02] | | | | |
| Normal | 5 | 9.59 | 3 (60 %) | 2 (40 %) | 0 | 0 |
| testis | | [8.93] | | | | |
| tissue | | | | | | |

For investigation of BRD9 expression in TGCT cell lines meta-analysis of previously published Illumina expression microarray data in embryonal carcinoma (2102 EP and NCCIT), seminoma (TCam-2), choriocarcinoma (JAR) and control cell lines (FS1 and MPAF) was performed ⁹⁴. The TGCT cell lines showed comparable expression levels while the control cell line MPAF (human adult fibroblasts) showed the lowest BRD9 expression (Figure 14 A). For analysis of BRD9 protein level Western Blot was performed. Here, again TGCT cell lines showed similar protein levels while MPAF displayed only a low BRD9 protein level (Figure 14 B).

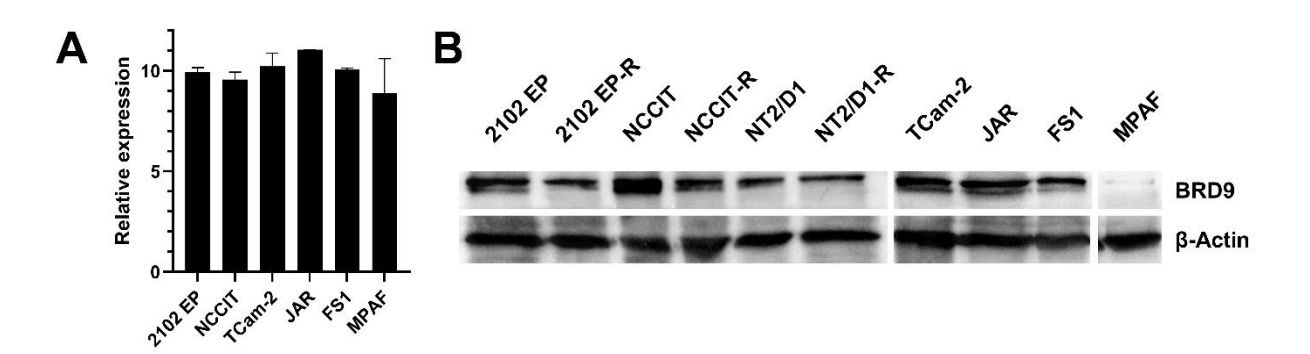


Figure 14: Expression of BRD9 in TGCT cell lines. (A) Meta-analysis of Illumina expression microarray data in 2102 EP, NCCIT, TCam-2, JAR, FS1 and MPAF cells. (B) BRD9 protein level in 2102 EP, 2102 EP-R, NCCIT, NCCIT-R, NT2/D1, NT2/D1-R, TCam-2, JAR, FS1 and MPAF cells with corresponding load control β-actin detected by Western Blot. Original Western Blot can be found in the appendix (Figure S 2). Modified from 1 .

These data suggest that BRD9 is expressed in TGCT tissues as well as cell lines. In addition, the lowest expression was detected in the control indicating a good starting point for further investigation of targeting BRD9 in TGCT cell lines using the inhibitor I-BRD9.

4.2 Inhibition of BRD9 decreases viability in TGCT cell lines in a dose- and time-dependent manner

The viability of TGCT cell lines (2102 EP, 2102 EP-R, NCCIT, NCCIT-R, NT2/D1, NT2/D1-R, TCam-2 and JAR) as well as two control cell lines (FS1 and MPAF) was investigated by XTT assay after treatment with I-BRD9. Measurement was performed after 24, 48 and 72 hours of treatment and five different concentrations (2, 10, 15, 20 and 25 µM) were tested. Initial induction of decreased viability was detected after 24 hours. A clear decrease was visible after 48 hours and even stronger after 72 hours which indicated a time-dependent effect. All TGCT cell lines showed the strongest reduction of viability after treatment with the highest concentration (25 µM). In NCCIT and NT2/D1 cells also 20 µM led to a similar decrease in viability as the highest concentration (25 µM). The cisplatin-resistant cell lines (2102 EP-R, NCCIT-R and NT2/D1-R) showed comparable effects as the parental cell lines (2102 EP, NCCIT and NT2/D1). In total, embryonal carcinoma cell lines and especially NCCIT cells were affected the most (Figure 15). The seminoma cell line TCam-2 displayed the lowest cytotoxic effect compared to the other TGCT cell lines. Choriocarcinoma cells (JAR) also showed a strong decrease of viability in the two highest concentrations (20 and 25 µM). On the other hand, control cell lines were only slightly affected. Sertoli cells (FS1) showed only a reduction of viability to 70 % in the highest concentration (25 μM) of I-BRD9 treatment while the fibroblast cell line (MPAF) showed no decrease in viability suggesting only low side-effects on somatic cells (Figure 16).

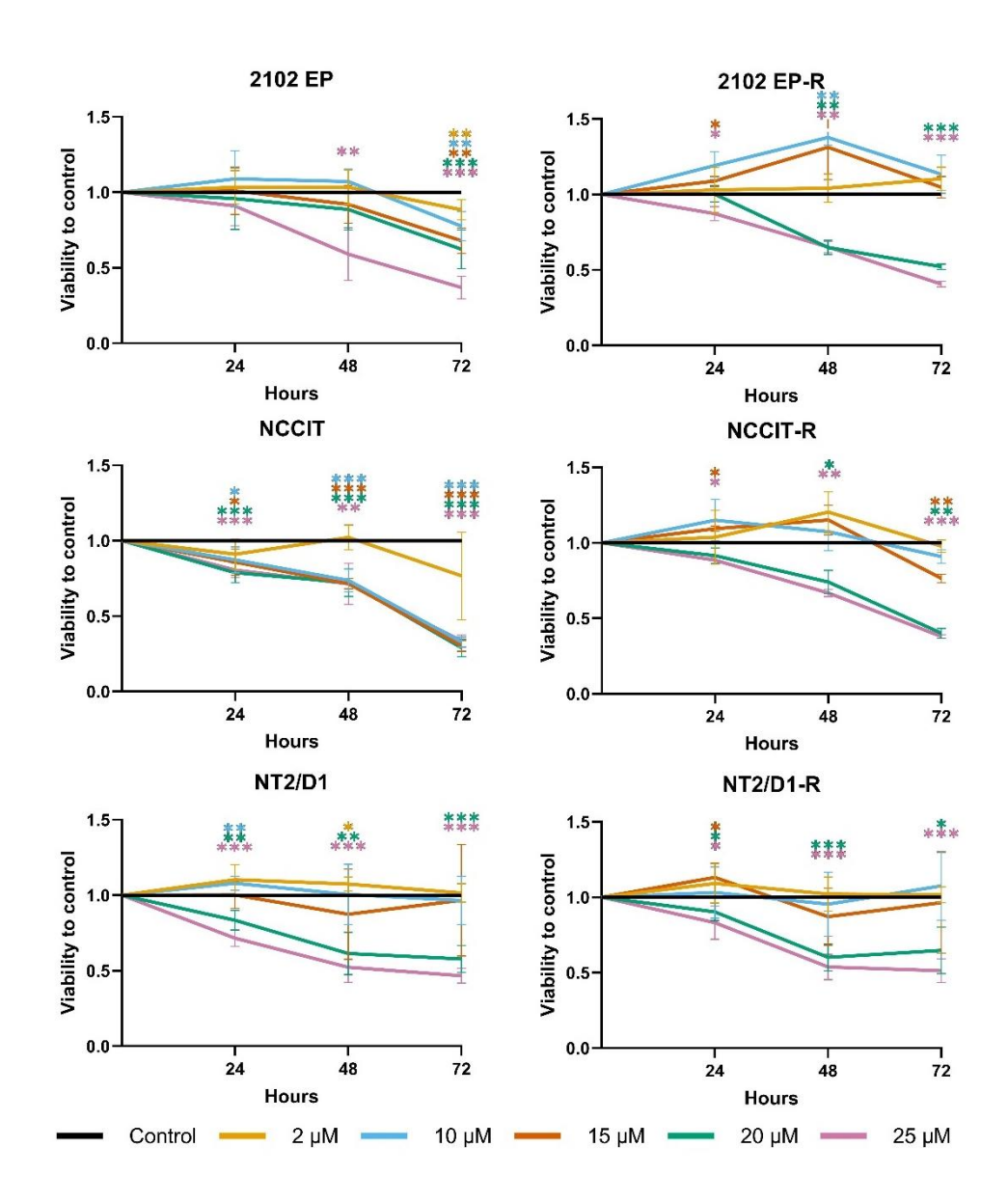


Figure 15: Viability of TGCT cell lines treated with I-BRD9. XTT assay in embryonal carcinoma cell lines as well as cisplatin-resistant subclones (2102 EP, 2102 EP-R, NCCIT, NCCIT-R, NT2/D1 and NT2/D1-R) was performed at three different time points (24, 48 and 72 hours) after treatment with I-BRD9 at five different concentrations (2, 10, 15, 20 and 25 μ M). The values were normalized to the corresponding DMSO control. Significance between I-BRD9 and DMSO treated control cells is indicated by asterisk (*p < 0.05; **p < 0.01; ***p < 0.001). The colors of asterisks indicate corresponding concentrations. n=3-6. Modified from 1 .

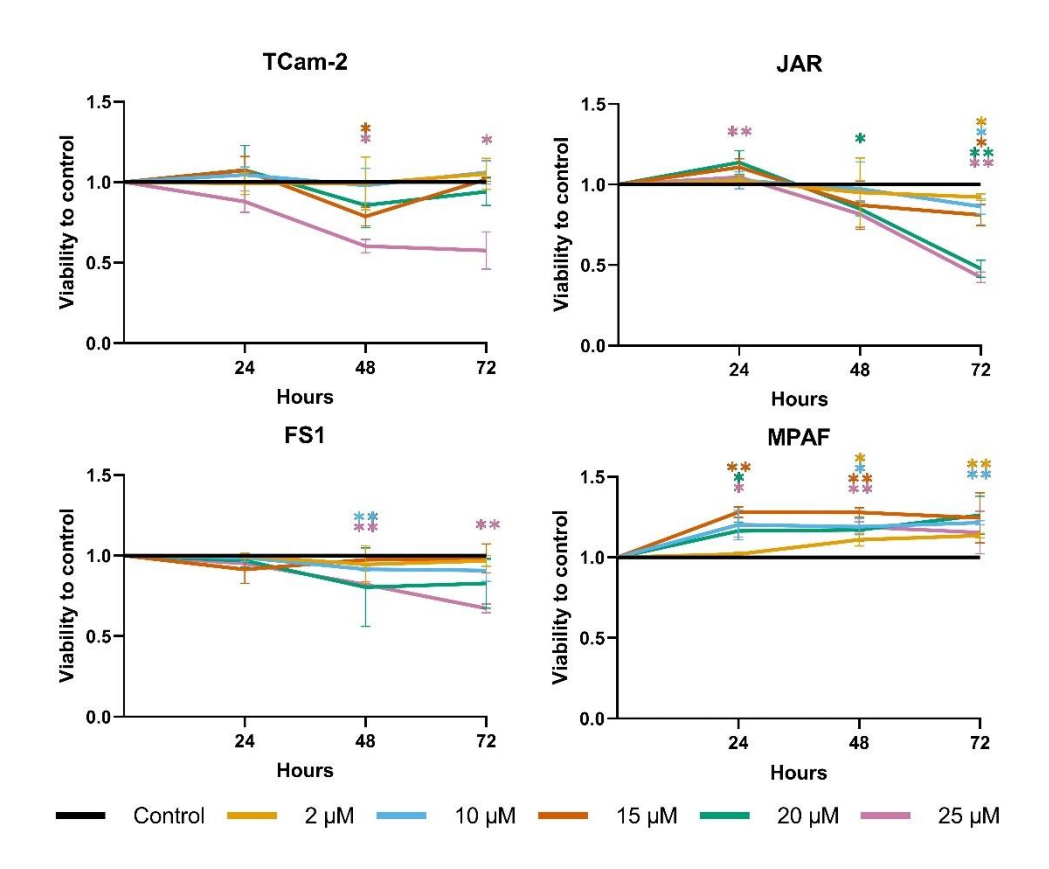


Figure 16: Viability of TGCT cell lines treated with I-BRD9. XTT assay in seminoma (TCam-2), choriocarcinoma (JAR) as well as control cell lines (FS1 and MPAF) was performed at three different time points (24, 48 and 72 hours) after treatment with I-BRD9 at five different concentrations (2, 10, 15, 20 and 25 μ M). The values were normalized to the corresponding DMSO control. Significance between I-BRD9 and DMSO treated control cells is indicated by asterisk (*p < 0.05; **p < 0.01; ***p < 0.001). The colors of asterisks indicate corresponding concentrations. n=3-6. Modified from 1 .

For comparison of therapeutic potency IC $_{50}$ values were calculated using logarithmic regression curves based on XTT assay data (Figure S 3, Figure S 4). The lowest IC $_{50}$ value and therefore the highest potency of I-BRD9 was determined in NCCIT cells at 6 μ M after 72 hours of treatment. The lowest potency of I-BRD9 in TGCT cell lines was found in TCam-2 cells after 72 hours at 29 μ M. In total, I-BRD9 showed very high potency in all TGCT cell lines after 72 hours. In 2102 EP, 2102 EP-R, NCCIT-R, NT2/D1 and NT2/D1-R cells the BRD9 inhibitor displayed also very high potency after 48 hours of treatment suggesting a high sensitivity of embryonal carcinomas towards I-BRD9. On the other hand, control cell line FS1 (sertoli cells) revealed low sensitivity after 24 hours (>500 μ M) and moderate sensitivity after 48 hours (64 μ M). After 72 hours I-BRD9 also showed high potency at 34 μ M in FS1 cells but the TGCT cell lines were all already sensitive to I-BRD9 in lower concentrations (6-29 μ M). Of note, in

human adult fibroblasts (MPAF) the BRD9 inhibitor showed only low potency at all time points (Table 2).

Table 2: IC₅₀ values of TGCT cell lines and control cell lines. IC₅₀ values [μM] were calculated based on XTT assays in 2102 EP, 2102 EP-R, NCCIT, NCCIT-R, NT2/D1, NT2/D1-R, TCam-2, JAR, FS1 and MPAF cells after treatment with I-BRD9 at three different time points (24, 48 and 72 hours). The values were grouped according to very high potency (green, 0-30 μM), high potency (orange, 31-50 μM), moderate potency (red, 51-500 μM) and low potency (white, >500 μM). Modified from 1 .

| | 24 h | 48 h | 72 h |
|-----------|------|------|------|
| 2102 EP | 201 | 30 | 21 |
| 2102 EP-R | 85 | 28 | 23 |
| NCCIT | 249 | 80 | 6 |
| NCCIT-R | 60 | 28 | 20 |
| NT2/D1 | 37 | 25 | 23 |
| NT2/D1-R | 44 | 27 | 26 |
| TCam-2 | 78 | 32 | 29 |
| JAR | >500 | 170 | 21 |
| FS1 | >500 | 64 | 34 |
| MPAF | >500 | >500 | >500 |

Taken together, viability assays showed a cytotoxic effect in all TGCT cell lines while control cell lines remained only slightly affected. Embryonal carcinoma cells showed the strongest effect after I-BRD9 treatment. The data indicate a time- and dose-dependent effect in all cell lines. IC₅₀ values also displayed very high potency to I-BRD9 after 72 hours and in some TGCT cell lines already after 48 hours. On the other hand, control cell lines showed lower potency compared to TGCT cell lines.

4.3 I-BRD9 led to induction of apoptosis and G1-phase cell cycle arrest in TGCT cell lines

To investigate the effect of I-BRD9 on apoptosis DAPI/ AnnexinV-based fluorescence activated cell sorting (FACS) was performed after 24 and 48 hours of treatment. TGCT cell lines (2102 EP, 2102 EP-R, NCCIT, NCCIT-R, NT2/D1, NT2/D1-R, TCam-2 and

JAR) and two control cell lines (FS1 and MPAF) were treated with 15 μM I-BRD9 or the solvent control DMSO. In 2102 EP, 2102 EP-R, NT2/D1-R and TCam-2 cells the highest induction of apoptosis was detectable already after 24 hours of treatment with I-BRD9 compared to the DMSO control. In NCCIT, NCCIT-R, NT2/D1and JAR cells an increase of apoptotic cells was visible after 24 hours but even stronger after 48 hours of treatment. The highest accumulation of apoptotic cells was detected in embryonal carcinoma cells (NCCIT-R) after 48 hours. In contrast, the control cell lines FS1 and MPAF showed no significant differences between I-BRD9 and DMSO treated cells (Figure 17).

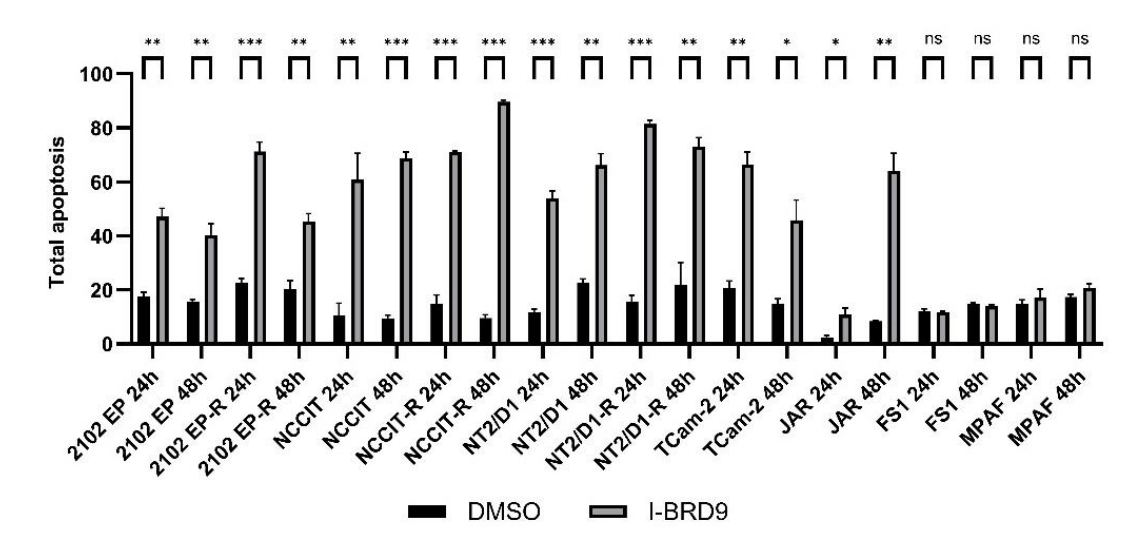


Figure 17: BRD9 inhibition induced apoptosis in TGCT cell lines. DAPI/ AnnexinV-based FACS analysis was performed in 2102 EP, 2102 EP-R, NCCIT, NCCIT-R, NT2/D1, NT2/D1-R, TCam-2, JAR, FS1 and MPAF cells after 24 and 48 hours of treatment with I-BRD9 (15 μ M) or solvent control DMSO. Asterisks indicate significant differences between treated cells and control group (ns: not significant; *p < 0.05; **p < 0.01; ***p < 0.001). n=3. Modified from 1 .

Cell cycle analysis was performed by Hoechst staining in 2102 EP, 2102 EP-R, NCCIT, NCCIT-R, NT2/D1, NT2/D1-R, TCam-2, JAR and FS1 cells treated with I-BRD9 (15 μM) or DMSO control. FACS analysis was performed after 24 and 48 hours. Induction of G1-phase cell cycle arrest was visible in all TGCT tumor cell lines after 24 hours of treatment with I-BRD9 in comparison to the DMSO control. In 2102 EP, 2102 EP-R and NT2/D1 cells an even stronger increase was visible after 48 hours. The highest accumulation of cells in G1-phase was detected in embryonal carcinoma cells (NCCIT and NT2/D1-R). The embryonal cell line 2102 EP showed the lowest effect on cell cycle

distribution after treatment with I-BRD9. The seminoma cell line TCam-2 as well as choriocarcinoma cells (JAR) displayed also strong induction after 24 hours of BRD9 inhibition. In contrast, control cell line FS1 (sertoli cells) showed no increase of cells in G1-phase (Figure 18).

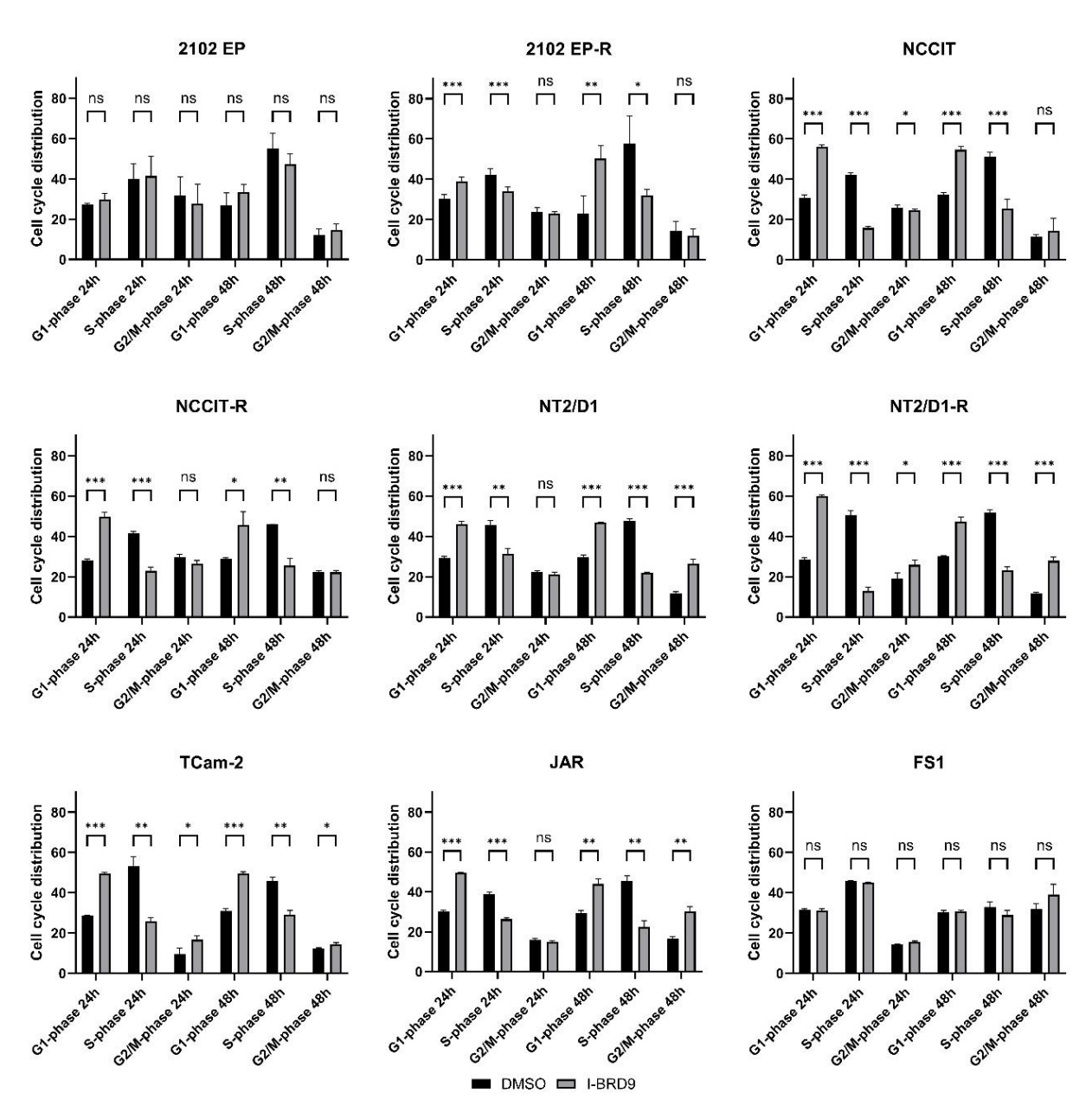


Figure 18: I-BRD9 induced G1-phase cell cycle arrest in TGCT cell lines. Staining of Hoechst in 2102 EP, 2102 EP-R, NCCIT, NCCIT-R, NT2/D1, NT2/D1-R, TCam-2, JAR and FS1 cells was analyzed via FACS after 24 and 48 hours of treatment. Cells were treated with I-BRD9 (15 μ M) or corresponding DMSO control. Asterisks indicate significant change between I-BRD9 treated and control cells (ns: not significant; *p < 0.05; **p < 0.01; ***p < 0.001). n=3-9. Modified from 1 .

BRD9 inhibition induced apoptosis and G1-phase cell cycle arrest in TGCT cell lines already after 24 hours of treatment with I-BRD9 in comparison to DMSO treated control cells. Embryonal carcinoma cells showed the strongest effect after BRD9 inhibition. On the other hand, I-BRD9 had no significant effect on control cells in apoptosis or cell cycle distribution analysis.

4.4 BRD9 inhibition in embryonal carcinoma and seminoma induces differentiation to an epithelial cell fate and loss of pluripotency

The impact of I-BRD9 on gene expression was analyzed by 3'mRNA sequencing after 24 hours of BRD9 inhibition in comparison to DMSO treated cells. The time point (24 hours) was chosen to analyze early gene expression changes before effects were observed in viability assays (48 and 72 hours). To get an overview of the different TGCT entities RNAseq was performed in embryonal carcinoma (2102 EP), seminoma (TCam-2) and control cells (MPAF).

In total, 2102 EP cells displayed 5536 significantly deregulated genes. 983 genes with a log₂ foldchange higher than 1 were upregulated and 983 genes with a log₂ foldchange lower than -1 were downregulated (Figure 19). In TCam-2 cells 753 genes with a log₂ foldchange higher than 1 showed upregulation while 898 genes with a log₂ foldchange lower than -1 were downregulated. In sum, 4833 genes were significantly deregulated after 24 hours of I-BRD9 treatment compared to the DMSO control (Figure 20). Control cells MPAF showed the lowest amount of significantly deregulated genes (4781). 1179 genes with a log₂ foldchange lower than -1 displayed downregulation and 695 genes with a log₂ foldchange higher than1 were upregulated after 24 hours of BRD9 inhibition in comparison to DMSO treated cells (Figure 21).

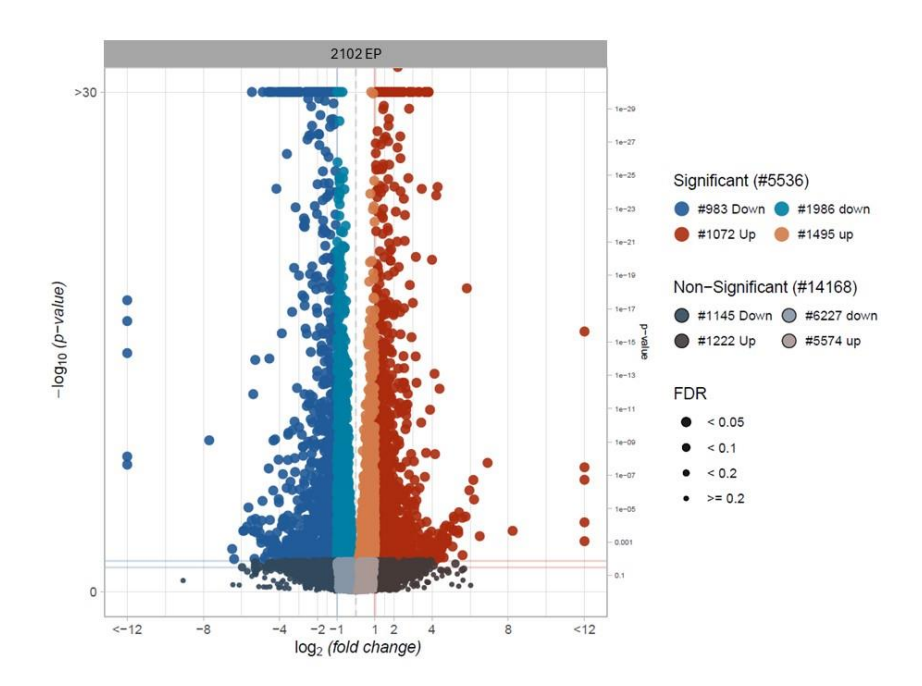


Figure 19: Differentially expressed genes in 2102 EP cells. Volcano plot displaying differentially expressed genes after 24 hours of treatment with I-BRD9 in comparison to DMSO control. Significantly upregulated genes are depicted in red (log₂ foldchange >1) or orange (log₂ foldchange between 0 and 1) and significantly downregulated genes are highlighted in dark (log₂ foldchange <-1) or light blue (log₂ foldchange between 0 and -1) (adjusted p-value < 0.05). FDR – false discovery rate. Modified from ¹.

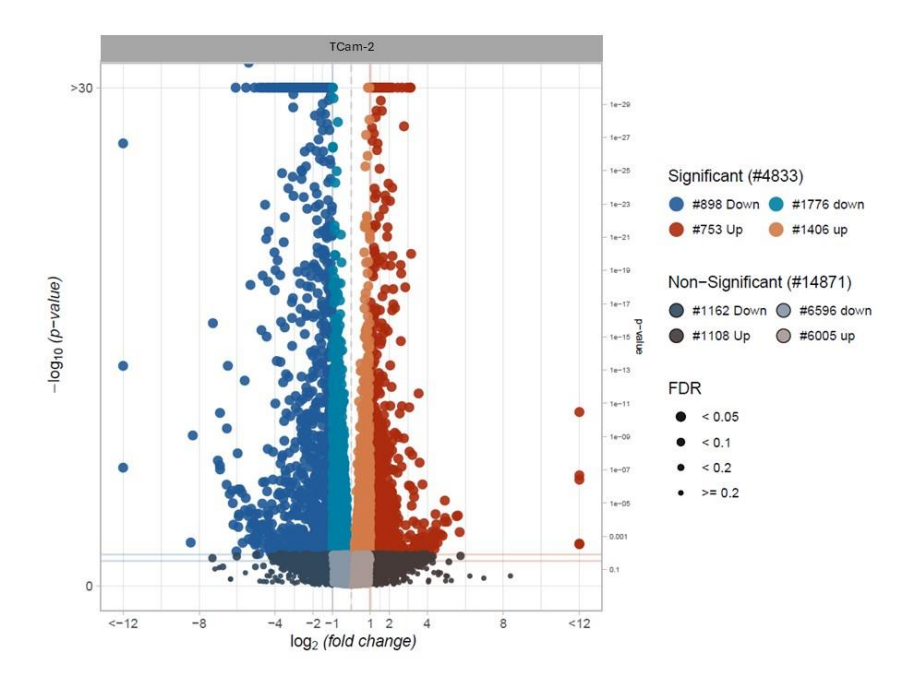


Figure 20: Differentially expressed genes in TCam-2 cells. Volcano plot displaying differentially expressed genes after 24 hours of treatment with I-BRD9 in comparison to DMSO control. Significantly upregulated genes are depicted in red (log₂ foldchange >1) or orange (log₂ foldchange between 0 and 1) and significantly downregulated genes are highlighted in

dark (log_2 foldchange <-1) or light blue (log_2 foldchange between 0 and -1) (adjusted p-value < 0.05). FDR – false discovery rate. Modified from ¹.

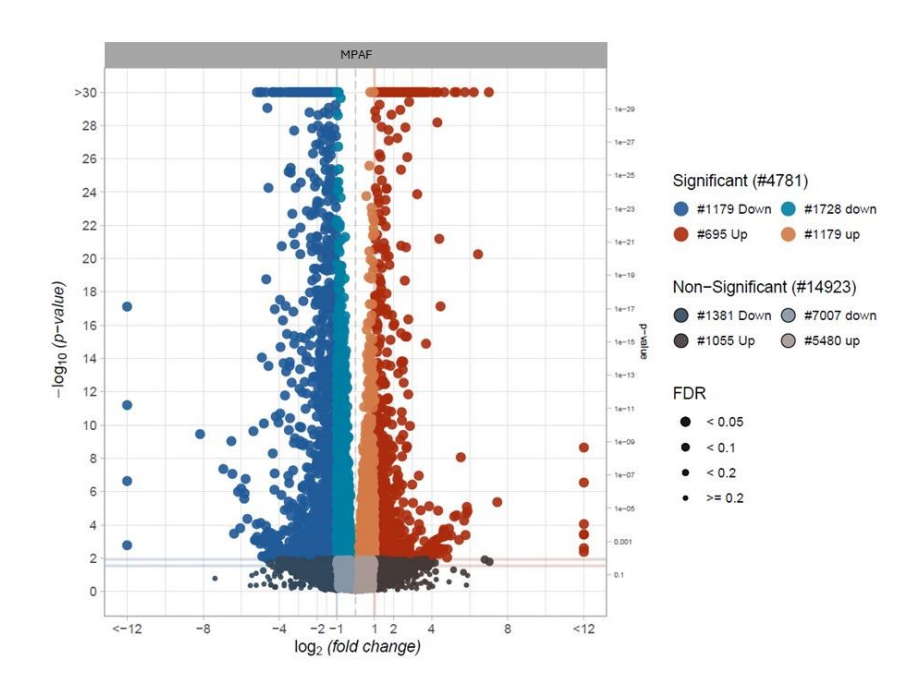


Figure 21: Differentially expressed genes in MPAF cells. Volcano plot displaying differentially expressed genes after 24 hours of treatment with I-BRD9 in comparison to DMSO control. Significantly upregulated genes are depicted in red (\log_2 foldchange >1) or orange (\log_2 foldchange between 0 and 1) and significantly downregulated genes are highlighted in dark (\log_2 foldchange <-1) or light blue (\log_2 foldchange between 0 and -1) (adjusted p-value < 0.05). FDR – false discovery rate.

First, enrichment analysis of significantly upregulated genes was performed. In 2102 EP (embryonal carcinoma) as well as TCam-2 (seminoma) cells the GO term "epithelium development" (GO:0060429) was among the TOP3 with deregulation of 197 genes in 2102 EP and 176 genes in TCam-2 cells (Figure 22 A, B, Figure S 5, Figure S 6). In control cells MPAF GO terms associated with metabolic processes like "organic acid metabolic process" (GO:0006082, 148 genes), "oxoacid metabolic process" (GO:0043436, 147 genes) and "cellular lipid metabolic process" (GO:0044255, 145 genes) were enriched (Figure 22 C). Of note, enrichment of epithelium development was not found in MPAF cells after BRD9 inhibition suggesting that this is a unique response of TGCT cell lines.

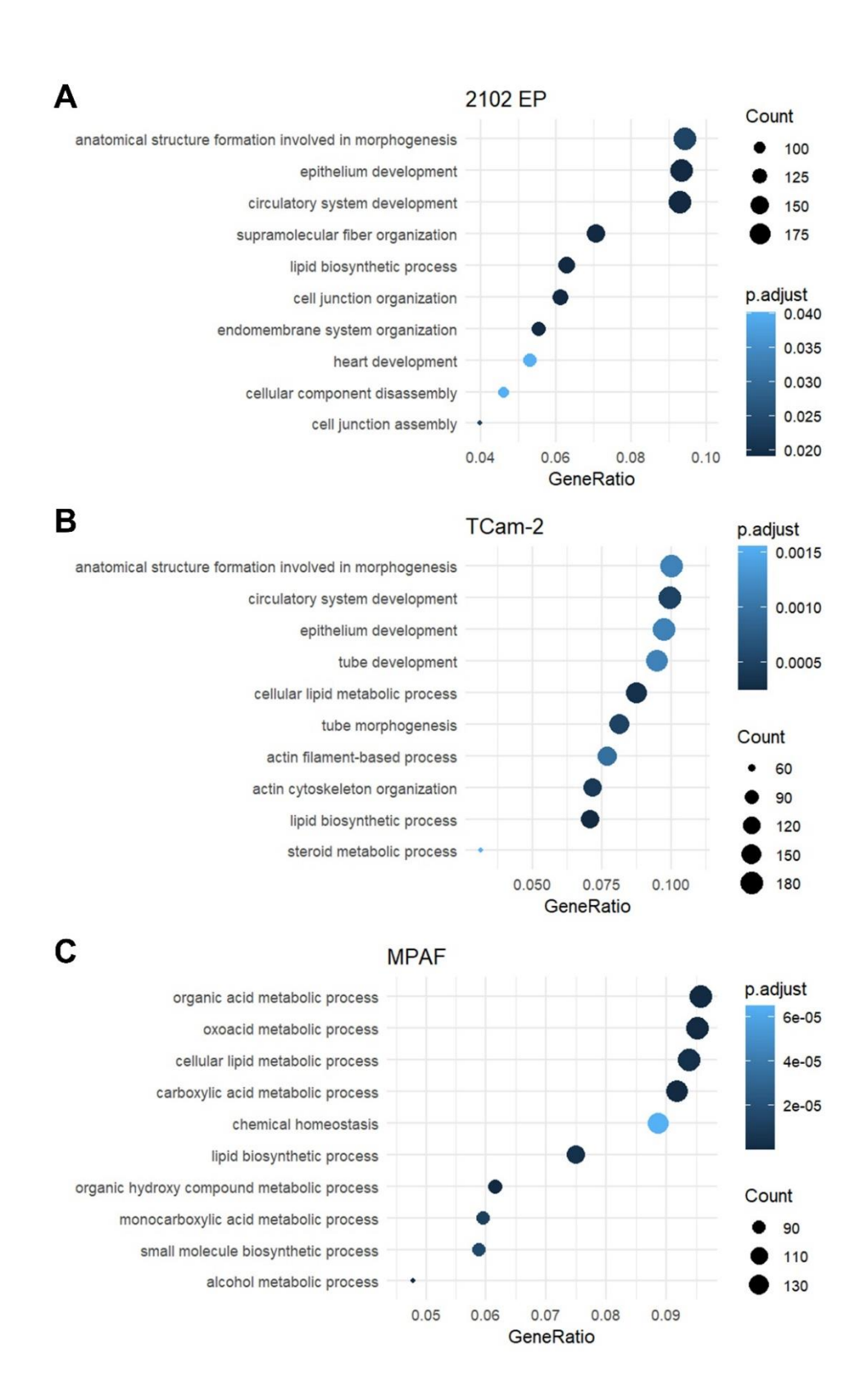


Figure 22: Epithelium development is enriched in 2102 EP and TCam-2 cells while metabolic processes are upregulated in MPAF cells. Dot plot of enrichment analysis of TOP 10 enriched biological processes based on all upregulated genes after 24 hours of I-BRD9 treatment compared to the DMSO control in (A) 2102 EP, (B) TCam-2 and (C) MPAF cells. Dot size displays the gene count associated with the GO term. Modified from ¹.

For validation in 2102 EP and TCam-2 cells different genes involved in epithelium development were selected based on the log₂ foldchange (log₂ foldchange >2). HSF4 was upregulated in both cell lines while SEMA3C, DLX6 and LEF1 were upregulated in 2102 EP cells and GATA5 as well as HEYL were enriched in TCam-2 cells. For 2102 EP cells SEMA3C and for TCam-2 cells GATA5 showed the strongest upregulation while HSF4 for 2102 EP and HEYL for TCam-2 cells showed the lowest log₂ foldchange (Figure 23 A). Validation was performed by qRT-PCR of the selected genes after 24 hours of treatment with I-BRD9 compared to DMSO treated cells. In 2102 EP cells, all four genes (HSF4, SEMA3C, DLX6 and LEF1) showed upregulation compared to the control. In line with the log₂ foldchanges in the RNAseq, SEMA3C showed the strongest upregulation while HSF4 was only slightly upregulated. TCam-2 cells also displayed upregulation of all three genes (HSF4, GATA5 and HEYL). HEYL showed the lowest upregulation while GATA5 was affected the most as already visible in the log₂ foldchanges (Figure 23 B). These data validate the upregulation of genes involved in epithelium development in 2102 EP and TCam-2 cells and suggest that differentiation of the TGCT cells was initiated.

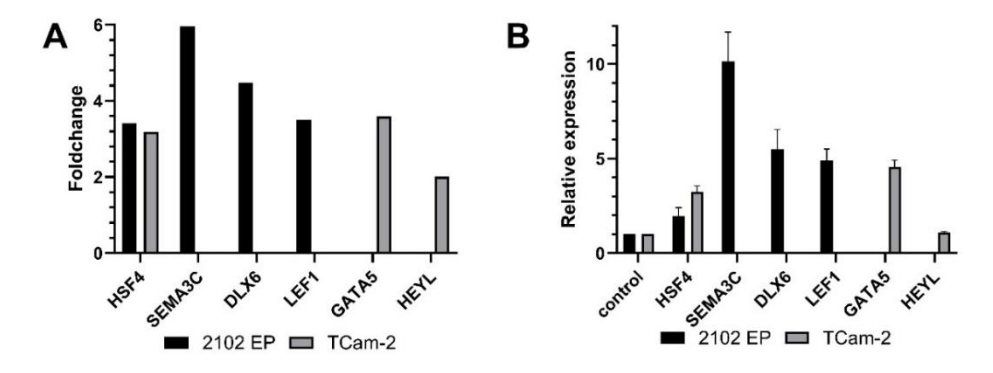


Figure 23: Genes associated with epithelium development were upregulated in 2102 EP and TCam-2 cells. (A) The log₂ foldchange of chosen validation genes in 2102 EP and TCam-2 cells after 24 hours of treatment with I-BRD9 in comparison to the DMSO control. (B) Relative expression of validation genes in 2102 EP and TCam-2 cells after BRD9 inhibition for 24 hours compared to DMSO treated control cells analyzed by qRT-PCR. Values were normalized to the housekeeping gene GAPDH. n=3. Modified from ¹.

Next, pathway analysis was performed for downregulated genes after 24 hours of treatment with I-BRD9 in comparison to DMSO treated control cells. In embryonal carcinoma (2102 EP) and seminoma (TCam-2) cells "signaling pathways regulating pluripotency of stem cells" were mostly affected (Figure 24 A, B). In addition, the

STRING interaction networks of genes associated with the GO term "stem cell population maintenance" (GO:0019827) in 2102 EP and TCam-2 cells were overlapping including pluripotency markers like NANOG, PRDM14 and KLF4 (Figure 24 D, E). In MPAF cells, pathway analysis revealed an enriched "p53 signaling pathway" while "signaling pathways regulating pluripotency of stem cells" were as expected not affected (Figure 24 C).

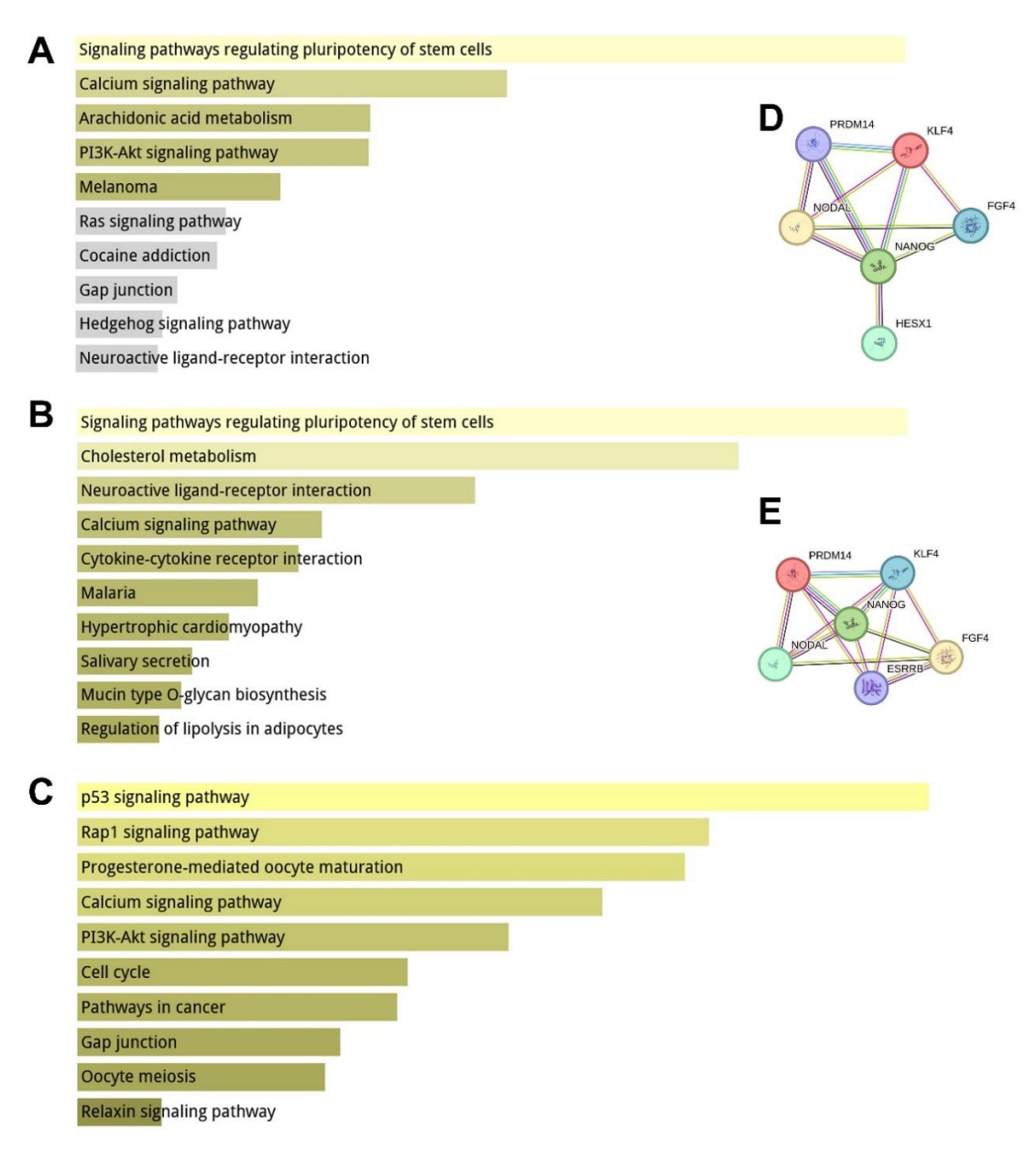


Figure 24: Downregulation of genes associated with stem cell population maintenance in 2102 EP and TCam-2 cells. Pathway analysis of downregulated genes in (A) 2102 EP, (B) TCam-2 and (C) MPAF cells after 24 hours of treatment with I-BRD9 compared to DMSO control analyzed with Enrichr. STRING interaction network of genes associated with stem cell population maintenance in (D) 2102 EP and (E) TCam-2 cells. Modified from ¹.

Downregulation of pluripotency markers was validated by qRT-PCR after 24 hours of BRD9 inhibition compared to the DMSO control. Five genes indicative of pluripotency were selected based on the log₂ foldchange (log₂ foldchange <-2). NANOG, NODAL KLF4, PRDM14 and FGF4 were all downregulated in both cell lines after 24 hours of I-BRD9 treatment. In 2102 EP cells, FGF4 showed the strongest downregulation while NODAL was the least affected. FGF4 was also the most affected gene in TCam-2 cells and KLF4 displayed the lowest downregulation (Figure 25 A). Relative mRNA levels were detected by qRT-PCR and showed downregulation for all genes in both cell lines. NANOG and FGF4 displayed the strongest downregulation while KLF4 was the least affected (Figure 25 B).

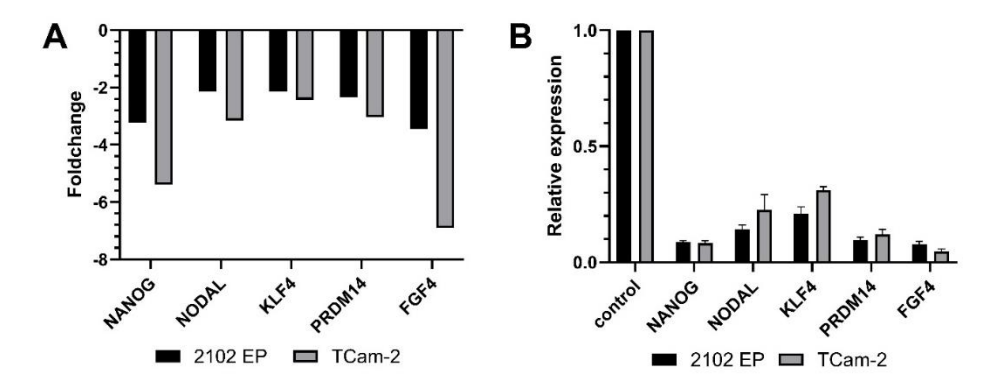


Figure 25: Stem cell population maintenance associated genes were downregulated in 2102 EP and TCam-2 cells. (A) The log₂ foldchange of chosen validation genes in 2102 EP and TCam-2 cells after BRD9 inhibition for 24 hours compared to DMSO treated cells. (B) Relative expression of validation genes in 2102 EP and TCam-2 cells after treatment with I-BRD9 for 24 hours in comparison with DMSO control analyzed by qRT-PCR. Normalization to the housekeeping gene GAPDH was performed. n=3. Modified from ¹.

Validation of downregulation of pluripotency markers was also performed on protein level by immunofluorescence staining. 2102 EP and TCam-2 cells were treated for 72 hours with I-BRD9 or DMSO and stainings against NANOG and PRDM14 were performed. For NANOG as well as PRDM14 a strong signal was detected in DMSO treated control cells while signal was absent after BRD9 inhibition in both cell lines (Figure 26, Figure 27).

Validation was successful on RNA and protein level for pluripotency markers in 2102 EP and TCam-2 cells.

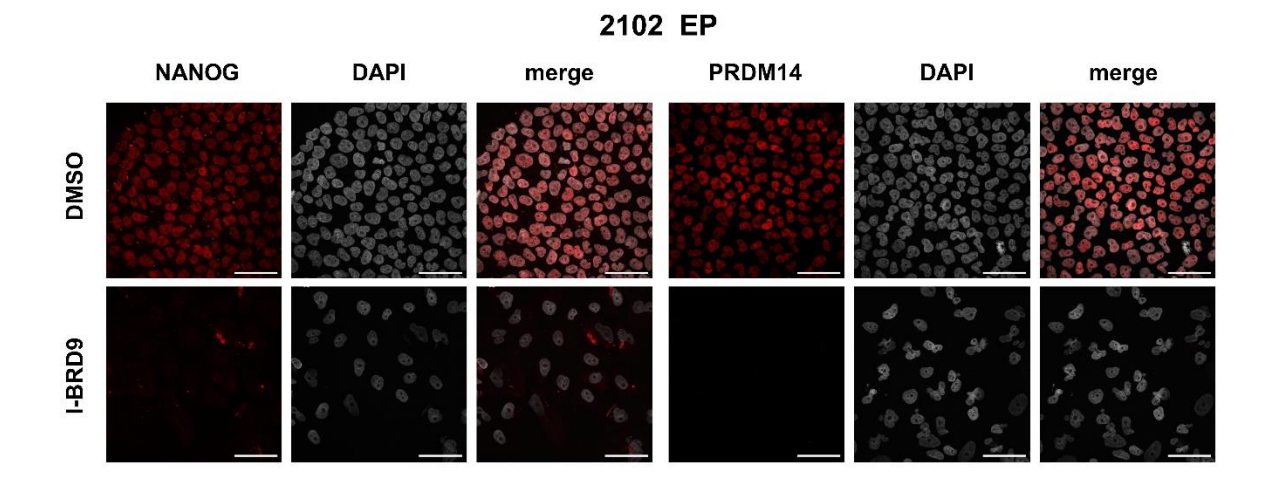


Figure 26: NANOG and PRDM14 were downregulated in 2102 EP cells on protein level. Immunofluorescence staining of NANOG (left panel) and PRDM14 (right panel) after 72 hours of BRD9 inhibition (lower panel) or DMSO control (upper panel) in 2102 EP cells. Target proteins (NANOG and PRDM14) were visualized in red while cell nuclei were depicted in grey. Nuclei were stained with DAPI. Scale bar: 50 μM. Modified from ¹.

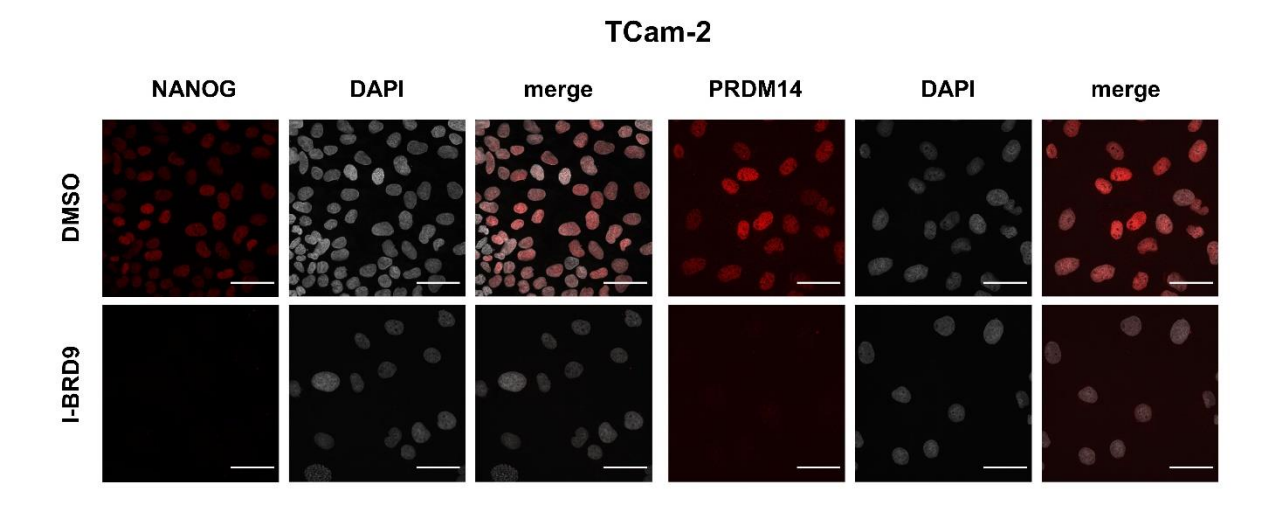


Figure 27: NANOG and PRDM14 were downregulated in TCam-2 cells on protein level. Immunofluorescence staining of NANOG (left panel) and PRDM14 (right panel) after 72 hours of BRD9 inhibition (lower panel) or DMSO control (upper panel) in TCam-2 cells. Target proteins (NANOG and PRDM14) were visualized in red while cell nuclei were depicted in grey. Nuclei were stained with DAPI. Scale bar: $50~\mu M$. Modified from 1 .

In summary, BRD9 inhibition led to induction of epithelial differentiation while pluripotency markers were downregulated in embryonal (2102 EP) and seminoma (TCam-2) cells. On the other hand, control cells (MPAF) showed upregulation of metabolic processes and downregulation of p53 signaling pathways.

4.5 Confirmation of induction of apoptosis and cell cycle arrest on transcriptome level

FACS analysis showed induction of apoptosis and cell cycle arrest after I-BRD9 treatment in TGCT cell lines compared to DMSO treated control cells (4.3). Here, the effect of BRD9 inhibition on the transcriptome level in context of deregulations in genes important for apoptosis and cell cycle was confirmed.

RNAseq analysis showed upregulation of genes involved in "apoptotic process" (GO term: 0006915) after 24 hours of I-BRD9 treatment. In embryonal carcinoma cells (2102 EP) a total of 38 genes associated with apoptotic processes were upregulated while in seminoma cells (TCam-2) 15 genes showed upregulation confirming induction of apoptosis by I-BRD9 treatment. TNF is the most upregulated gene in both 2102 EP (log₂ foldchange: 4.8) and TCam-2 (log₂ foldchange: 3.6) (Figure 28 A, B). On the other hand, control cells (MPAF) also showed upregulation of 18 genes involved in apoptotic processes (Figure 28 C). This contrasts with the FACS analysis where MPAF cells displayed no significant changes in apoptotic cells after 24 or 48 hours of treatment with I-BRD9 (4.3).

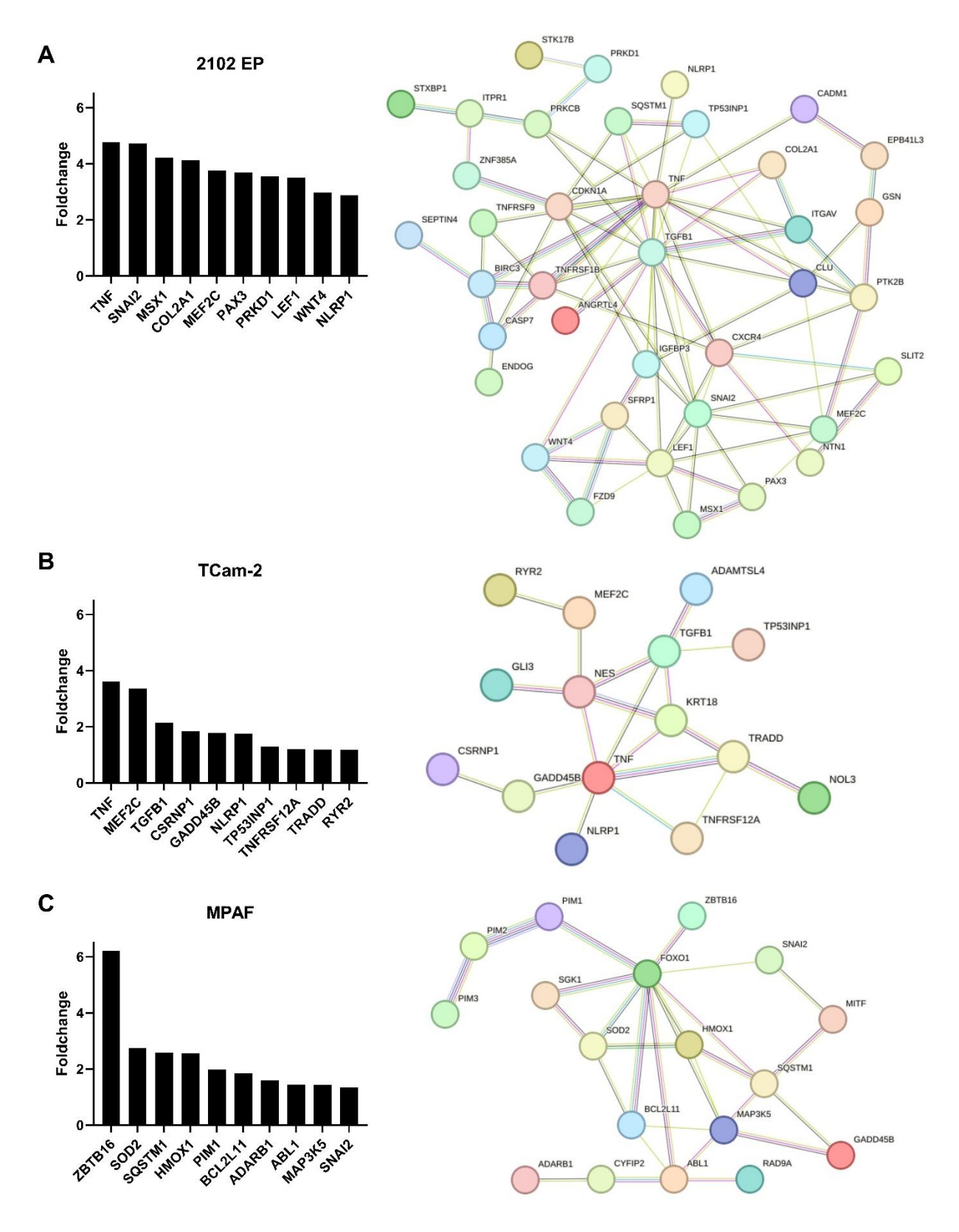


Figure 28: Transcriptome analysis confirmed induction of apoptosis. RNAseq analysis was performed in 2102 EP, TCam-2 and MPAF cells after 24 hours of I-BRD9 treatment. STRING interaction network of genes involved in the GO term "apoptotic process" as well as log₂ foldchanges of TOP10 upregulated genes for (A) 2102 EP, (B) TCam-2 and (C) MPAF cells. n=3.

In embryonal carcinoma cells (2102 EP) 11 genes associated with "cell cycle process" (GO term: 0022402) were downregulated while seminoma cells (TCam-2) displayed downregulation of 23 genes. CHEK2 was downregulated in both 2102 EP (log₂ foldchange: 1.3) and TCam-2 (log₂ foldchange: 1.3) (Figure 29). This is in line with the findings of FACS analysis revealing induction of cell cycle arrest after 24 hours of I-BRD9 treatment (4.3).

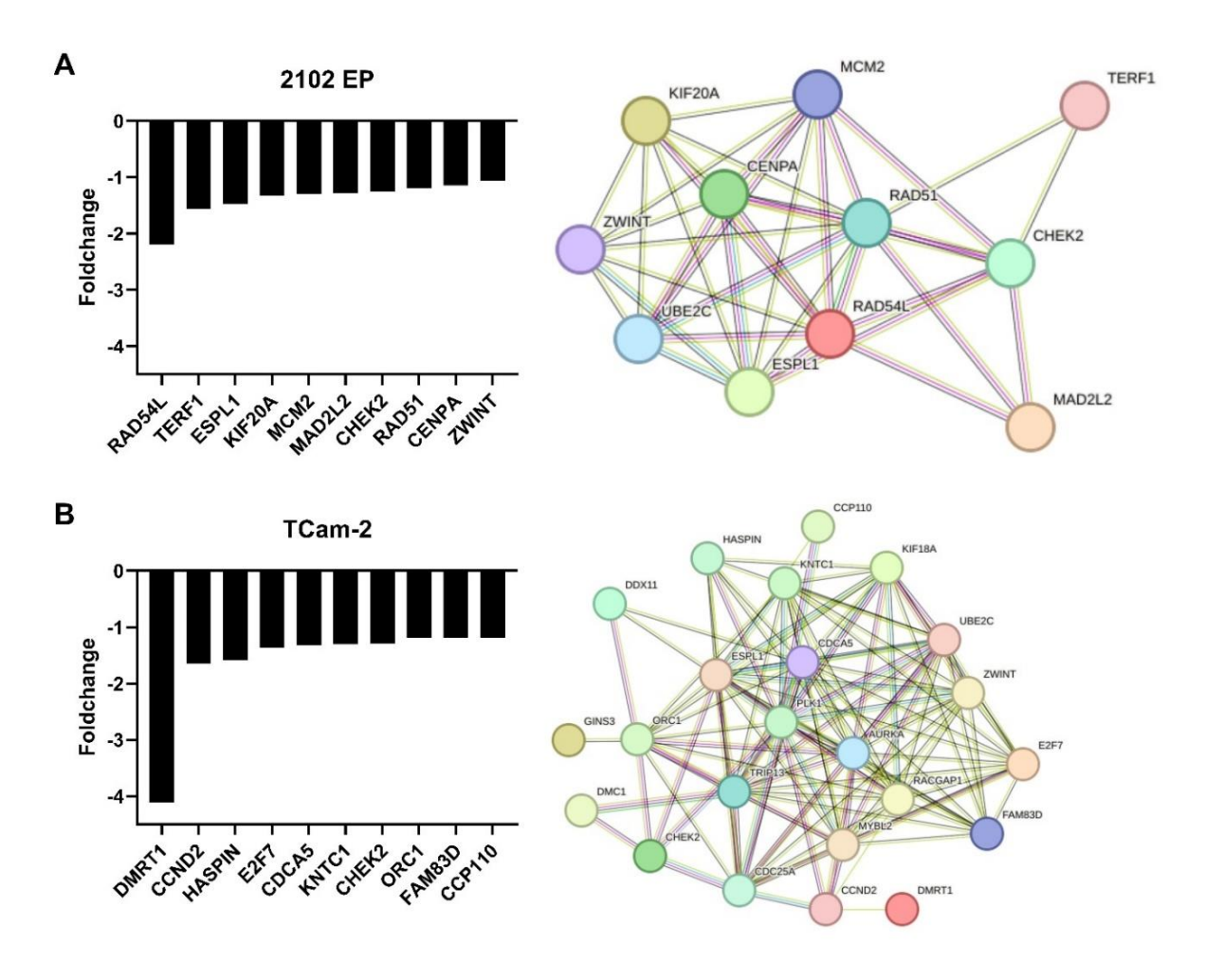


Figure 29: Transcriptome analysis confirmed induction of cell cycle arrest. RNAseq analysis was performed in 2102 EP, TCam-2 and MPAF cells after 24 hours of I-BRD9 treatment. STRING interaction network of downregulated genes involved in cell cycle processes and log₂ foldchanges of TOP10 downregulated genes in (A) 2102 EP and (B) TCam-2 cells. n=3.

Induction of apoptosis in 2102 EP and TCam-2 cells was confirmed on RNA level by the upregulation of genes associated with apoptotic processes. In contrast, also MPAF cells showing no induction of apoptosis in FACS analysis displayed upregulation of genes involved in apoptotic processes. Cell cycle distributions found in 2102 EP and TCam-2 cell by FACS analysis were validated on RNA level by downregulation of genes involved in cell cycle processes.

5 DISCUSSION

This project showed that the inhibition of BRD9 with the inhibitor I-BRD9 might be an effective treatment alternative for TGCTs. Application of I-BRD9 resulted in severe effects like decrease of viability, induction of apoptosis as well as G1-phase cell cycle arrest in TGCT cell lines while the control cells remained only slightly affected. Transcriptome analysis revealed loss of the pluripotency state along with differentiation towards an epithelial cell fate.

First, the expression of the target BRD9 was analyzed. Meta-analysis of microarray data in TGCT tissues revealed heterogeneous expression with the highest expression in embryonal carcinoma while the lowest expression was found in GCNIS. Normal testis tissue showed also high expression of BRD9 on RNA level. On the other hand, a TMA displayed the highest BRD9 protein levels in GCNIS while normal testis tissue revealed the lowest expression. In TGCT cell lines meta-analysis of microarray data showed expression of BRD9 in all TGCT cell lines while the control cell line MPAF displayed the lowest expression. On protein level a comparable BRD9 abundance was visible compared to RNA level. BRD9 expression in TGCTs on protein level along with low abundance in controls indicated a good starting point for targeting BRD9 in TGCT cell lines. Viability assays after treatment with I-BRD9 displayed cytotoxic effects in a dose- and time-dependent manner in all TGCT cell lines. The strongest cytotoxicity was detected in the embryonal carcinoma cell line NCCIT while the sertoli cells (FS1) were only slightly affected and the fibroblasts (MPAF) showed no effect by the I-BRD9 treatment. In line, the IC₅₀ values showed the highest sensitivity for I-BRD9 in NCCIT cells (6 µM) while MPAF cells revealed IC₅₀ values above 500 µM. FACS analysis showed induction of apoptosis already after 24 hours of treatment with I-BRD9 in all TGCT cell lines and in most cell lines an even stronger induction after 48 hours. The control cells (FS1 and MPAF) displayed no significant increase in apoptosis. Again, an embryonal carcinoma cell line (NCCIT-R) showed the strongest effect. Cell cycle distribution analysis via FACS revealed G1-phase cell cycle arrest already 24 hours after BRD9 inhibition in all TGCT cell lines. While the strongest arrest was visible in embryonal carcinoma cells (NCCIT and NT2/D1-R) the sertoli cells (FS1) showed no induction of cell cycle arrest. Transcriptome analysis in embryonal carcinoma (2102 EP) and seminoma (TCam-2) revealed downregulation of a prominent network of pluripotency markers along with upregulation of genes involved in epithelium

development. Of note, these changes on transcriptome level were not detected in the fibroblasts (MPAF).

In our experiments the embryonal carcinoma cell lines showed the strongest effects after BRD9 inhibition indicating I-BRD9 as a possible alternative treatment option especially for embryonal carcinomas. In line, the BRD4 inhibitor JQ1 also displayed stronger impact on apoptosis in embryonal carcinoma cells compared to seminomas ⁹⁵

I-BRD9 application showed no significant differences between parental and cisplatinresistant subclones in our analyses. The role of BRD9 in cisplatin resistance is still elusive. In locally advanced cervical cancer (LACC) methylation of the BRD9 promoter region and therefore low expression levels of BRD9 led to higher sensitivity to cisplatinradiotherapy ¹⁴⁵. Furthermore, in BRD9 overexpressing gastric cancer cells BRD9 inhibitors enhanced the sensitivity to cisplatin ¹⁴⁶. Zhou et al. found that in ovarian cancer cells I-BRD9 treatment reduced homologous recombination (HR) and resensitized the cells to cisplatin. Three BRD-containing proteins (BRD9, ZMYND8 and ASH1L) comprise a high HR signature and positively influence HR. BRD9 especially plays an important role in homologous recombination by orchestrating RAD54-RAD51 interaction. BRD9 is recruited by RAD51 leading to the binding of BRD9 to K515 acetylation on RAD54 which is induced by DNA damage. Therefore, BRD9 enhances the interaction of RAD54 and RAD51. Upon binding, RAD51 forms filaments on singlestrand DNA leading to the search for homologous sequences on the intact DNA strand which are used as a model for error-free repair. This leads to the conclusion that BRD9 might be a possible treatment target for HR-proficient tumors 147. Deficiencies in homologous recombination mechanisms (HRR) are known to be involved in cisplatin ³⁹. For example, in ovarian and breast cancer BRCA1 and BRCA2 which code for proteins of the HRR machinery comprise mutations. BRCA2 has a key function in HR while BRCA1 is also involved in cell cycle-checkpoint control, chromatin remodeling and DNA repair indicating its role in carcinogenesis. BRCA1 and BRCA2 together with RAD51 induce HR and double-strand break repair. Cells that express mutated BRCA1 and BRCA2 are more sensitive to ionizing radiation and the following repair is errorprone ⁵³. Not only BRCA1, BRCA2 and RAD51, but also other genes (BRAD1, BRIP1, ATM, NBS1, CHEK2 and PALB2) of the HR pathway are known to be involved in inherited susceptibility for different cancer types. The first step of HR is the sensing of double-strand breaks. Here, NBS1 is necessary to recruit ATM to the damaged site leading to induction of checkpoint activation. ATM in combination with CHEK2 initiates phosphorylation of downstream proteins including p53 and BRCA1. BARD1 and BRIP1 assist BRCA1 in the assembly with other proteins involved in the repair. PALB2 is a linker between BRCA1 and BRCA2 and mediates the recruitment of RAD51 initiating the HR by DNA synthesis ¹⁴⁸. CHEK2 and ATM are the most common breast cancer susceptibility genes while BRIP1 is highly associated with susceptibility in ovarian cancer ^{149,150}. BARD1 and PALB2 are also involved in breast cancer susceptibility ^{151,152}. In general, deficiency in HRR is correlated with higher sensitivity to cisplatin. These findings suggest that BRD9 might play a role in cisplatin resistance but in this study the question cannot be answered. The origin of the cisplatin resistance in our cisplatin-resistant cell lines is unclear. Therefore, BRD9 involvement in resistance mechanisms needs to be investigated.

Interestingly, the control cell lines FS1 (sertoli cells) showed only slight sensitivity to I-BRD9 indicating weak side-effects on healthy testis tissue and the control cell line MPAF (fibroblasts) revealed no sensitivity to I-BRD9 application indicative for only slight or no effect on somatic cells. In fact, I-BRD9 was already tested in a mouse xenograft with colon adenocarcinoma cells and no side-effects were reported ¹¹⁹. Nevertheless, side-effects were only studied in control cells implying the need for further investigation of possible side-effects in healthy testis tissue.

Interfering with the epigenetic landscape and targeting bromodomain-containing proteins has already been shown to be effective. In colon cancer cells depletion of BRD8 significantly reduced cell viability and induced G1-phase cell cycle arrest and apoptosis ¹⁵³. The BRD4 inhibitor JQ1 led to induction of apoptosis as well as G1/G0-phase cell cycle arrest in TGCT cell lines ⁹⁵. Similar results were obtained by the epigenetic readers LP99 (targeting BRD7 and BRD9) as well as MZ-1 which is a proteolysis targeting chimera (PROTAC) targeting BRD4. Both reduced cell viability and induced apoptosis and cell cycle arrest in TGCT cell lines ¹⁵⁴. BRD9 inhibition showed already antitumor effects in different tumor entities. BI-7273 and BI-9564 both targeting BRD9 resulted in reduced growth of acute myeloid leukemia cells (AML) ¹¹⁰. The effect of I-BRD9 was also studied in AML cells resulting in reduced proliferation dependent on cell cycle inhibition and apoptosis ¹¹⁷. In rhabdoid tumor cells I-BRD9 led to reduced cell proliferation and induced G1-phase cell cycle arrest ¹²⁰. Application

of I-BRD9 in colon cancer cells decreased cell growth in vitro and arrested tumor growth in xenografted mice after BRD9 inhibition in vivo ¹¹⁹. In gallbladder cancer I-BRD9 significantly affected cell proliferation and reduced tumor growth in mouse tumor models ¹¹⁸. Inhibition of BRD9 in uterine fibroid cells reduced cell proliferation as well as induced apoptosis and G1-phase cell cycle arrest ¹⁵⁵. Taken together, BRD9 inhibition by I-BRD9 led to reduced viability, cell cycle arrest as well as apoptosis in different tumor entities which is in line with our findings in TGCT cell lines.

Despite the inhibition of BRD9 also degradation and depletion of BRD9 revealed severe effects in different tumor entities. The BRD9 degrader QA-68 induces ubiquitination and degradation of BRD9 therefore reducing cell proliferation of AML cells. The authors also investigated BRD9 CRISPR knockout as well as doxycyclineinduced knockdown of BRD9 in AML cell lines again resulting in decreased cell growth ¹⁵⁶. Another BRD9 degrader, dBRD9-A, led to reduced viability as well as cell cycle arrest in synovial sarcoma cell lines. Furthermore, an in vivo xenograft model treated with the BRD9 degrader showed decreased tumor progression ¹⁵⁷. In AML cells the shRNA-mediated BRD9 depletion resulted in reduced cell survival as well as induction of G0/G1-phase cell cycle arrest and apoptosis ¹⁵⁸. Depletion of BRD9 by siRNA in squamous cell lung cancer cells resulted in inhibited cell proliferation ¹⁰⁸. In prostate cancer using shRNA for knockdown of BRD9 led to decreased cell viability and furthermore a xenograft mouse model treated with shRNA targeting BRD9 revealed reduced tumor growth. In addition, the BRD9 PROTAC degrader dBRD9 decreased cell proliferation in prostate cancer cell lines ¹⁵⁹. In summary, the studies show that interfering with BRD9 by inhibition, depletion or degradation resulted in reduced cell viability as well as induction of cell cycle arrest and apoptosis in different tumor entities which is in line with the effects of I-BRD9 application in TGCT cell lines and stresses the possibility of targeting BRD9 as potential treatment option.

Treatment with I-BRD9 led to loss of pluripotency as well as differentiation towards an epithelial cell fate in embryonal carcinoma (2102 EP) and seminoma (TCam-2) cells. In fact, retinoic acid induced differentiation was already studied in different testicular germ cell tumor cell lines. Application of retinoic acid in embryonal carcinoma cells led to alterations of expression of WNT2B, FZD5, FZD6, FZD10, SFRP1 and SFRP4 resulting in a reprogrammed WNT signaling pathway and therefore induction of canonical WNT signaling ¹⁶⁰. The embryonal carcinoma cell line NT2/D1 differentiates

towards a neuronal cell fate after retinoic acid treatment along with reduction of cell growth and tumorigenicity ^{123,161}. Retinoic acid application in the embryonal carcinoma cell line NTera2 led to significant downregulation of genes involved in DNA mismatch repair like PMS2, MLH1, MSH2 and EXO1 as well as pluripotency factors including OCT4 and NODAL ¹⁶². In fact, exit of pluripotency along with induction of differentiation seems to be a common response of GCT reacting to drugs. In TGCT cell lines the inhibition of BRD4 by JQ1 led to downregulation of pluripotency markers including LIN28, ZSCAN10 and UTF1 along with upregulation of mesodermal differentiation marker HAND1 leading to the conclusion that the cells exit the pluripotency state and differentiate towards a mesodermal cell fate 95. Funke et al. found that neddylation pathway inhibition by the NAE1 inhibitor MLN4924 induced upregulation of cell differentiation markers like HAND1, CLDN1, SOX15 and CDX2 in 2102 EP cells indicating mesoderm/ endoderm differentiation. Again, downregulation of pluripotency markers including SOX21, SOX2, TCFL1, KLF15 and HESX1 was detected indicative for loss of pluripotency and induction of mesodermal/ endodermal differentiation ¹⁶³. In fact, this is in line with our findings showing downregulation of a prominent network of pluripotency markers including NANOG, KLF4, PRDM14 and NODAL while genes involved in epithelium development were upregulated. In conclusion, loss of pluripotency along with differentiation seems to be a common aspect in TGCT cell lines after application of different drugs.

Of note, differentiation therapy is an approach where differentiating agents induce tumor reprogramming and therefore leading to reduce proliferative capacity and induce terminal differentiation 164 . Application of berberin, a plant-alkaloid, reduced cancer stemness markers including N-MYC, β -catenin, CD133, NOTCH2, SOX2 and Nestin along with increase of neuronal differentiation markers like NCAM, MAP2 and β -III tubulin generating viable neurons in neuroblastoma cells 165 . Treatment with differentiating agents salinomycin and thioridazine resulted in differentiation of embryonal carcinoma cells as well as decreased expression of pluripotency markers like OCT4. In xenografted mice thioridazine application increased survival and decreased the amount of pluripotent cells in the tumor and therefore reduced tumorigenicity 166 . This underlines our conclusion, that I-BRD9 treatment in TGCT cells could induce terminal differentiation and therefore reduce the risk of progression of the tumor as well as reduction of cytotoxicity of standard chemotherapies.

The next step of testing the suitability of I-BRD9 as a potential treatment option for TGCTs would be to use other models than cell lines. Cell line-derived and patient-derived xenograft models could be used. The cell line-derived xenografts are easily available and have a rapid growth rate while they lack heterogeneity as well as the tumor microenvironment. Patient-derived xenograft models enable studies retaining the heterogeneity, mutations as well as microenvironment and the model allows for personalized medicine. A limitation is the use of immune suppressed mice ¹⁶⁷. Another possibility is the use of 3D culture methods from embryonic or adult stem cells which comprise self-organizing abilities leading to the formation of organoids allowing for studying human pathologies in vitro. In addition, patient-derived organoids can be used for personalized medicine ¹⁶⁸. Cancer organoids resemble human tumors and enable not only drug screening but additionally basic research ¹⁶⁹. An in vitro testis organoid model was established to study reproductive toxicants providing a promising model for reproductive toxicology investigations ¹⁷⁰. Unfortunately, no TGCT organoids are described yet indicating necessity for further research.

In conclusion, the treatment of TGCT cell lines with I-BRD9 led to severe effects like reduction of cell viability as well as induction of cell cycle arrest in G1-phase and apoptosis while the control cell lines remained only slightly effected. I-BRD9 induced loss of pluripotency in embryonal carcinoma and seminoma cells along with differentiation towards an epithelial cell fate indicating terminal differentiation as a benefit of BRD9 inhibition. Most importantly, the findings suggest I-BRD9 as a potential alternative treatment option for TGCTs.

6 BIBLIOGRAPHY

- 1. Hansen A, Sanders C, Fronhoffs F, Funke K, Kristiansen G, Schorle H. BRD9 inhibition as potential treatment option for testicular germ cell tumors. *Andrology*. Published online April 1, 2025:1-14. doi:10.1111/andr.70038
- 2. Ben Maamar M, Nilsson EE, Skinner MK. Epigenetic transgenerational inheritance, gametogenesis and germline development†. *Biol Reprod.* 2021;105(3):570-592. doi:10.1093/biolre/ioab085
- 3. Kojima Y, Sasaki K, Yokobayashi S, et al. Evolutionarily Distinctive Transcriptional and Signaling Programs Drive Human Germ Cell Lineage Specification from Pluripotent Stem Cells. *Cell Stem Cell*. 2017;21(4):517-532.e5. doi:10.1016/j.stem.2017.09.005
- 4. Saitou M, Yamaji M. Primordial Germ Cells in Mice. *Cold Spring Harb Perspect Biol.* 2012;4(11):a008375. doi:10.1101/cshperspect.a008375
- 5. Nicholls PK, Schorle H, Naqvi S, et al. Mammalian germ cells are determined after PGC colonization of the nascent gonad. *Proc Natl Acad Sci U S A*. 2019;116(51):25677-25687. doi:10.1073/pnas.1910733116
- 6. Tang WWC, Kobayashi T, Irie N, Dietmann S, Surani MA. Specification and epigenetic programming of the human germ line. *Nat Rev Genet*. 2016;17(10):585-600. doi:10.1038/nrg.2016.88
- 7. Nettersheim D, Jostes S, Schneider S, Schorle H. Elucidating human male germ cell development by studying germ cell cancer. *Reproduction*. 2016;152(4):R101-R113. doi:10.1530/REP-16-0114
- 8. Weber S, Eckert D, Nettersheim D, et al. Critical Function of AP-2gamma/TCFAP2C in Mouse Embryonic Germ Cell Maintenance1. *Biology of Reproduction*. 2010;82(1):214-223. doi:10.1095/biolreprod.109.078717
- Lin Y, Gill ME, Koubova J, Page DC. Germ Cell-Intrinsic and -Extrinsic Factors Govern Meiotic Initiation in Mouse Embryos. Science. 2008;322(5908):1685-1687. doi:10.1126/science.1166340

- Neto FTL, Bach PV, Najari BB, Li PS, Goldstein M. Spermatogenesis in humans and its affecting factors. Seminars in Cell & Developmental Biology. 2016;59:10-26. doi:10.1016/j.semcdb.2016.04.009
- 11. Laronda MM. Factors within the Developing Embryo and Ovarian Microenvironment that Influence Primordial Germ Cell Fate. Sex Dev. 2023;17(2-3):134-144. doi:10.1159/000528209
- 12. Oosterhuis JW, Looijenga LHJ. Human germ cell tumours from a developmental perspective. *Nat Rev Cancer*. 2019;19(9):522-537. doi:10.1038/s41568-019-0178-9
- 13. Roelen BAJ, Chuva de Sousa Lopes SM. Stay on the road: from germ cell specification to gonadal colonization in mammals. *Philos Trans R Soc Lond B Biol Sci*. 377(1865):20210259. doi:10.1098/rstb.2021.0259
- 14. Cancer. Accessed January 28, 2025. https://www.who.int/health-topics/cancer#tab=tab_1
- 15. Ferlay J, Ervik M, Lam F, et al. Global Cancer Observatory: Cancer Today. Lyon, France: International Agency for Research on Cancer. doi:Available from: https://gco.iarc.who.int/today, accessed [28/1/2025].
- 16. Ehrlich Y, Margel D, Lubin MA, Baniel J. Advances in the treatment of testicular cancer. *Transl Androl Urol*. 2015;4(3):381-390. doi:10.3978/j.issn.2223-4683.2015.06.02
- 17. van de Geijn GJM, Hersmus R, Looijenga LHJ. Recent developments in testicular germ cell tumor research. *Birth Defects Res C Embryo Today*. 2009;87(1):96-113. doi:10.1002/bdrc.20140
- 18. Fukawa T, Kanayama H omi. Current knowledge of risk factors for testicular germ cell tumors. *International Journal of Urology*. 2018;25(4):337-344. doi:10.1111/iju.13519

- 19. Greene MH, Kratz CP, Mai PL, et al. Familial testicular germ cell tumors in adults: 2010 summary of genetic risk factors and clinical phenotype. *Endocr Relat Cancer*. 2010;17(2):R109-R121. doi:10.1677/ERC-09-0254
- 20. Oosterhuis JW, Looijenga LHJ. Testicular germ-cell tumours in a broader perspective. *Nat Rev Cancer*. 2005;5(3):210-222. doi:10.1038/nrc1568
- 21. Cuevas-Estrada B, Montalvo-Casimiro M, Munguia-Garza P, Ríos-Rodríguez JA, González-Barrios R, Herrera LA. Breaking the Mold: Epigenetics and Genomics Approaches Addressing Novel Treatments and Chemoresponse in TGCT Patients. *Int J Mol Sci.* 2023;24(9):7873. doi:10.3390/ijms24097873
- 22. Irie N, Weinberger L, Tang WWC, et al. SOX17 Is a Critical Specifier of Human Primordial Germ Cell Fate. Cell. 2015;160(1-2):253-268. doi:10.1016/j.cell.2014.12.013
- 23. de Jong J, Stoop H, Gillis A, et al. Differential expression of SOX17 and SOX2 in germ cells and stem cells has biological and clinical implications. *The Journal of Pathology*. 2008;215(1):21-30. doi:10.1002/path.2332
- 24. Nonaka D. Differential Expression of SOX2 and SOX17 in Testicular Germ Cell Tumors. *American Journal of Clinical Pathology*. 2009;131(5):731-736. doi:10.1309/AJCP7MNCNBCRN8NO
- 25. Oldenburg J, Berney DM, Bokemeyer C, et al. Testicular seminoma and non-seminoma: ESMO-EURACAN Clinical Practice Guideline for diagnosis, treatment and follow-up☆. *Annals of Oncology*. 2022;33(4):362-375. doi:10.1016/j.annonc.2022.01.002
- 26. Koši Kunac A, Gnjidić M, Antunac Golubić Z, Gamulin M. Treatment of germ cell testicular cancer. *Acta Clin Croat*. 2020;59(3):496-504. doi:10.20471/acc.2020.59.03.14
- 27. Daugaard G, Gundgaard MG, Mortensen MS, et al. Surveillance for stage I nonseminoma testicular cancer: outcomes and long-term follow-up in a population-based cohort. *J Clin Oncol*. 2014;32(34):3817-3823. doi:10.1200/JCO.2013.53.5831

- 28. Ghosh S. Cisplatin: The first metal based anticancer drug. *Bioorganic Chemistry*. 2019;88:102925. doi:10.1016/j.bioorg.2019.102925
- 29. Dasari S, Tchounwou PB. Cisplatin in cancer therapy: molecular mechanisms of action. *Eur J Pharmacol*. 2014;740:364-378. doi:10.1016/j.ejphar.2014.07.025
- 30. Zhang C, Xu C, Gao X, Yao Q. Platinum-based drugs for cancer therapy and anti-tumor strategies. *Theranostics*. 2022;12(5):2115-2132. doi:10.7150/thno.69424
- 31. Kelland L. The resurgence of platinum-based cancer chemotherapy. *Nat Rev Cancer*. 2007;7(8):573-584. doi:10.1038/nrc2167
- 32. Alderden RA, Hall MD, Hambley TW. The Discovery and Development of Cisplatin. *J Chem Educ*. 2006;83(5):728. doi:10.1021/ed083p728
- 33. Ries L, Young J, Keel G, Eisner M, Lin Y, Horner MJ. SEER Survival Monograph: Cancer Survival Among Adults: U.S. SEER Program, 1988-2001, Patient and Tumor Characteristics. In: *SEER*. National Cancer Institute, SEER Program, NIH Pub. No. 07-6215, Bethesda, MD, 2007.
- 34. Vries G de, Rosas-Plaza X, Vugt MATM van, Gietema JA, Jong S de. Testicular cancer: Determinants of cisplatin sensitivity and novel therapeutic opportunities. *Cancer Treatment Reviews*. 2020;88. doi:10.1016/j.ctrv.2020.102054
- 35. Jordan P, Carmo-Fonseca* M. Molecular mechanisms involved in cisplatin cytotoxicity. *Cell Mol Life Sci.* 2000;57(8-9):1229-1235. doi:10.1007/PL00000762
- 36. Koster R, Timmer-Bosscha H, Bischoff R, Gietema JA, de Jong S. Disruption of the MDM2–p53 interaction strongly potentiates p53-dependent apoptosis in cisplatin-resistant human testicular carcinoma cells via the Fas/FasL pathway. *Cell Death Dis*. 2011;2(4):e148. doi:10.1038/cddis.2011.33
- 37. Wermann H, Stoop H, Gillis AJ, et al. Global DNA methylation in fetal human germ cells and germ cell tumours: association with differentiation and cisplatin resistance.

 The Journal of Pathology. 2010;221(4):433-442. doi:10.1002/path.2725

- 38. Singh R, Fazal Z, Freemantle SJ, Spinella MJ. Mechanisms of cisplatin sensitivity and resistance in testicular germ cell tumors. *Cancer Drug Resist*. 2019;2(3):580-594. doi:10.20517/cdr.2019.19
- 39. Lugones Y, Loren P, Salazar LA. Cisplatin Resistance: Genetic and Epigenetic Factors Involved. *Biomolecules*. 2022;12(10):1365. doi:10.3390/biom12101365
- 40. Galluzzi L, Senovilla L, Vitale I, et al. Molecular mechanisms of cisplatin resistance. *Oncogene*. 2012;31(15):1869-1883. doi:10.1038/onc.2011.384
- 41. Jostes S, Nettersheim D, Schorle H. Epigenetic drugs and their molecular targets in testicular germ cell tumours. *Nat Rev Urol*. 2019;16(4):245-259. doi:10.1038/s41585-019-0154-x
- 42. Safaei R, Howell SB. Copper transporters regulate the cellular pharmacology and sensitivity to Pt drugs. *Critical Reviews in Oncology/Hematology*. 2005;53(1):13-23. doi:10.1016/j.critrevonc.2004.09.007
- 43. Ishida S, McCormick F, Smith-McCune K, Hanahan D. Enhancing tumor-specific uptake of the anticancer drug cisplatin with a copper chelator. *Cancer Cell*. 2010;17(6):574-583. doi:10.1016/j.ccr.2010.04.011
- 44. More SS, Akil O, Ianculescu AG, Geier EG, Lustig LR, Giacomini KM. Role of the Copper Transporter, CTR1, in Platinum-Induced Ototoxicity. *J Neurosci*. 2010;30(28):9500-9509. doi:10.1523/JNEUROSCI.1544-10.2010
- 45. Chen HHW, Kuo MT. Role of Glutathione in the Regulation of Cisplatin Resistance in Cancer Chemotherapy. *Met Based Drugs*. 2010;2010:430939. doi:10.1155/2010/430939
- 46. Kasahara K, Fujiwara Y, Nishio K, et al. Metallothionein content correlates with the sensitivity of human small cell lung cancer cell lines to cisplatin. *Cancer Res*. 1991;51(12):3237-3242.

- 47. Masters JR, Thomas R, Hall AG, et al. Sensitivity of testis tumour cells to chemotherapeutic drugs: role of detoxifying pathways. *Eur J Cancer*. 1996;32A(7):1248-1253. doi:10.1016/0959-8049(96)00033-0
- 48. Wood RD, Araújo SJ, Ariza RR, et al. DNA damage recognition and nucleotide excision repair in mammalian cells. *Cold Spring Harb Symp Quant Biol*. 2000;65:173-182. doi:10.1101/sqb.2000.65.173
- 49. Bellmunt J, Paz-Ares L, Cuello M, et al. Gene expression of ERCC1 as a novel prognostic marker in advanced bladder cancer patients receiving cisplatin-based chemotherapy. *Ann Oncol.* 2007;18(3):522-528. doi:10.1093/annonc/mdl435
- 50. Dabholkar M, Bostick-Bruton F, Weber C, Bohr VA, Egwuagu C, Reed E. ERCC1 and ERCC2 expression in malignant tissues from ovarian cancer patients. *J Natl Cancer Inst*. 1992;84(19):1512-1517. doi:10.1093/jnci/84.19.1512
- 51. Vaisman A, Varchenko M, Umar A, et al. The role of hMLH1, hMSH3, and hMSH6 defects in cisplatin and oxaliplatin resistance: correlation with replicative bypass of platinum-DNA adducts. *Cancer Res.* 1998;58(16):3579-3585.
- 52. Mello JA, Acharya S, Fishel R, Essigmann JM. The mismatch-repair protein hMSH2 binds selectively to DNA adducts of the anticancer drug cisplatin. *Chem Biol*. 1996;3(7):579-589. doi:10.1016/s1074-5521(96)90149-0
- 53. Narod SA, Foulkes WD. BRCA1 and BRCA2: 1994 and beyond. *Nat Rev Cancer*. 2004;4(9):665-676. doi:10.1038/nrc1431
- 54. Bryant HE, Schultz N, Thomas HD, et al. Specific killing of BRCA2-deficient tumours with inhibitors of poly(ADP-ribose) polymerase. *Nature*. 2005;434(7035):913-917. doi:10.1038/nature03443
- 55. Farmer H, McCabe N, Lord CJ, et al. Targeting the DNA repair defect in BRCA mutant cells as a therapeutic strategy. *Nature*. 2005;434(7035):917-921. doi:10.1038/nature03445

- 56. Ratnam K, Low JA. Current development of clinical inhibitors of poly(ADP-ribose) polymerase in oncology. *Clin Cancer Res.* 2007;13(5):1383-1388. doi:10.1158/1078-0432.CCR-06-2260
- 57. Mego M, Cierna Z, Svetlovska D, et al. PARP expression in germ cell tumours. *J Clin Pathol.* 2013;66(7):607-612. doi:10.1136/jclinpath-2012-201088
- 58. Cavallo F, Graziani G, Antinozzi C, et al. Reduced Proficiency in Homologous Recombination Underlies the High Sensitivity of Embryonal Carcinoma Testicular Germ Cell Tumors to Cisplatin and Poly (ADP-Ribose) Polymerase Inhibition. *PLoS One*. 2012;7(12):e51563. doi:10.1371/journal.pone.0051563
- 59. Galluzzi L, Vitale I, Michels J, et al. Systems biology of cisplatin resistance: past, present and future. *Cell Death Dis.* 2014;5(5):e1257. doi:10.1038/cddis.2013.428
- 60. Martinez-Rivera M, Siddik ZH. Resistance and gain-of-resistance phenotypes in cancers harboring wild-type p53. *Biochem Pharmacol*. 2012;83(8):1049-1062. doi:10.1016/j.bcp.2011.12.026
- 61. Peng HQ, Hogg D, Malkin D, et al. Mutations of the p53 gene do not occur in testis cancer. *Cancer Res.* 1993;53(15):3574-3578.
- 62. Gutekunst M, Oren M, Weilbacher A, et al. p53 Hypersensitivity Is the Predominant Mechanism of the Unique Responsiveness of Testicular Germ Cell Tumor (TGCT) Cells to Cisplatin. *PLoS One*. 2011;6(4):e19198. doi:10.1371/journal.pone.0019198
- 63. Romano FJ, Rossetti S, Conteduca V, et al. Role of DNA repair machinery and p53 in the testicular germ cell cancer: a review. *Oncotarget*. 2016;7(51):85641-85649. doi:10.18632/oncotarget.13063
- 64. Duale N, Lindeman B, Komada M, et al. Molecular portrait of cisplatin induced response in human testis cancer cell lines based on gene expression profiles. *Mol Cancer*. 2007;6:53. doi:10.1186/1476-4598-6-53

- 65. Koster R, di Pietro A, Timmer-Bosscha H, et al. Cytoplasmic p21 expression levels determine cisplatin resistance in human testicular cancer. *J Clin Invest*. 2010;120(10):3594-3605. doi:10.1172/JCI41939
- 66. Juliachs M, Muñoz C, Moutinho CA, et al. The PDGFRβ–AKT Pathway Contributes to CDDP-Acquired Resistance in Testicular Germ Cell Tumors. *Clinical Cancer Research*. 2014;20(3):658-667. doi:10.1158/1078-0432.CCR-13-1131
- 67. Kim PKM, Mahidhara R, Seol DW. The role of caspase-8 in resistance to cancer chemotherapy. *Drug Resistance Updates*. 2001;4(5):293-296. doi:10.1054/drup.2001.0223
- 68. Kroemer G, Mariño G, Levine B. Autophagy and the integrated stress response. *Mol Cell*. 2010;40(2):280-293. doi:10.1016/j.molcel.2010.09.023
- 69. Donnelly A, Blagg BSJ. Novobiocin and Additional Inhibitors of the Hsp90 C-Terminal Nucleotide-binding Pocket. *Curr Med Chem*. 2008;15(26):2702-2717.
- 70. Ren JH, He WS, Nong L, et al. Acquired Cisplatin Resistance in Human Lung Adenocarcinoma Cells Is Associated with Enhanced Autophagy. *Cancer Biotherapy and Radiopharmaceuticals*. 2010;25(1):75-80. doi:10.1089/cbr.2009.0701
- 71. Yu H, Su J, Xu Y, et al. p62/SQSTM1 involved in cisplatin resistance in human ovarian cancer cells by clearing ubiquitinated proteins. *Eur J Cancer*. 2011;47(10):1585-1594. doi:10.1016/j.ejca.2011.01.019
- 72. Országhová Z, Kalavska K, Mego M, Chovanec M. Overcoming Chemotherapy Resistance in Germ Cell Tumors. *Biomedicines*. 2022;10(5):972. doi:10.3390/biomedicines10050972
- 73. Oechsle K, Honecker F, Cheng T, et al. Preclinical and clinical activity of sunitinib in patients with cisplatin-refractory or multiply relapsed germ cell tumors: a Canadian Urologic Oncology Group/German Testicular Cancer Study Group cooperative study. *Annals of Oncology*. 2011;22(12):2654-2660. doi:10.1093/annonc/mdr026

- 74. Castillo-Avila W, Piulats JM, Garcia Del Muro X, et al. Sunitinib inhibits tumor growth and synergizes with cisplatin in orthotopic models of cisplatin-sensitive and cisplatin-resistant human testicular germ cell tumors. *Clin Cancer Res.* 2009;15(10):3384-3395. doi:10.1158/1078-0432.CCR-08-2170
- 75. Yaba A, Bozkurt ER, Demir N. mTOR expression in human testicular seminoma. Andrologia. 2016;48(6):702-707. doi:10.1111/and.12504
- 76. Mego M, Svetlovska D, Miskovska V, et al. Phase II study of everolimus in refractory testicular germ cell tumors. *Urol Oncol*. 2016;34(3):122.e17-22. doi:10.1016/j.urolonc.2015.10.010
- 77. Fenner M, Oing C, Dieing A, et al. Everolimus in patients with multiply relapsed or cisplatin refractory germ cell tumors: results of a phase II, single-arm, open-label multicenter trial (RADIT) of the German Testicular Cancer Study Group. *J Cancer Res Clin Oncol*. 2019;145(3):717-723. doi:10.1007/s00432-018-2752-z
- 78. De Giorgi U, Schepisi G, Gurioli G, et al. Olaparib as salvage treatment for advanced germ cell tumors after chemotherapy failure: Results of the open-label, single-arm, IGG-02 phase II trial. *JCO*. 2020;38(15_suppl):5058-5058. doi:10.1200/JCO.2020.38.15_suppl.5058
- 79. Castellano DE, Quinn DI, Feldman DR, et al. A phase II study of ribociclib in men with unresectable, incurable teratoma with recent progression. *JCO*. 2019;37(7_suppl):517-517. doi:10.1200/JCO.2019.37.7_suppl.517
- 80. Vaughn DJ, Hwang WT, Lal P, Rosen MA, Gallagher M, O'Dwyer PJ. Phase 2 trial of the cyclin-dependent kinase 4/6 inhibitor palbociclib in patients with retinoblastoma protein-expressing germ cell tumors. *Cancer*. 2015;121(9):1463-1468. doi:10.1002/cncr.29213
- 81. Funke K, Düster R, Wilson PDG, Arévalo L, Geyer M, Schorle H. Transcriptional CDK Inhibitors as Potential Treatment Option for Testicular Germ Cell Tumors. *Cancers (Basel)*. 2022;14(7):1690. doi:10.3390/cancers14071690

- 82. Cierna Z, Mego M, Miskovska V, et al. Prognostic value of programmed-death-1 receptor (PD-1) and its ligand 1 (PD-L1) in testicular germ cell tumors. *Ann Oncol*. 2016;27(2):300-305. doi:10.1093/annonc/mdv574
- 83. Fankhauser CD, Curioni-Fontecedro A, Allmann V, et al. Frequent PD-L1 expression in testicular germ cell tumors. *Br J Cancer*. 2015;113(3):411-413. doi:10.1038/bjc.2015.244
- 84. Adra N, Einhorn LH, Althouse SK, et al. Phase II trial of pembrolizumab in patients with platinum refractory germ-cell tumors: a Hoosier Cancer Research Network Study GU14-206. *Ann Oncol*. 2018;29(1):209-214. doi:10.1093/annonc/mdx680
- 85. Tsimberidou A, Vo HH, Subbiah V, et al. Pembrolizumab in Patients with Advanced Metastatic Germ Cell Tumors. *Oncologist*. 2021;26(7):558-e1098. doi:10.1002/onco.13682
- 86. Kawai K, Tawada A, Onozawa M, et al. Rapid Response to Pembrolizumab in a Chemo-Refractory Testicular Germ Cell Cancer with Microsatellite Instability-High. *Onco Targets Ther*. 2021;14:4853-4858. doi:10.2147/OTT.S323898
- 87. Mego M, Svetlovska D, Chovanec M, et al. Phase II study of avelumab in multiple relapsed/refractory germ cell cancer. *Invest New Drugs*. 2019;37(4):748-754. doi:10.1007/s10637-019-00805-4
- 88. Schmidtova S, Kalavska K, Gercakova K, et al. Disulfiram Overcomes Cisplatin Resistance in Human Embryonal Carcinoma Cells. *Cancers (Basel)*. 2019;11(9):1224. doi:10.3390/cancers11091224
- 89. Schmidtova S, Kalavska K, Liskova V, et al. Targeting of Deregulated Wnt/β-Catenin Signaling by PRI-724 and LGK974 Inhibitors in Germ Cell Tumor Cell Lines. *Int J Mol Sci.* 2021;22(8):4263. doi:10.3390/ijms22084263
- 90. Bauer S, Mühlenberg T, Leahy M, et al. Therapeutic Potential of Mdm2 Inhibition in Malignant Germ Cell Tumours. *European Urology*. 2010;57(4):679-687. doi:10.1016/j.eururo.2009.06.014

- 91. Oing C, Skowron MA, Bokemeyer C, Nettersheim D. Epigenetic treatment combinations to effectively target cisplatin-resistant germ cell tumors: past, present, and future considerations. *Andrology*. 2019;7(4):487-497. doi:10.1111/andr.12611
- 92. Albany C, Hever-Jardine MP, Von Herrmann KM, et al. Refractory testicular germ cell tumors are highly sensitive to the second generation DNA methylation inhibitor guadecitabine. *Oncotarget*. 2017;8(2):2949-2959. doi:10.18632/oncotarget.13811
- 93. Albany C, Fazal Z, Singh R, et al. A phase 1 study of combined guadecitabine and cisplatin in platinum refractory germ cell cancer. *Cancer Med*. 2020;10(1):156-163. doi:10.1002/cam4.3583
- 94. Nettersheim D, Jostes S, Fabry M, et al. A signaling cascade including ARID1A, GADD45B and DUSP1 induces apoptosis and affects the cell cycle of germ cell cancers after romidepsin treatment. *Oncotarget*. 2016;7(46):74931-74946. doi:10.18632/oncotarget.11647
- 95. Jostes S, Nettersheim D, Fellermeyer M, et al. The bromodomain inhibitor JQ1 triggers growth arrest and apoptosis in testicular germ cell tumours in vitro and in vivo. *J Cell Mol Med*. 2017;21(7):1300-1314. doi:10.1111/jcmm.13059
- 96. Choudhary C, Kumar C, Gnad F, et al. Lysine acetylation targets protein complexes and co-regulates major cellular functions. *Science*. 2009;325(5942):834-840. doi:10.1126/science.1175371
- 97. Filippakopoulos P, Picaud S, Mangos M, et al. Histone Recognition and Large-Scale Structural Analysis of the Human Bromodomain Family. *Cell*. 2012;149(1):214-231. doi:10.1016/j.cell.2012.02.013
- 98. Tamkun JW, Deuring R, Scott MP, et al. brahma: a regulator of Drosophila homeotic genes structurally related to the yeast transcriptional activator SNF2/SWI2. *Cell.* 1992;68(3):561-572. doi:10.1016/0092-8674(92)90191-e
- 99. Haynes SR, Dollard C, Winston F, Beck S, Trowsdale J, Dawid IB. The bromodomain: a conserved sequence found in human, Drosophila and yeast proteins. *Nucleic Acids Res.* 1992;20(10):2603.

- 100. Zeng L, Zhou MM. Bromodomain: an acetyl-lysine binding domain. *FEBS Letters*. 2002;513(1):124-128. doi:10.1016/S0014-5793(01)03309-9
- 101. Taniguchi Y. The Bromodomain and Extra-Terminal Domain (BET) Family:

 Functional Anatomy of BET Paralogous Proteins. *Int J Mol Sci.* 2016;17(11):1849.

 doi:10.3390/ijms17111849
- 102. Zaware N, Zhou MM. Bromodomain biology and drug discovery. *Nat Struct Mol Biol*. 2019;26(10):870-879. doi:10.1038/s41594-019-0309-8
- 103. Pan Z, Zhao Y, Wang X, et al. Targeting bromodomain-containing proteins: research advances of drug discovery. *Mol Biomed*. 2023;4:13. doi:10.1186/s43556-023-00127-1
- 104. Lou W, Gao K, Xu C, Li Q. Bromodomain-containing protein 9 is a prognostic biomarker associated with immune infiltrates and promotes tumor malignancy through activating notch signaling pathway in negative HIF-2α clear cell renal cell carcinoma. *IUBMB Life*. 2021;73(11):1334-1347. doi:10.1002/iub.2547
- 105. Mashtalir N, D'Avino AR, Michel BC, et al. Modular Organization and Assembly of SWI/SNF Family Chromatin Remodeling Complexes. *Cell*. 2018;175(5):1272-1288.e20. doi:10.1016/j.cell.2018.09.032
- 106. Zhu X, Liao Y, Tang L. Targeting BRD9 for Cancer Treatment: A New Strategy. *Onco Targets Ther.* 2020;13:13191-13200. doi:10.2147/OTT.S286867
- 107. Hohmann AF, Martin LJ, Minder JL, et al. Sensitivity and engineered resistance of myeloid leukemia cells to BRD9 inhibition. *Nat Chem Biol*. 2016;12(9):672-679. doi:10.1038/nchembio.2115
- 108. Huang H, Wang Y, Li Q, Fei X, Ma H, Hu R. miR-140-3p functions as a tumor suppressor in squamous cell lung cancer by regulating BRD9. *Cancer Letters*. 2019;446:81-89. doi:10.1016/j.canlet.2019.01.007

- 109. Clark PGK, Vieira LCC, Tallant C, et al. LP99: Discovery and Synthesis of the First Selective BRD7/9 Bromodomain Inhibitor. *Angew Chem Int Ed Engl*. 2015;54(21):6217-6221. doi:10.1002/anie.201501394
- 110. Martin LJ, Koegl M, Bader G, et al. Structure-Based Design of an in Vivo Active Selective BRD9 Inhibitor. *Journal of Medicinal Chemistry*. 2016;59(10):4462. doi:10.1021/acs.jmedchem.5b01865
- 111. Theodoulou NH, Bamborough P, Bannister AJ, et al. The Discovery of I-BRD9, a Selective Cell Active Chemical Probe for Bromodomain Containing Protein 9 Inhibition. *J Med Chem.* 2016;59(4):1425-1439. doi:10.1021/acs.jmedchem.5b00256
- 112. Berman HM, Westbrook J, Feng Z, et al. The Protein Data Bank. *Nucleic Acids Research*. 2000;28(1):235-242. doi:10.1093/nar/28.1.235
- 113. Zhang S, Chitu V, Stanley ER, Elliott BE, Greer PA. Fes tyrosine kinase expression in the tumor niche correlates with enhanced tumor growth, angiogenesis, circulating tumor cells, metastasis and infiltrating macrophages. *Cancer Res.* 2011;71(4):1465-1473. doi:10.1158/0008-5472.CAN-10-3757
- 114. Bagnyukova TV, Restifo D, Beeharry N, et al. DUSP6 regulates drug sensitivity by modulating DNA damage response. *Br J Cancer*. 2013;109(4):1063-1071. doi:10.1038/bjc.2013.353
- 115. Yan Y, Zhang L, Xu T, et al. SAMSN1 Is Highly Expressed and Associated with a Poor Survival in Glioblastoma Multiforme. *PLoS One*. 2013;8(11):e81905. doi:10.1371/journal.pone.0081905
- 116. Sattler S, Reiche D, Sturtzel C, et al. The Human C-Type Lectin-Like Receptor CLEC-1 is Upregulated by TGF-β and Primarily Localized in the Endoplasmic Membrane Compartment. *Scandinavian Journal of Immunology*. 2012;75(3):282-292. doi:10.1111/j.1365-3083.2011.02665.x
- 117. Zhou L, Yao Q, Li H, Chen J. Targeting BRD9 by I-BRD9 efficiently inhibits growth of acute myeloid leukemia cells. *Transl Cancer Res.* 2021;10(7):3364-3372. doi:10.21037/tcr-21-42

- 118. Qiang J, Zhao C, Shi LQ, et al. BRD9 promotes the progression of gallbladder cancer via CST1 upregulation and interaction with FOXP1 through the PI3K/AKT pathway and represents a therapeutic target. *Gene Ther*. 2024;31(11-12):594-606. doi:10.1038/s41434-024-00488-4
- 119. Zhu Q, Gu X, Wei W, Wu Z, Gong F, Dong X. BRD9 is an essential regulator of glycolysis that creates an epigenetic vulnerability in colon adenocarcinoma. *Cancer Med*. 2022;12(2):1572-1587. doi:10.1002/cam4.4954
- 120. Krämer KF, Moreno N, Frühwald MC, Kerl K. BRD9 Inhibition, Alone or in Combination with Cytostatic Compounds as a Therapeutic Approach in Rhabdoid Tumors. *Int J Mol Sci.* 2017;18(7):1537. doi:10.3390/ijms18071537
- 121. Andrews PW, Goodfellow PN, Shevinsky LH, Bronson DL, Knowles BB. Cell-surface antigens of a clonal human embryonal carcinoma cell line: Morphological and antigenic differentiation in culture. *International Journal of Cancer*. 1982;29(5):523-531. doi:10.1002/ijc.2910290507
- 122. Teshima S, Shimosato Y, Hirohashi S, et al. Four new human germ cell tumor cell lines. *Lab Invest*. 1988;59(3):328-336.
- 123. Andrews PW. Retinoic acid induces neuronal differentiation of a cloned human embryonal carcinoma cell line *in vitro*. *Developmental Biology*. 1984;103(2):285-293. doi:10.1016/0012-1606(84)90316-6
- 124. Damjanov I, Horvat B, Gibas Z. Retinoic acid-induced differentiation of the developmentally pluripotent human germ cell tumor-derived cell line, NCCIT. *Lab Invest.* 1993;68(2):220-232.
- 125. Josephson R, Ording CJ, Liu Y, et al. Qualification of Embryonal Carcinoma 2102Ep

 As a Reference for Human Embryonic Stem Cell Research. *Stem Cells*.

 2007;25(2):437-446. doi:10.1634/stemcells.2006-0236
- 126. Fichtner A, Bohnenberger H, Elakad O, et al. Proteomic profiling of cisplatin-resistant and cisplatin-sensitive germ cell tumour cell lines using quantitative mass spectrometry. *World J Urol.* 2022;40(2):373-383. doi:10.1007/s00345-022-03936-1

- 127. Skowron MA, Vermeulen M, Winkelhausen A, et al. CDK4/6 inhibition presents as a therapeutic option for paediatric and adult germ cell tumours and induces cell cycle arrest and apoptosis via canonical and non-canonical mechanisms. *Br J Cancer*. 2020;123(3):378-391. doi:10.1038/s41416-020-0891-x
- 128. Pattillo R, Ruckert A, Hussa R, Bernstein R, Delfs E. The JAr cell line continuous human multi-hormone production and controls. *In Vitro Cellular & Developmental Biology Plant*. Published online August 29, 1971. Accessed March 11, 2025. https://www.semanticscholar.org/paper/The-JAr-cell-line-continuous-human-multi-hormone-Pattillo-Ruckert/729fda8a2b51843fd194722055fe01e92f51de82
- 129. Mizuno Y, Gotoh A, Kamidono S, Kitazawa S. [Establishment and characterization of a new human testicular germ cell tumor cell line (TCam-2)]. *Nihon Hinyokika Gakkai Zasshi*. 1993;84(7):1211-1218. doi:10.5980/jpnjurol1989.84.1211
- 130. Schumacher V, Gueler B, Looijenga LHJ, et al. Characteristics of testicular dysgenesis syndrome and decreased expression of SRY and SOX9 in Frasier syndrome.
 Molecular Reproduction and Development. 2008;75(9):1484-1494.
 doi:10.1002/mrd.20889
- 131. Eckert D, Nettersheim D, Heukamp LC, Kitazawa S, Biermann K, Schorle H. TCam-2 but not JKT-1 cells resemble seminoma in cell culture. *Cell Tissue Res*. 2008;331(2):529-538. doi:10.1007/s00441-007-0527-y
- 132. Sasaki S, Katayama PK, Roesler M, Pattillo RA, Mattingly RF, Ohkawa K. Cytogenetic analysis of choriocarcinoma cell lines. *Nihon Sanka Fujinka Gakkai Zasshi*. 1982;34(12):2253-2256.
- 133. Hartmann K, Bennien J, Wapelhorst B, et al. Current insights into the sulfatase pathway in human testis and cultured Sertoli cells. *Histochem Cell Biol*. 2016;146(6):737-748. doi:10.1007/s00418-016-1503-y
- 134. Hussein SM, Batada NN, Vuoristo S, et al. Copy number variation and selection during reprogramming to pluripotency. *Nature*. 2011;471(7336):58-62. doi:10.1038/nature09871

- 135. Edgar R, Domrachev M, Lash AE. Gene Expression Omnibus: NCBI gene expression and hybridization array data repository. *Nucleic Acids Res.* 2002;30(1):207-210. doi:10.1093/nar/30.1.207
- 136. Ewels PA, Peltzer A, Fillinger S, et al. The nf-core framework for community-curated bioinformatics pipelines. *Nat Biotechnol*. 2020;38(3):276-278. doi:10.1038/s41587-020-0439-x
- 137. Dobin A, Davis CA, Schlesinger F, et al. STAR: ultrafast universal RNA-seq aligner. *Bioinformatics*. 2012;29(1):15. doi:10.1093/bioinformatics/bts635
- 138. Patro R, Duggal G, Love MI, Irizarry RA, Kingsford C. Salmon provides fast and biasaware quantification of transcript expression. *Nat Methods*. 2017;14(4):417-419. doi:10.1038/nmeth.4197
- 139. R: The R Project for Statistical Computing. Accessed November 13, 2024. https://www.r-project.org/
- 140. Love MI, Huber W, Anders S. Moderated estimation of fold change and dispersion for RNA-seq data with DESeq2. *Genome Biol*. 2014;15(12):550. doi:10.1186/s13059-014-0550-8
- 141. Huber W, Carey VJ, Gentleman R, et al. Orchestrating high-throughput genomic analysis with Bioconductor. *Nat Methods*. 2015;12(2):115-121. doi:10.1038/nmeth.3252
- 142. Szklarczyk D, Kirsch R, Koutrouli M, et al. The STRING database in 2023: protein–protein association networks and functional enrichment analyses for any sequenced genome of interest. *Nucleic Acids Res.* 2022;51(D1):D638-D646. doi:10.1093/nar/gkac1000
- 143. Chen EY, Tan CM, Kou Y, et al. Enrichr: interactive and collaborative HTML5 gene list enrichment analysis tool. *BMC Bioinformatics*. 2013;14:128. doi:10.1186/1471-2105-14-128

- 144. Livak KJ, Schmittgen TD. Analysis of Relative Gene Expression Data Using Real-Time Quantitative PCR and the 2–ΔΔCT Method. *Methods*. 2001;25(4):402-408. doi:10.1006/meth.2001.1262
- 145. Contreras-Romero C, Pérez-Yépez EA, Martinez-Gutierrez AD, et al. Gene Promoter-Methylation Signature as Biomarker to Predict Cisplatin-Radiotherapy Sensitivity in Locally Advanced Cervical Cancer. *Front Oncol.* 2022;12:773438. doi:10.3389/fonc.2022.773438
- 146. Wang Y, Jiang XY, Yu XY. BRD9 controls the oxytocin signaling pathway in gastric cancer via CANA2D4, CALML6, GNAO1, and KCNJ5. *Transl Cancer Res*. 2020;9(5):3354-3366. doi:10.21037/tcr.2020.03.67
- 147. Zhou Q, Huang J, Zhang C, et al. The bromodomain containing protein BRD-9 orchestrates RAD51–RAD54 complex formation and regulates homologous recombination-mediated repair. *Nat Commun*. 2020;11:2639. doi:10.1038/s41467-020-16443-x
- 148. Yamamoto H, Hirasawa A. Homologous Recombination Deficiencies and Hereditary Tumors. *Int J Mol Sci.* 2021;23(1):348. doi:10.3390/ijms23010348
- 149. Suszynska M, Ratajska M, Kozlowski P. BRIP1, RAD51C, and RAD51D mutations are associated with high susceptibility to ovarian cancer: mutation prevalence and precise risk estimates based on a pooled analysis of ~30,000 cases. *J Ovarian Res*. 2020;13:50. doi:10.1186/s13048-020-00654-3
- 150. Toss A, Tenedini E, Piombino C, et al. Clinicopathologic Profile of Breast Cancer in Germline ATM and CHEK2 Mutation Carriers. *Genes (Basel)*. 2021;12(5):616. doi:10.3390/genes12050616
- 151. Weber-Lassalle N, Borde J, Weber-Lassalle K, et al. Germline loss-of-function variants in the BARD1 gene are associated with early-onset familial breast cancer but not ovarian cancer. *Breast Cancer Res.* 2019;21:55. doi:10.1186/s13058-019-1137-9

- 152. Rahman N, Seal S, Thompson D, et al. PALB2, which encodes a BRCA2-interacting protein, is a breast cancer susceptibility gene. *Nat Genet*. 2007;39(2):165-167. doi:10.1038/ng1959
- 153. Lashgari A, Fauteux M, Maréchal A, Gaudreau L. Cellular Depletion of BRD8 Causes p53-Dependent Apoptosis and Induces a DNA Damage Response in Non-Stressed Cells. *Sci Rep.* 2018;8:14089. doi:10.1038/s41598-018-32323-3
- 154. Müller MR, Burmeister A, Skowron MA, et al. Therapeutical interference with the epigenetic landscape of germ cell tumors: a comparative drug study and new mechanistical insights. *Clin Epigenetics*. 2022;14:5. doi:10.1186/s13148-021-01223-1
- 155. Yang Q, Vafaei S, Falahati A, et al. Bromodomain-Containing Protein 9 Regulates Signaling Pathways and Reprograms the Epigenome in Immortalized Human Uterine Fibroid Cells. *Int J Mol Sci.* 2024;25(2):905. doi:10.3390/ijms25020905
- 156. Weisberg E, Chowdhury B, Meng C, et al. BRD9 degraders as chemosensitizers in acute leukemia and multiple myeloma. *Blood Cancer J.* 2022;12(7):110. doi:10.1038/s41408-022-00704-7
- 157. Brien GL, Remillard D, Shi J, et al. Targeted degradation of BRD9 reverses oncogenic gene expression in synovial sarcoma. van Lohuizen M, Sawyers CL, eds. eLife. 2018;7:e41305. doi:10.7554/eLife.41305
- 158. Del Gaudio N, Di Costanzo A, Liu NQ, et al. BRD9 binds cell type-specific chromatin regions regulating leukemic cell survival via STAT5 inhibition. *Cell Death Dis*. 2019;10(5):338. doi:10.1038/s41419-019-1570-9
- 159. Alpsoy A, Utturkar SM, Carter BC, et al. BRD9 is a critical regulator of androgen receptor signaling and prostate cancer progression. *Cancer Res.* 2021;81(4):820-833. doi:10.1158/0008-5472.CAN-20-1417
- 160. Snow GE, Kasper AC, Busch AM, et al. Wnt pathway reprogramming during human embryonal carcinoma differentiation and potential for therapeutic targeting. *BMC Cancer*. 2009;9:383. doi:10.1186/1471-2407-9-383

- 161. Freemantle SJ, Kerley JS, Olsen SL, Gross RH, Spinella MJ. Developmentally-related candidate retinoic acid target genes regulated early during neuronal differentiation of human embryonal carcinoma. *Oncogene*. 2002;21(18):2880-2889. doi:10.1038/sj.onc.1205408
- 162. Rudolph C, Melau C, Nielsen JE, et al. Involvement of the DNA mismatch repair system in cisplatin sensitivity of testicular germ cell tumours. *Cell Oncol*. 2017;40(4):341-355. doi:10.1007/s13402-017-0326-8
- 163. Funke K, Einsfelder U, Hansen A, et al. Genome-scale CRISPR screen reveals neddylation to contribute to cisplatin resistance of testicular germ cell tumours. *Br J Cancer*. Published online April 6, 2023:1-13. doi:10.1038/s41416-023-02247-5
- 164. Leszczyniecka M, Roberts T, Dent P, Grant S, Fisher PB. Differentiation therapy of human cancer: basic science and clinical applications. *Pharmacology & Therapeutics*. 2001;90(2):105-156. doi:10.1016/S0163-7258(01)00132-2
- 165. Naveen CR, Gaikwad S, Agrawal-Rajput R. Berberine induces neuronal differentiation through inhibition of cancer stemness and epithelial-mesenchymal transition in neuroblastoma cells. *Phytomedicine*. 2016;23(7):736-744. doi:10.1016/j.phymed.2016.03.013
- 166. Loehr AR, Pierpont TM, Gelsleichter E, et al. Targeting Cancer Stem Cells with Differentiation Agents as an Alternative to Genotoxic Chemotherapy for the Treatment of Malignant Testicular Germ Cell Tumors. *Cancers (Basel)*. 2021;13(9):2045. doi:10.3390/cancers13092045
- 167. Abdolahi S, Ghazvinian Z, Muhammadnejad S, Saleh M, Asadzadeh Aghdaei H, Baghaei K. Patient-derived xenograft (PDX) models, applications and challenges in cancer research. *J Transl Med*. 2022;20:206. doi:10.1186/s12967-022-03405-8
- 168. Clevers H. Modeling Development and Disease with Organoids. *Cell.* 2016;165(7):1586-1597. doi:10.1016/j.cell.2016.05.082

- 169. Tang XY, Wu S, Wang D, et al. Human organoids in basic research and clinical applications. *Signal Transduct Target Ther*. 2022;7:168. doi:10.1038/s41392-022-01024-9
- 170. Cham TC, Ibtisham F, Al-Dissi A, Honaramooz A. An *in vitro* testicular organoid model for the study of testis morphogenesis, somatic cell maturation, endocrine function, and toxicological assessment of endocrine disruptors. *Reproductive Toxicology*. 2024;128:108645. doi:10.1016/j.reprotox.2024.108645

7 APPENDIX

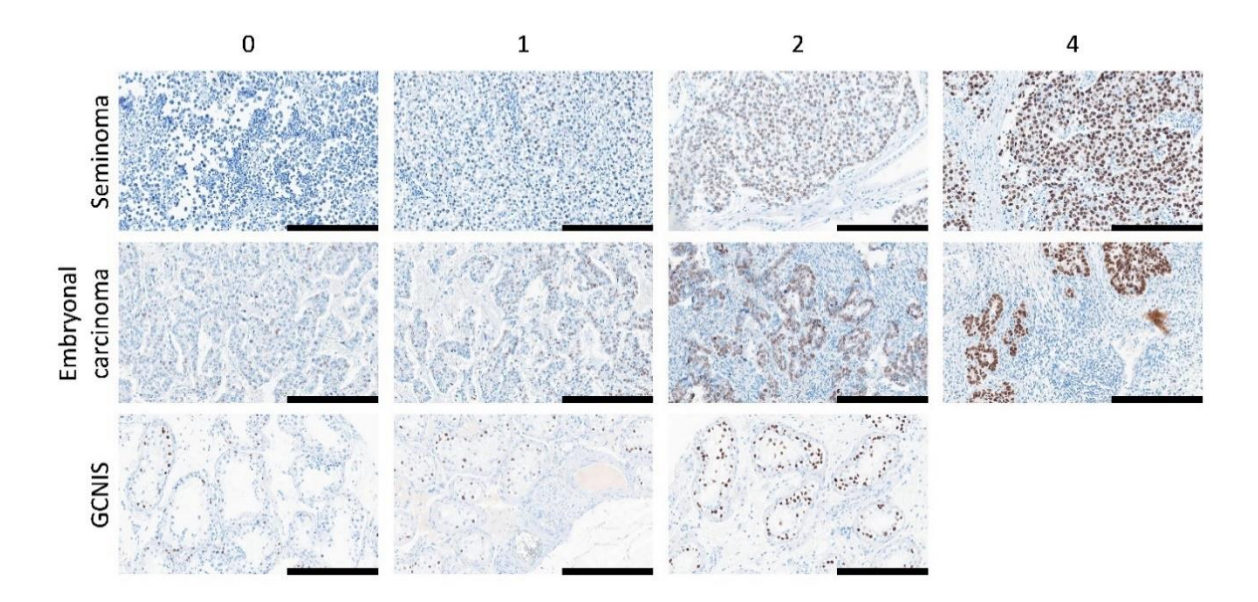


Figure S 1: Example images for the staining intensities of SALL4 in seminomas, embryonal carcinomas and GCNIS. Staining intensity was scored as negative (0), weak (1), moderate (2) and strong (3). The example images for GCNIS show the heterogeneity of SALL4 expression. GCNIS – germ cell neoplasia in situ.

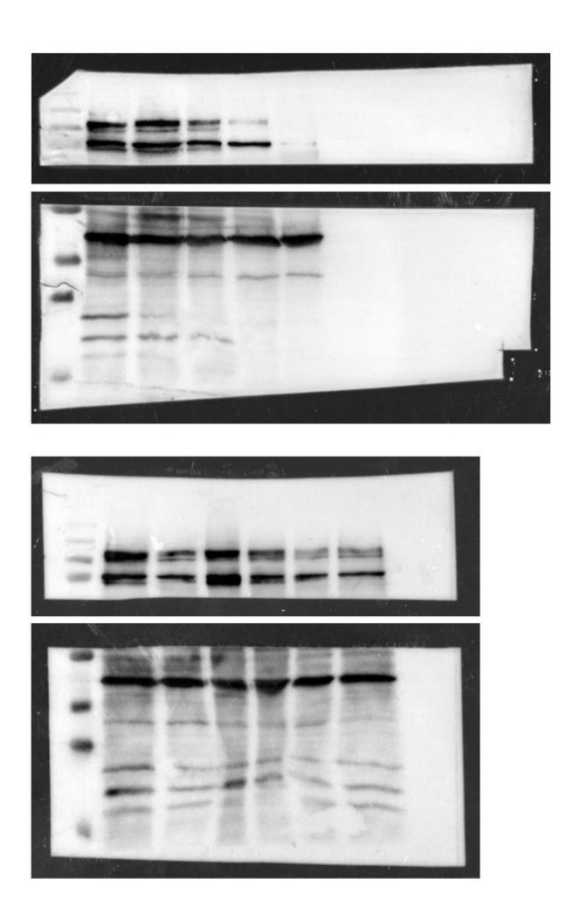


Figure S 2: Original Western Blot images of BRD9 protein level and corresponding load control β-actin in different TGCT cell lines as well as control cell lines. Modified from ¹.

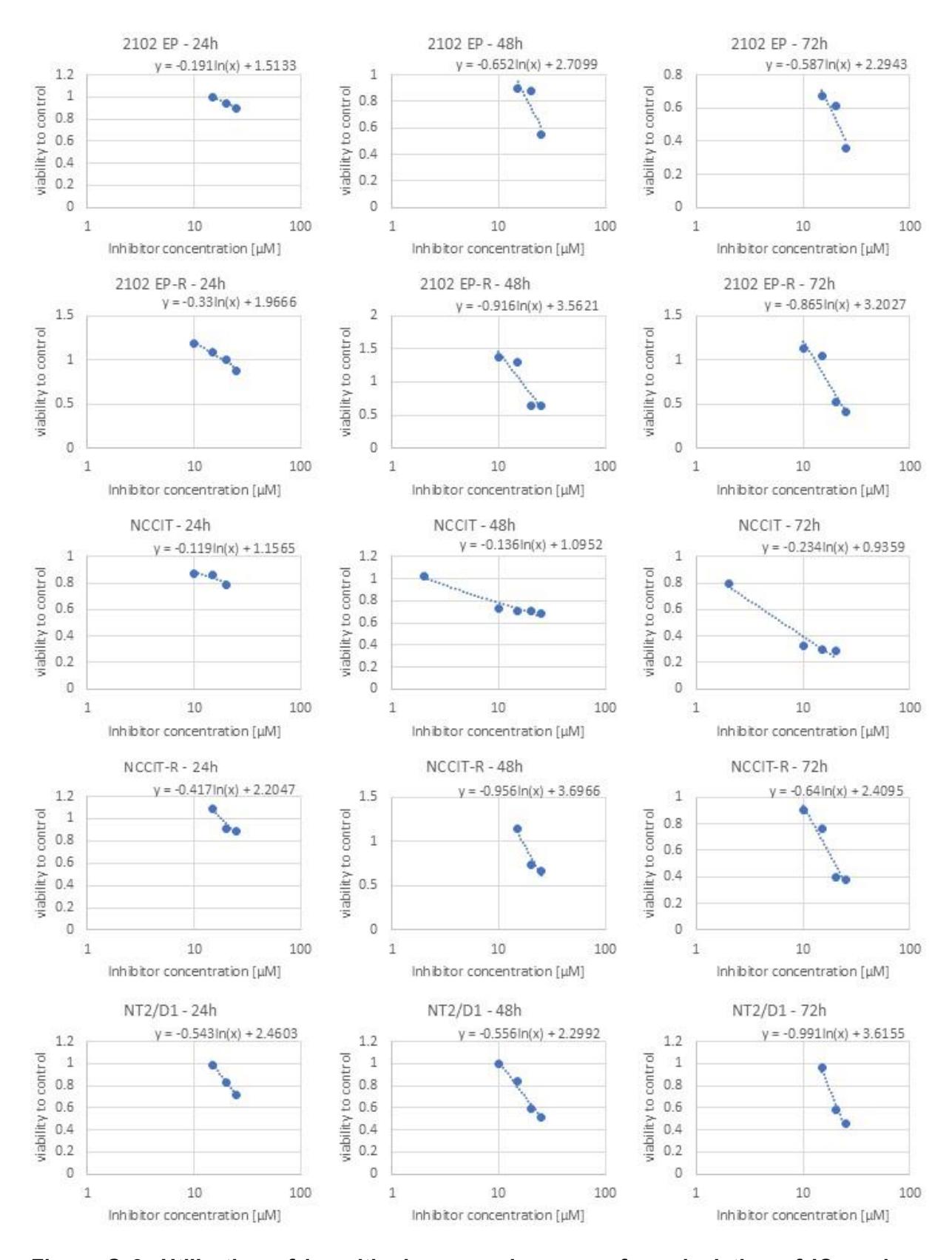


Figure S 3: Utilization of logarithmic regression curve for calculation of IC_{50} values based on XTT assay data (Figure 15).

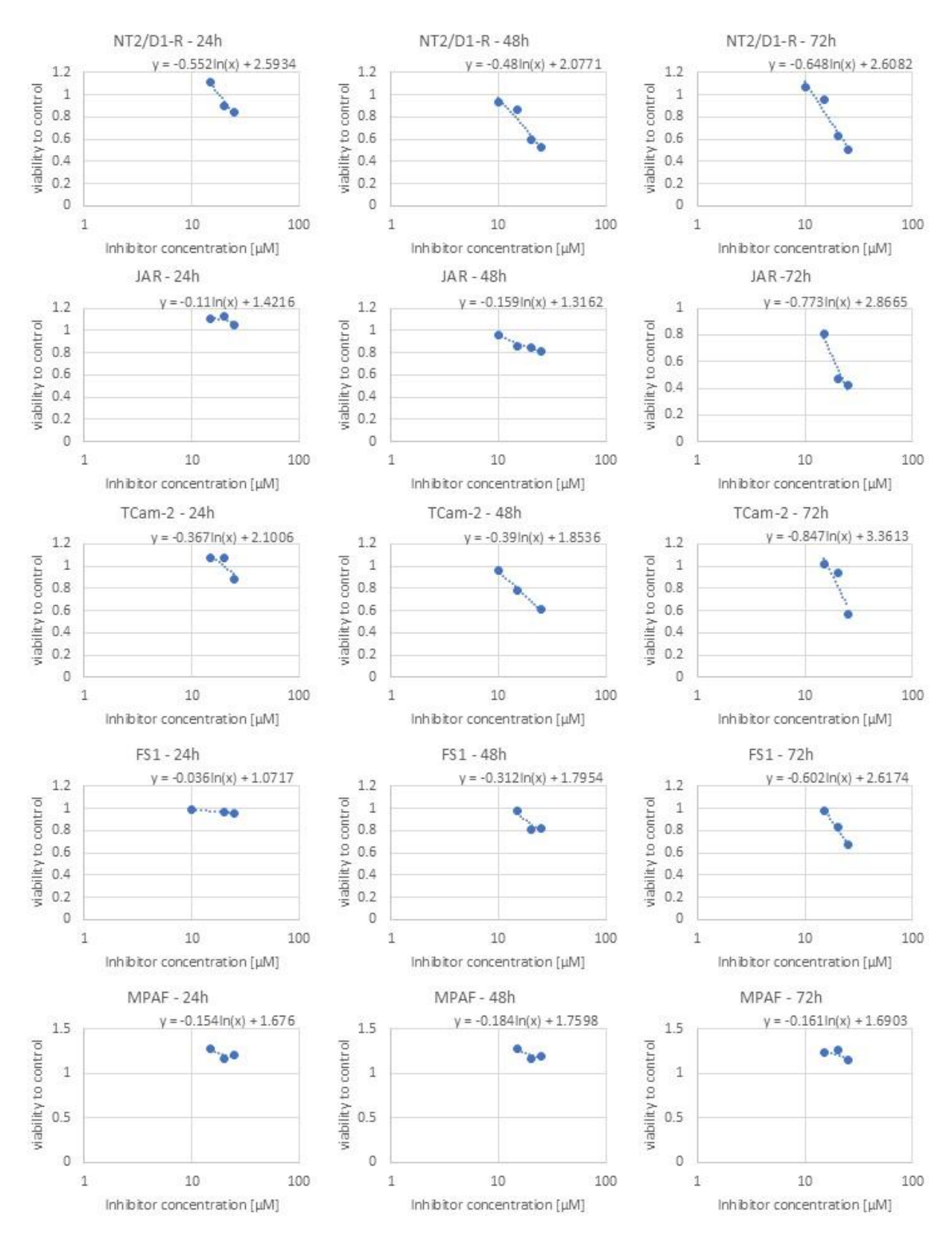


Figure S 4: Utilization of logarithmic regression curve for calculation of IC_{50} values based on XTT assay data (Figure 15).

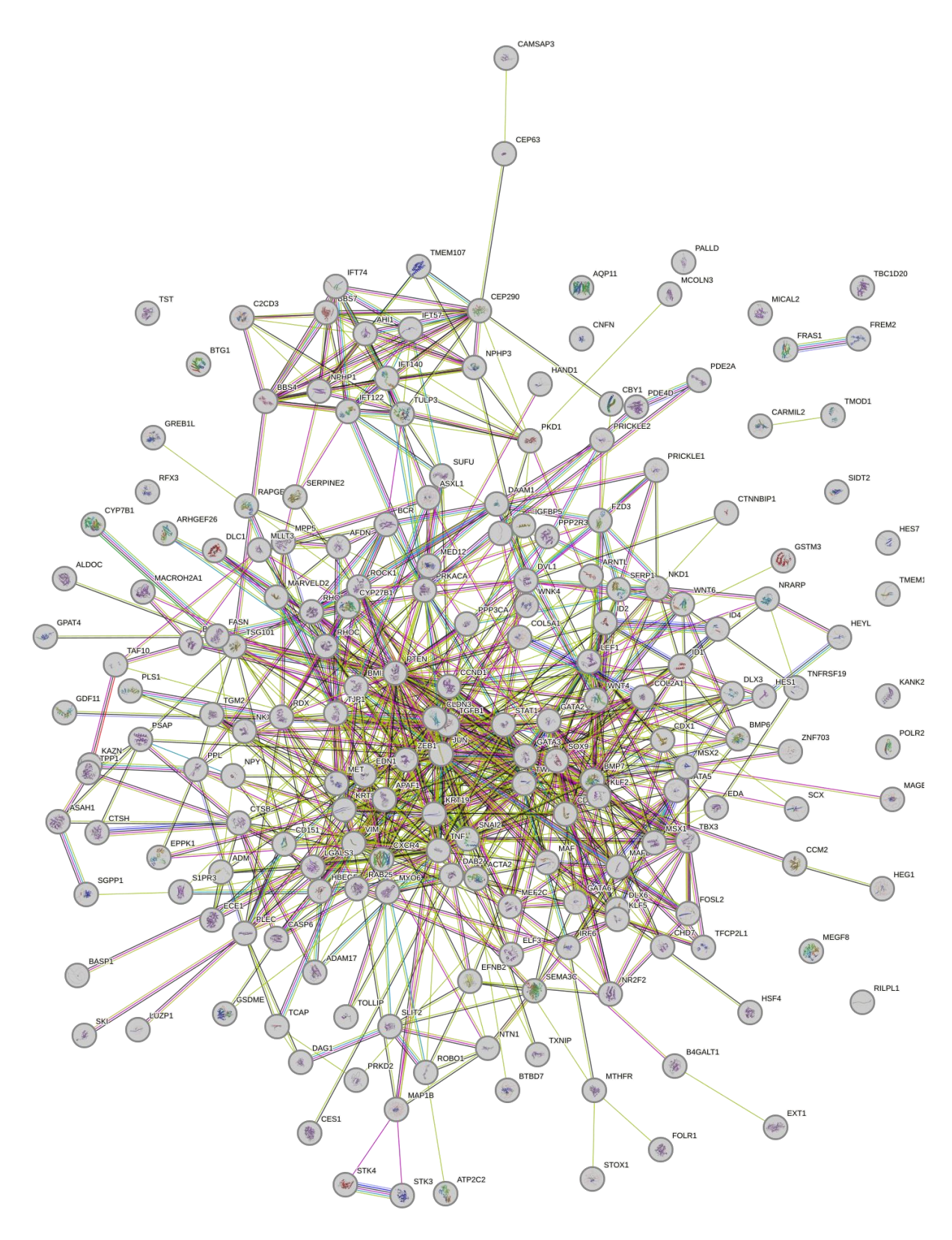


Figure S 5: STRING-based interaction analysis of all upregulated genes associated with epithelium development in 2102 EP cells after 24h of treatment with I-BRD9. Modified from ¹.

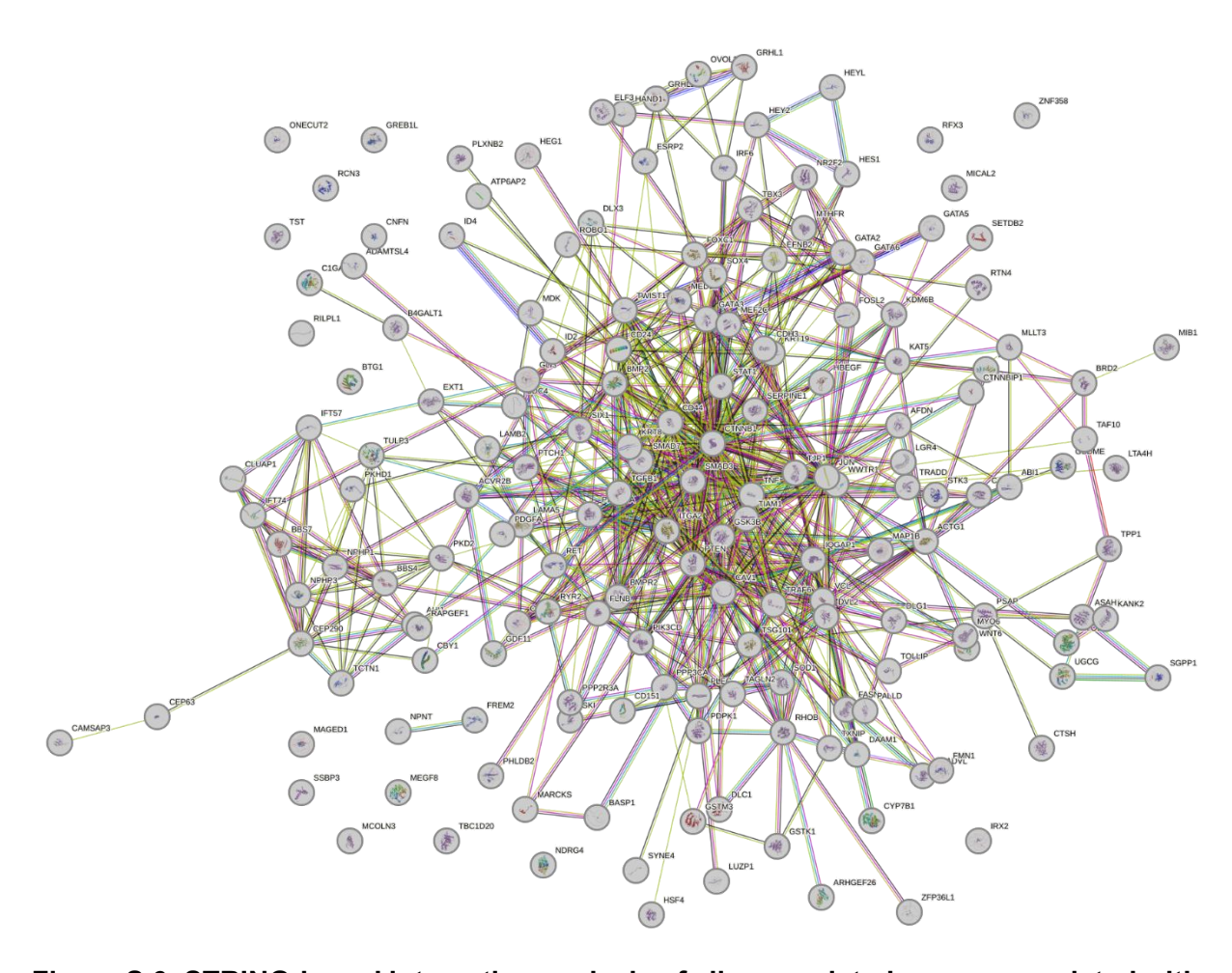


Figure S 6: STRING-based interaction analysis of all upregulated genes associated with epithelium development in TCam-2 cells after 24h of treatment with I-BRD9. Modified from ¹.

8 ACKNOWLEDGEMENT

Ich möchte mich vor allem bei meinem Doktorvater Prof. Dr. Hubert Schorle bedanken, der mir zunächst die Möglichkeit gab, meine Masterarbeit bei ihm im Labor zu schreiben und anschließend auch für meine Promotion zu bleiben. Er stand mir während der gesamten Zeit meiner Promotion bei Fragen und Diskussion zur Seite und hat mich in meinem wissenschaftlichen Arbeiten sehr gefördert.

Weiterhin möchte ich mich bei den Mitgliedern meiner Promotionskommission bedanken: Prof. Dr. Gruß, für die freundliche Bereitschaft das 2. Gutachten dieser Arbeit zu übernehmen, PD Dr. Gregor Kirfel als Vorsitzender der Kommission sowie Prof. Dr. Matthias Geyer als fachgruppenfremdes Mitglied.

Darüber hinaus danke ich Prof. Dr. Glen Kristiansen, Dr. Christine Sanders und Dr. Florian Fronhoffs für die freundliche und produktive Kooperation und hilfreichen Diskussionen.

Ein besonderer Dank gilt auch Dr. Kai Funke, der mich seit meiner Masterarbeit und zum Beginn meiner Promotion betreut hat und immer für Fragen hilfsbereit und mit einem Lächeln im Gesicht zur Seite stand. Er hat meine selbständige Arbeitsweise stark gefördert und mir seine fachliche Expertise weitergegeben.

Mein Dank gilt auch den ehemaligen und derzeitigen Mitarbeitern der AG Schorle (Gaby Beine, Greta Zech, Dr. Lena Arévalo, Dr. Gina Merges, Dr. Simon Schneider, Dr. Rashidul Islam, Anđela Kovačević, Annalena Liesen, Eva Ordziniak, Christoph Wiesejahn, Lea Descher, Necal Sehil, Andrea Jäger, Angela Egert und Ahmad Chebli) für den wissenschaftlichen Austausch aber vor allem auch für die schöne Zeit auch im privaten Umfeld. Die Gespräche in den Mittagspausen, das gemeinsame Kochen aber auch private Aktivitäten haben die Zeit meiner Promotion sehr bereichert, die mir immer gerne in Erinnerung bleiben wird.

Außerdem möchte ich mich auch bei meiner Familie und meinem Partner für die bedingungslose Unterstützung in dieser aufregenden Zeit bedanken. Ein besonderer Dank gilt meinen Eltern, die immer an mich und meine Ziele geglaubt haben. Ohne euch hätte ich es nicht bis hier hingeschafft.